ANALYSIS OF MICROEARTHQAUKES WITH CORRELATION METHOD AT SALAVATLI GEOTHERMAL AREA, AYDIN

by
Esra Kalkan
B.S., Geophysical Engineering, İstanbul University, 2007

Submitted to
Boğaziçi University
Kandilli Observatory and Earthquake Research Institute
in partial fulfillment of the requirements for the degree of
Master of Science

Graduate Program in Geophysical Engineering
Boğaziçi University
2013

ACKNOWLEDGEMENT

I would like to express my gratitude to my advisor Prof. Dr. Cemil Gürbüz for the useful comments, remarks and engagement through the learning process of this master thesis. His invaluable guidance and proffesional excellence throughout my goal provide a motivation to expose this study.

I am a grateful to my co-advisor Assoc. Prof. Dr. Ekrem Zor for his helpful guidance and significant determinations about my study. His propositions about my performance elicit to complete my study with a self-confidence.

I would like to thank MENDERES JEOTERMAL ELEKTRİK ÜRETİM A.Ş. (MEGE) to allow us use their geothermal data.

I am deeply greatful to my dear and closest friend Pınar Büyükakpınar who is there with me all along, supporting me, giving me courage, making me smile at diffucult times and her brilliant advices. There is no word enough to describe her precence for me. I also thank my lovely friend Sezim Ezgi Güvercin Işık for her endless help. She listened to me whenever I needed help and gived her guidance about computer programming. Without their support it is not possible to finish my thesis. I would also like to thank all of my friends and members of Kandilli Observatory and Earthquake Research Institute for encouraging me to continue on and finish up my thesis. My research would not have been possible without their helps.

I also thank all my closest friends, especially Kübra Kan and Hazal Kan for their spiritually support.

I would like to acknowledge the spiritual and material support of my dad Kenan Kalkan, my mom Sırrıye Kalkan and my dearly beloved sister Kısmet Kübra Kalkan who helped me to conceive the importance of education and encouraged me through all my life. This goal would not be realized without their concerns and patiences.

Dedicated to my lovely beloved sister Kısmet Kübra Kalkan

ABSTRACT
ANALYSIS OF MICROEARTHQAUKES WITH CORRELATION METHOD AT SALAVATLI GEOTHERMAL AREA, AYDIN

Induced seismicity typically refers to minor earthquakes and tremors that are caused by human activity that alters the stresses and strains on the Earth's crust. Earthquakes which are smaller magnitude are called micro-earthquakes. Micro-earthquakes could be observed in areas which includes energy technologies that involve injection or withdrawal of fluids from the subsurface. Micro-earthquakes are the result from these kind of process. Geothermal areas are good example of that kind of areas. So we chose Salavatlı, Aydın geothermal area to study.

The main aim of this study is to find similar micro-earthquakes with correlation method to check if they come from same source or location. So the data which was collected from 9 broad-band stations which were installed at the study area,between June of 2010 and April of 2013 were used for this aim. 977 micro-earthquakes were located with SEISAN. 815 of them could be used for the correlation analysis due to quality of data. GISMO correlation toolbox was used for this process. The duration of waveforms are 10 seconds because the longest micro-earthquake in this study is 8 seconds. We took lower limit as 0.9 for the correlation co-efficient. 34 event of similar waveforms were found.

When we examined location of all micro-earthquakes, we saw that they were scattered over the study area. This might be caused from wrong P or S wave pickings or inadequate crustal velocity model. So, firstly, we decided to check the initial velocity model by using VELEST software. For the VELEST processing 334 best located micro-earthquakes were selected on the base some criterias. After getting minimum 1D velocity model for the study area, all micro-earthquakes were relocated again and then mapped. The location of most of them altered and get better. Then with final 1D velocity model, events of similar waveforms were map. In general, when monthly location of micro-earthquakes were checked, the direction of the injected water from re-injection wells could be clearly seen on the seismicity maps.

ÖZET
AYDIN, SALAVATLI JEOTERMAL ALANINDA KORELASYON METODU İLE MİKRO DEPREM ANALİZİ

İndüklenmiş sismik genel olarak, insan aktivitesi sonucu yerin içinde meydana gelen gerilim değişiminin, küçük depremlere ve yer sarsıntılarına sebebiyet vermesini içermektedir. Küçük manyetüdlü depremler, mikro depremler olarak adlandırılır. Mikro depremler, yer altından su çekilmesi veya basınçlı bir şekilde enjekte edilmesini içeren enerji teknolojilerinde gözlemlenebilmektedir. Mikro depremler, bu tür aşamalardan kaynaklanmaktadır. Jeotermal alanlar, bu gibi alanlar için iyi bir örnektir. Bu sebepten dolayı Aydın, Salavatlı jeotermal bölgesi bu çalışma için seçilmiştir.

Çalışmanın asıl amacı, korelasyon yöntemiyle benzer mikro depremleri bulmak ve bu depremlerin aynı kaynaktan ya da aynı yerden gelip gelmediğine bakmaktır. Bunun için, çalışma alanında kurulmuş olan dokuz adet geniş-bantlı deprem istasyonundan Haziran 2010 ve Nisan 2013 aralığında veri toplanmıştır. 977 adet mikro depremin yeri, SEISAN programıyla belirlenmiştir. Kayıt kalitesinden dolayı, bu depremlerin 815 tanesi korelasyon için kullanılabilmiştir. Korelasyon süreci için, GISMO korelasyon programı kullanılmıştır. Bu çalışmadaki depremlerin en uzun süreli olanı 8 saniye olduğundan dolayı korelasyon için dalga uzunluğu 10 saniye olarak seçilmiştir. Minimum korelasyon kat sayısı olarak ise, 0.9 alınmıştır. 34 adet benzer dalga formu içeren grup bulunmuştur.

Bütün depremlerin yerleri incelendiğinde, çalışma alanına yayılmış bir şekilde olduğunu görüldü. Bunun sebebi , yanlış P ya da S okumaları ya da yetersiz bir hız modeli olabilir. Bu sebeple, yapılacak ilk iş başlangıç modelini kontrol etmek ve çalışma alanı için uygun 1 boyutlu hız modelini VELEST ile bulmak oldu. 334 adet iyi çözülmüş mikro deprem kullanılarak uygun bir hız modeli elde edildi. Hız modeli bulunduktan sonra bütün depremler tekrar çözülerek, haritalandırıldı. Çoğu depremin lokasyonu değişerek, daha iyileşmiş oldu. Daha sonra elde edilen 1 boyutlu hız modeli ile depremlerin lokasyonları yenilenerek, yeniden haritaya aktarıldı. Genel olarak aylık mikro depremlerin lokasyonları incelendiğinde, enjekte edilen suyun hareket yönünün sismik haritalarda gözlemleme olanağı doğmuştur.

TABLE OF CONTENTS

LIST OF FIGURES

LIST OF TABLES

LIST OF SYMBOLS / ABBREVIATIONS

σ	Variance
i	Integer
μ	Mean
τ	Lag
E	Expected value operator
N	North
S	South
E	East
W	West
Hz	Hertz
R	Correlation function
1-D	One Dimensional
Corr	Correlation
CSS	Carbon capture and storage
EGS	Enhanced geothermal system
GCF	Guralp compressed format
GISMO	GI Seismology Matlab Objects
GMT	Generic mapping tools
GPS	Global Positioning System
HYPO71	Earthquake Location Program
ML	Local magnitude
MEQ	Micro earthquake

MMM	Menderes Metamorphic Massive
MTA	Mineral Research and Exploration General Directorate
RMS	Root mean square
SAC	Seismic analysis code
SEISAN	The earthquake analysis software
TUBITAK	Scientific & Technological Research Council of Turkey
TPOA	Turkish Petroleum Corporation

1. INTRODUCTION

The most earthquakes occured in the world have natural causes. However some earthquakes are related to human activities and have no relation with natural causes. These earthquakes have also smaller magnitude and also small in intensity of ground shaking. These type of earthquakes are called “induces seismic events” or “induced earthquakes”. Induces seismic events have been documented since 1920s (i.e.; the impoundement of large earthquakes behind dams, controlled exploisons, underground nuclear tests.). Induces sesismic events are also observed in energy Technologies that involve injection or withdrawal of fluids from the surface. For example, geothermal energy, oil and gas production, carbon capture and storage (CSS) involve fluid injection and withdrawal.

In these kind of energy technologies, geothermal energy has an important place. Since fluid injection and withdrawal of fluid is backbone of it. Geothermal energy exists because of the substantial heat in the Earth and the temperature increase with depths below Earth’s surface. Geothermal development usually try to keep a mass balance between fluid volumes produced and fluids replaced by injection to enlarge the longevity of the energy resource. This fluid balance helps to keep fairly constant reservoir pressure close to minimum, pre-production value and can aid in reducing the potential for induced seismicity.

There are three types of geothermal resources are recognized: (1) vapor-dominated, the steam is contained in the pores or fractures of hot rock; (2) liquid-dominated, the hot water is contained in the rock; and (3) hot dry rock , where the resource is simply hot and currently dry rock that requires an Enhanced Geothermal System (EGS) to facilitate development. Each of these types has different injection processes and these processes can cause induced seismicity. In hot dry rock type of geothermal resources, regions have sufficiently high temperature at reasonably shallow depths for potential commercial development of enhanced geothermal systems (EGS). Our study area is a mixture of hot dry rock and liquid dominated. The EGS system requires the injection of a liquid at sufficient pressure in one well to overcome the confining pressures at depth and to thereby force open incipient fractures and planes of weakness or to create new fractures to allow fluids to flow more freely through the subsurface rock. The new fractures location can be determined by monitoring the microseismic response at the surface or downhole . Figure 1.1 shows the schema of EGS system.

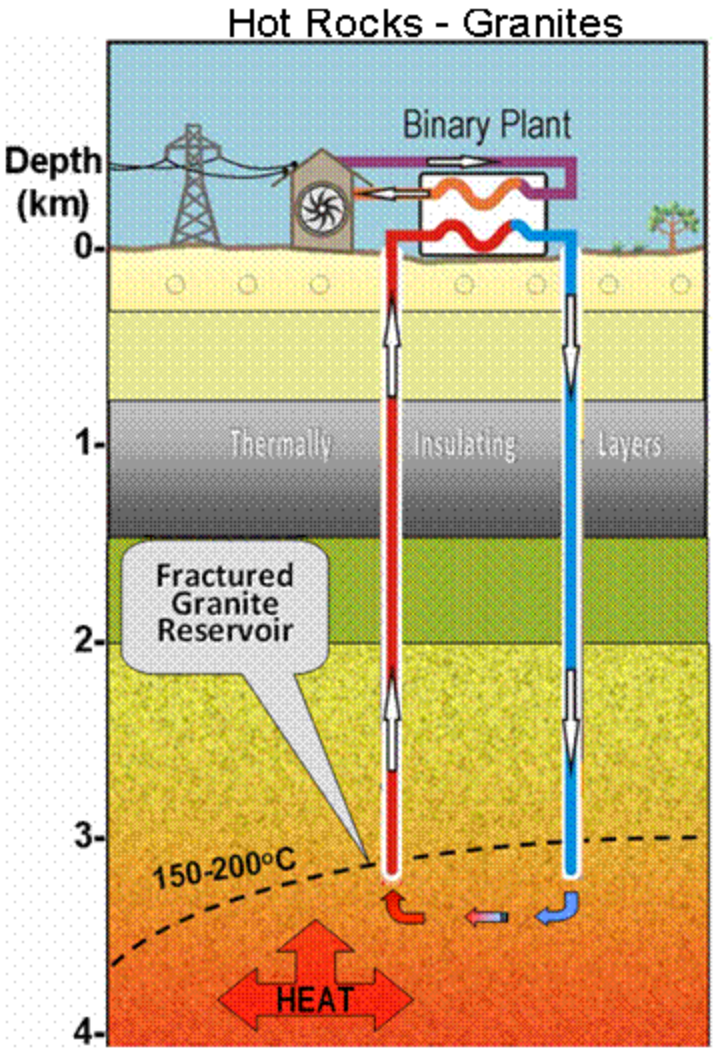

Figure 1.1. EGS development (Taken from Clean Energy Australia Pty Ltd.).

Blue pipe represents the injection well is accompanied by the red pipe represents the production well. The production well is drilled to intersect the fractures generated by the injection well at a depth and proper lateral distance from the injection well. The distance should be chosen to allow the injected water to be sufficiently heated by the surrounding rock as it is circulated to the production well and pumped to the surface. Once at the surface the hot water can be flashed to steam or used to heat a secondary fluid that can be used in a binary cycle process.

In our study area reinjection operations used. The reinjection operation provides the following benefits: (1) keeps the pressure close to initial in the reservoir, (2) prevent the contamination,and (3) enhancing heat recovery by heat mining. Not reinjecting or partly

reinjecting in our country geothermal fields has resulted in pressure losses of reservoirs and in turn productivity losses of the wells, and contamination of most fertile soils of agricultural areas. As more geothermal fields are being operated soon, and actual operations are extended in some fields conducting or no-conducting reinjection operations with their pronounced resulting effects will become most important issue in Turkish geothermal industry in very near future.

Micro Earthquake (MEQ) data can use to assess permeability structures in geothermal fields. Location of MEQs can give some clue about flow injection pattern and determine reservoir boundaries.

The first seismically monitored geothermal area is Salavatlı geothermal area in Turkey. There are three reinjection and four production wells in the study area. This geothermal field is in operation since 1990. There were some problems to follow coloured mixed meterial with the cold water. When it reinjected, it was not observed at the production wells. Since there is a flow injection and re-injection process, microearthquakes are likely to happen in that area. So, nine brodband sesismometers were installed to investigate flow direction of the injected water. Our aim was to find similar microearthquakes with correlation method and to check if they come from same source or location.

Geology of the area is explained in Chapter 2. Correlation function is used to measure how two sequences are correlated or agree with each other or alike one another. In this study GISMO toolbox was used for correlation. The methods are explained in detailed in Chapter 3. In Chapter 4, data collection and data analysis were explained. To look for similiar microearthquakes , data collected from May 2010 to April 2013 was used in the analysis. At first data format was GCF (Guralp Compress Format). Then the data was converted to SAC (Seismic Analysis Code) and SEISAN (The Earthquake Analysis Program). Monthly data was checked for microearthquakes and located with SEISAN then they map with GMT (Generic Mapping Tool). SAC formated data was used for correlation analysis. The correlation coefficient was chosen as 0.9. From this analysis 34 events of similar waveforms were found. VELEST is the best way to minimize the RMS residuals, to fit the best locations to the arrival times and to derive a 1D minimum model for the region. All the microearthquakes were relocated and there was an improvement in the distribution of earthquakes.

In Chapter 5, results of the correlation analysis and relocation of earthquakes with new velocity model were given.

2. GEOLOGICAL STRUCTURE

Salavatlı Geothermal field is situated at middle of the Menderes Metamorphic Massive (MMM) and at the northern half of actual Büyük Menderes Graben. Büyük Menderes Graben has several fields which are suitable for the formation of geothermal resources. Most of these fields have developed at reservoirs with medium enthalpies, with 120-180°C temperatures. These temperatures are being raised through to the asymmetrical axis of the Graben and reach up to 240°C. At different lithological units of metamorphic basement generally devolop the geothermal resorvoirs. A typical characteristic of this Basement is the location of originally deep situated gneisses over the upper units of metamorphic as result of a regional overthrusting.

Our study area, Salavatlı Field is located at east of the Aydın, in northern side of Menderes River. Büyük Menderes Graben is relatively wider and filled by thick young sediments. The alluvial plain is extending about 6.5 km at the north of river bed. Observable graben forming faults occurred only after this margin. There is a series of ENE-WSW or NW-SE gravity faults with falling blocks at south. Holocene aged terraces and Pliocene aged coarse clastics outcrop at stepped blocks which were separated with these faults.

Geological Map of the study area based on Karamanderesi (1994) and revised by Serpen and Aksoy (2010) are being given in Figure 2.1. Main gravity faults divide the field in two parts. At the North part of the field, there are Metemorphic Basement and Miocene sedimentary units and at the South part of the field Pliocene and Quaternary deposits. Miocene units located as filling NW-SE oriented old grabens over the Metamorphic Basement at NW quarter of the area. But, the ENE-WSW oriented young graben system are filled by the Pliocene deposits.

There are two wells which names as AS-1 and AS-2 had been previously drilled by MTA in the area. Their locations were chosen to cut two main young graben faults which were considered as dipping about 40˚ by Karamanderesi (1994). However, there is no sign to conclude that this target has been reached. To discover the area properly, seven more wells have been drilled. Their location were depend on the low resistivity anomalies. They intersect Quaternary to Recent Alluvial deposits, Pliocene and Miocene deposits, gneiss, micaschist, marble, quartzschist succession. The minimum depth to the top of Metamorphic Basement is

316 m and maximum depth is 1280 m, and this surface being deeper to south of the field (Figure 2.2).

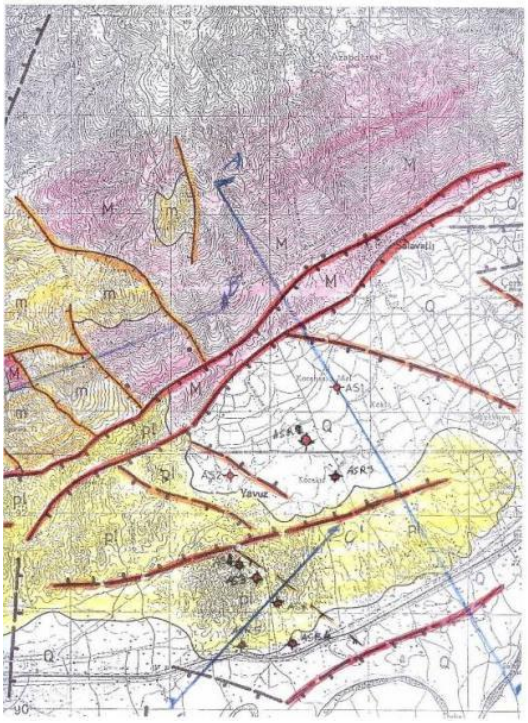

Figure 2.1. Geological Map of the Salavatlı Geothermal Area.

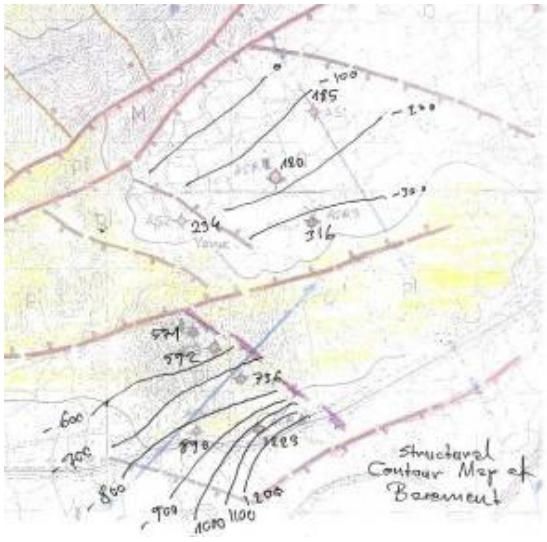

Figure 2.2. Structural contour map of basement.

Geophysical resistivity surveys helped to get reliable results (Şahin, 1985; and SUMET, 2010). Resistivity level maps show the distribution of large low resistivity anomalies in this area. These zones cover nearly 15 sq.km area. Areas with resistivities lower than 7 and 5 Ohmm's cover about 10 sq.km area, too. Very low resistivity area located

especially at the hills between Yavuz Village and Menderes Plain and goes down to at least 1000-1200 m depths. This area is extending through to north of Köşk from Yavuz. A subsurface structural geological map based on the depth to resistive basement information gathered by last resistivity survey is being shown in Figure 2.3. This map also exposes the covered old Miocene gravity faults which can also be observed in the NW, outside of the field in northern neighboring hills. This structural pattern is being considered as important for the interpretation of reinjection and seismic monitoring studies.

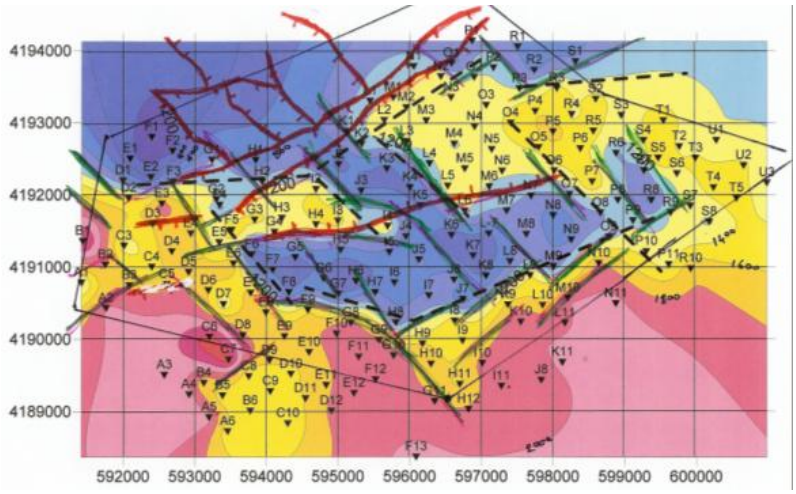

Figure 2.3. Structural geology map according to the resistive basement depths.

Old Miocene and recent graben forming fault systems provide channels for the infiltration of surface waters considerably deep levels and contact with high temperature rock medium. The recharge region must be the northern slopes where the metamorphic basement outcropped. Heated water already finds ascending channels especially along intersecting zones of different fault sets. The main geothermal reservoir is situated in the Metamorphic Basement. Temperature logs of the completed wells and typical low resistivity zones are identified in this Basement. Productive zones at drilled wells are generally encountered in marbles or calcschists. But, some other limited permeability zones may also be encountered in gneiss or quartz rich micaschists. Some large loss of circulation fluids have occurred when the main fault zones had been intersected.

3. METHODOLOGY

Correlation function is used to measure how two sequences are correlated or agree with each other or alike one another. Since, waveforms of microearthquakes were used, correlation has a high importance in this study. Similarity between waveforms was measured by two programs: Correlation macro written in Seismic Analysis Code (SAC) and GISMO (correlation toolbox). Finding and making earthquake clusters is rather easy with correlation. In this chapter, correlation types are defined. Also how GISMO program works is explained.

Correlation is integral of the product of two series with one shifted relative to other or as the average product of the two sequences with one shifted.

$$\text{Corr (g,h)} = \int_{-\infty}^{\infty} g\,(t+\tau)h(\tau)d\tau \qquad (3.1)$$

Corr (g,h) $\leftrightarrow G(f).H*(f)$ called correlation theorem. If g and h are real functions H*(f)= H(-f), here * denotes complex conjugate.

Correlation plays a central part in the study of time series. There are two types of correlation: Autocorrelation and Cross-Correlation.

3.1. Autocorrelation

The cross-correlation of a signal with itself is called autocorrelation. It is the similarity between observations as a function of the time lag between them. It helps to find repeating patterns, such as the presence of a periodic signal concealed by noise, or to identify the missing fundamental frequency in a signal implied by its harmonic frequencies. It is commonly used in signal processing for analyzing functions or series of values, such as time domain signals.

The correlation between values of the process at different times, as a function of the two times or of the time lag are described by the autocorrelation of a random process describes. Let X be some repeatable process, and i be some point in time after the start of that process. (i could be an integer for a discrete-time process or a real number for a continuous-time process.) Then X_i is the value produced by a given run of the process at time i. Suppose that the process is further known to have defined values for mean μ_i and variance σ_i^2 for all times i. Then the definition of the autocorrelation between times s and t is

$$R(s,t) = \frac{E\,[(X_t - \mu_t)(X_s - \mu_s)]}{\sigma_t \sigma_s} \tag{3.2}$$

where "E" is the expected value operator. However, this expression is not well-defined for all time series or processes, because the variance may be zero (for a constant process) or infinite. If the function R is well-defined, its value must lie in the range [−1, 1]. 1 represents excellent correlation and −1 excellent anti-correlation.

If X_t is a second-order stationary process then the mean μ and the variance σ^2 are time-independent, and more than that the autocorrelation depends only on the lag between t and s while the correlation depends only on the time-distance between the pair of values but not on their position in time. That also implies that the autocorrelation can be expressed as a function of the time-lag, and that this would be an even function of the lag $\tau = s - t$. This gives the more familiar form

$$R(\tau) = \frac{\mathrm{E}\,[(X_t - \mu)(X_{t+\tau} - \mu)]}{\sigma^2} \tag{3.3}$$

and the fact that this is an even function can be stated as

$$R(\tau) = R(-\tau) \tag{3.4}$$

It is common practice in some disciplines, other than statistics and time series analysis, to drop the normalization by σ^2 and use the term "autocorrelation" interchangeably with "autocovariance". However, the normalization is important both because the interpretation of the autocorrelation as a correlation provides a scale-free measure of the strength of statistical dependence, and because the normalization has an effect on the statistical properties of the estimated autocorrelations.

In signal processing, the above definition is often used without the normalization, that is, without subtracting the mean and dividing by the variance. When the autocorrelation function is normalized by mean and variance, it is sometimes referred to as the autocorrelation coefficient (Dunn, 2005).

3.2. Cross Correlation

Cross-correlation is a measure of similarity of two waveforms as a function of a time-lag applied to one of them. Cross-correlation is also known as a sliding dot product or sliding inner-product. It helps to search a long-signal for a shorter, known feature.

For continuous functions, f and g, the cross-correlation is defined as:

$$(f \star g)(t) \stackrel{\text{def}}{=} \int_{-\infty}^{\infty} f^*(\tau) g(t+\tau) d\tau \tag{3.5}$$

Similarly, for discrete functions, the cross-correlation is defined as:

$$(f \star g)[n] \stackrel{\text{def}}{=} \int_{m=-\infty}^{\infty} f^*[m]\, g[n+m] \tag{3.6}$$

The cross-correlation is similar to the convolution of two functions.

In an autocorrelation, which is the cross-correlation of a signal with itself, there will always be a peak at a lag of zero unless the signal is a trivial zero signal.

For example, take two real valued functions **f** and **g** differing only by an unknown shift along the x-axis. The cross-correlation can use to find how much **g** must be shifted along the x-axis to make it identical to **f**. The **g** function is slided along the x-axis by the formula, calculating the integral of their product at each position. When the functions match, the value of **(f * g)** is maximized. This is because when peaks (positive areas) are aligned, they make a large contribution to the integral. Similarly, when troughs (negative areas) align, they also make a positive contribution to the integral because the product of two negative numbers is positive.

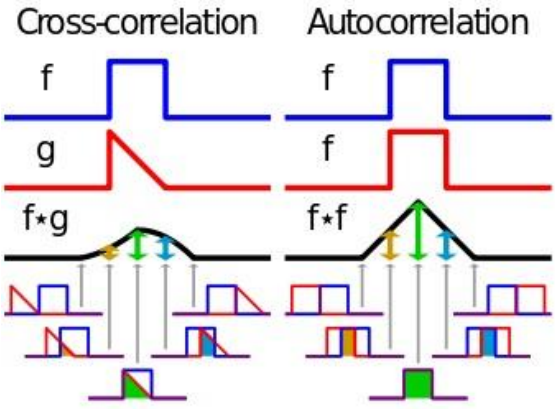

Figure 3.1. Comparision cross-correlation and autocorrelation.

3.3. GISMO (GI Seismology and MATLAB Objects)

The GISMO software is a collection of Matlab toolboxes for seismic waveform analysis built on a common platform (Reyes and West, 2011). The core products include the waveform toolbox and correlation toolbox.

GISMO software uses waveforms for correlation rather than travel times. All waveforms have to be the same duration. Ten seconds duration data were used for GISMO run. It correlates waveforms by using GISMO routines. When all the waveforms were put in program, their raw form, similarity matrix, maximum correlation coefficient, lag matrix, realign traces, hierarchical cluster tree, event clusters, interferogram of clusters's waveform, main clusters's waveforms, cluster's data interval were given as the output of the program.

3.3.1. The Waveform Toolbox

The waveform object allows to work all kind of form from any resources and to make basic waveform research quick and easy. It has many features. Users could use any data stream, make mathematical functions such as adding, extraction, division, multiplication etc., fitler, crop, subset, stack, normalize, taper etc., make statics, waveform operations, use countles waveforms, plot the waveforms, object architecture provides a stable base for writing more complex programs.

3.3.2. The Correlation Toolbox

This toolbox provides an environment for analyzing waveforms with a suite of related cross-correlation techniques based on a common data object. It is built on the waveform toolbox. The overarching goal of the toolbox is to provide a set of functions for performing routine manipulations on a large set of waveforms (tens to thousands) which may bare some similarity to each other - cross correlation, stacking, eventing, plotting, interferometry etc. To load SAC format data into the correlation toolbox, a cshell program was used. With correlation toolbox, user's use commands and could crop and filter traces, cross correlate waveforms, find similarity matrix, maximum correlation coefficient, lag matrix, realign traces, find hierarchical cluster tree, make event clusters, interferogram of clusters's waveform, find residuel waveform, plot main clusters's waveforms, main cluster's data interval and overlay traces.

4. DATA ACQUISITION AND PROCESSING

4.1. Installation of Seismic Stations

In this thesis, the data were provided by nine broadband stations which were installed in Salavatlı Jeotermal Area, Aydın. Seismic network covers an area of 20 km^2. The data were collected between June, 2010 and April 2013.

At the begining, there were seven broadband stations. They were installed in May, 2010. Pits were dug for the seismometers through loose surface cover. There was no outcroping rock in the study area. Seismometers were buried to a depth of 1m at the first phase. Moreover, location of three stations were changed in August 2010 due to high noise levels. The aim of station location change was to monitore movement of reinjected water with high quality. During the second phase of the installation of seismometers of the three sites and central station were buried to a depth of 1.5 m in order to reduce high noise level. There was a big improvement in the signal to noise ratio and it was about ten fold.

The number of stations increased to 9 by adding two new stations to the network in 15 October 2010 (Figure 4.1). There were two main reason of adding stations. The first reason was to cover study area properly. The second reason was to increase quality of the earthquake location. Table 4.1 shows all changes done in the network which were done during the study.

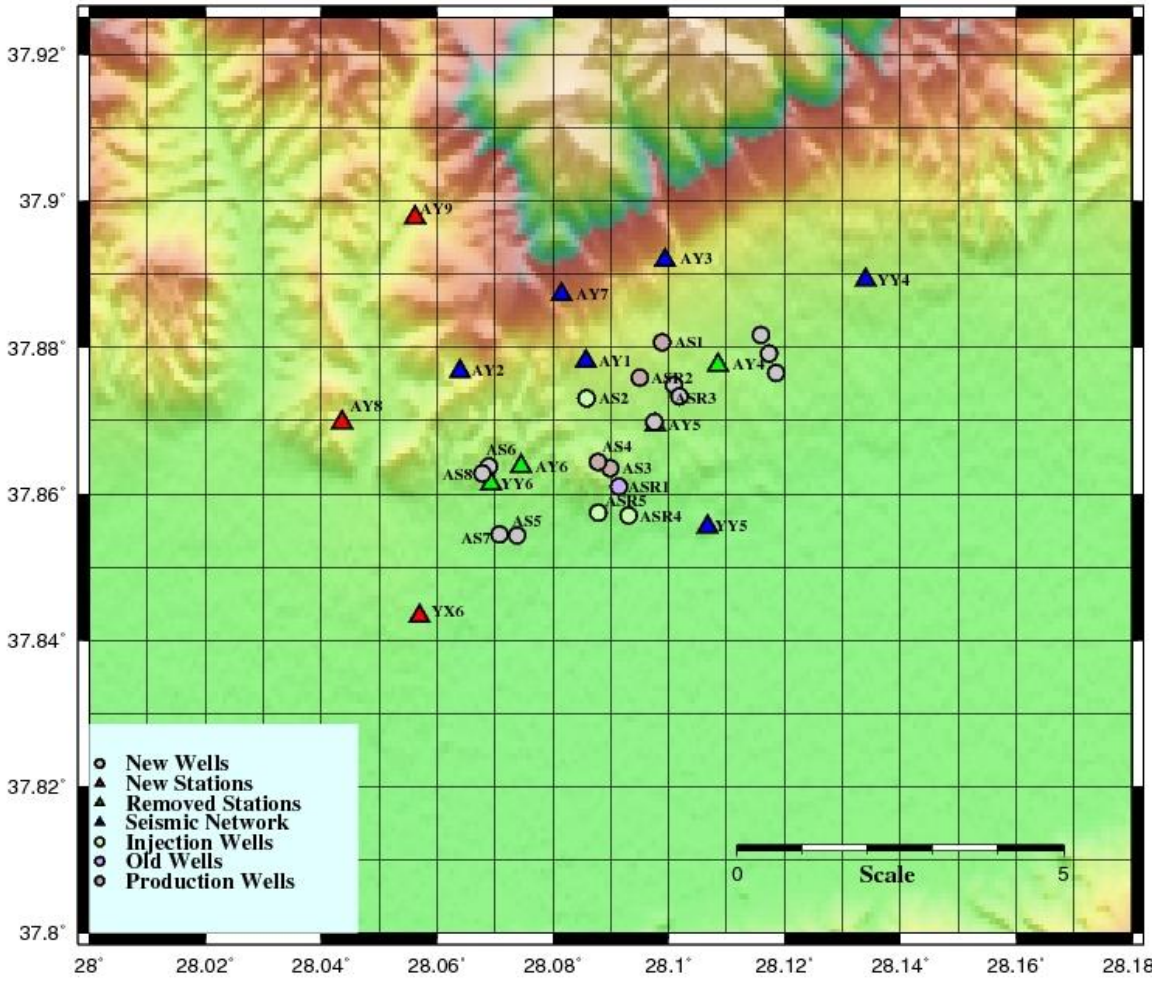

Figure 4.1. Location of stations and wells.

Seismometer were placed far away from the main roads and factories, and if possible as close as possible to outcropping rocks in order to avoid noisy conditions and high attenuation associated with tuffs, soils, sediments and other soft surface deposits. A flat base was constructed with cement for the insturment to be mounted upon. Figure 4.2 shows improvement of the signal to noise ratio before and after this process. The yellow line represents 20th June 2010 and the red lines represents 18th November 2011.

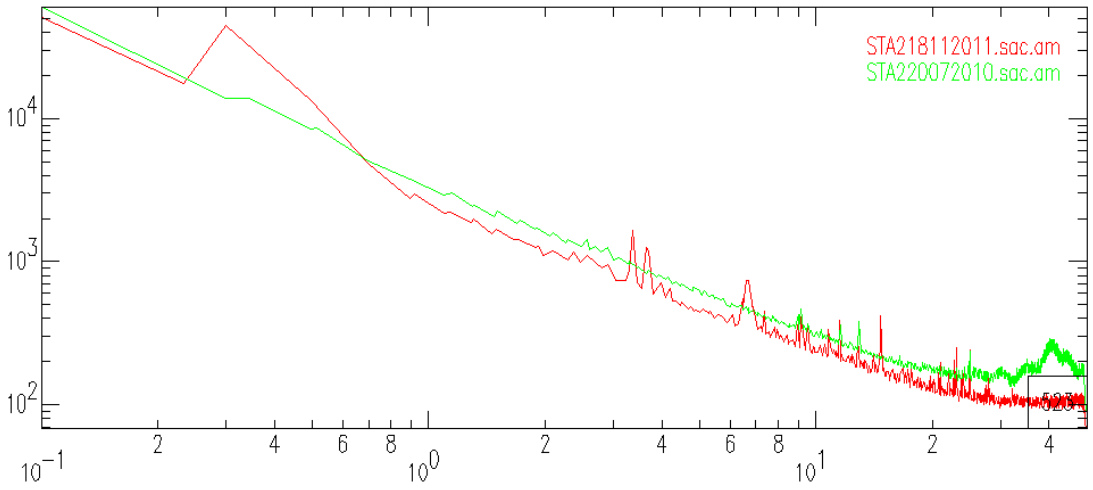

Figure 4.2. Improvement of the signal/noise ratio .

The seismometers which were used in this study, are designed by GÜRALP Systems and their model is CMG-6TD. The model is an ultra-lightweight three component digital output seismometer. The recording was continuous with a sample rate of 100 samples/s. Each seismic station consisted of a hard disk of 4 Gb memory , a GPS receiver, solar panel and a 12V battery (Figure 4.4).

Figure 4.4. CMG-6TD with supplied GPS and installation site of a station.

Table 4.1. Information about stations and their installation dates.

STATION NAME	LATITUDE	LONGTITUDE	START TIME AND CHANGES
AYD10	37˚ 52’ 41.2’’	28˚ 05’ 08.6’’	25.05.201 A10 (6457-4MB)
AYD20	37˚ 52’ 36.4’’	28˚ 03’ 50.4’’	26.05.2010 A20 (6454-2MB) 17.11.2011 A20 (6443-4MB)
AYD30	37˚ 53’ 36.4’’	28˚ 05’ 58.1’’	A30 (6454-4MB) 24.05.2010
AYD40 AYD41 AYD42	37˚ 52’ 34.6’’ 37˚ 53’ 21.4’’ 37˚ 53’ 10.0’’	28˚ 06’ 38.8’’ 28˚ 08’ 06.4’’ 28˚ 07’ 23.7’’	A40 (6444-2MB) 26.05.2010 A41 (6443-2MB) 17.08.2010 A42(6456-4MB) 16.10.2011
AYD50 AYD51	37˚ 52’ 10.1’’ 37˚ 51’ 19.9’’	28˚ 05’ 58.7’’ 28˚ 06’ 24.2’’	A50 (6419-4MB) 25.05.2010 A51 (6419-4MB) 18.08.2010
AYD60 AYD61 AYD62	37˚ 51’ 49.7’’ 37˚ 51’ 41.9’’ 37˚ 50’ 35.8’’	28˚ 04’ 28.4’’ 28˚ 04’ 04.6’’ 28˚ 03’ 25.2’’	A60 (6716-4MB) 25.05.2010 A61 (6456-2MB) 18.08.2010 A62 (6373-8MB) 24.08.2011
AYD70	37˚ 53’ 13.8’’	28˚ 04’ 53.6’’	A70 (6764-4MB) 24.05.2010
AYD80 AYD08	37˚ 52’ 11.2’’	28˚ 02’ 37.1’’	A80 (6390-2MB) 16.10.2010 A08 (6429-4MB) 28.12.2011
AYD90	37˚ 53’ 52.0’’	28˚ 03’ 22.5’’	A90 (6444-2MB) 15.10.2010 A90 (6390-4MB) 28.02.2012

4.2. Data Preparation

Recorded data were collected from the stations by transferring the data to an external hard disk, later data transferred to a laptop computer and they were displayed in the field in order to check the instrument state of health. Every one hour data was written to a file and was extracted from external hard disk to PC with GCF format. Then GCF formatted data was converted to SAC (Seismic Analysis Code) with the help of a cshell program. After that, the data which were in SAC format, were converted to SEISAN format. There are few commands to convert SAC data to SEISAN format. After all these process, the data became ready to read in SEISAN program.

4.3. Finding Microearthquakes and Locating Them

The durations of the microearthquakes are all under 10 seconds and their magnitudes are near to 0.0. Given the low signal to noise ratio, it needs very careful examination of the records to find microearthquakes. Because of these reasons, every one hour data was displayed and checked with ten minutes periods with the help of SEISAN program. The vertical component data of all the stations were displayed at the same time to look for microearthquakes.

4.3.1. Construction of Initial Velocity Model

Crustal velocity model was constructed to locate the events. In order to determine crustal velocity model, we examined various geophysical data. There are well log data for all the wells in the study area. Each geological unit with depth is given up to the basement rock. The Depth of the basement varies among wells. It becomes deeper in the south towards the Menderes River. For crustal velocity model, we needed also P and S wave velocity information in each layer. Turkish Petroleum Company had done seismic reflection study in the region in October 2000 (Figure 4.5). There are 2 E-W and 4 N-S profiles crossing the study area. One of the E-W profile was interpreted by Ciftci *et al*. (2010). In addition to TPAO seismic reflection study, MTA had also conducted a seismic reflection survey between Köşk and Sultanhisar towns. This survey also covers the study area. Information obtained from these studies with the well log data were used to estimate velocity of the layers. Velocity

information obtained from the reflection surveys was enough only to get top part of the velocity model up to 2 – 3 km depth. Below this depth, velocity structure are derived from three different earthquake data analysis studies. They are surface wave dispersion analysis (Tezel *et al*., 2007), receiver function analysis (Tezel *et al*., 2010) and velocity model determined from the aftershocks of Denizli earthquakes near to the study area by applying the VELEST software (Özalaybey *et al*., 2010). The constructed velocity model obtained is given in Table 4.2.

Table 4.2. Velocity model used in location of the earthquakes.

Depth (km)	P wave velocity (km/s)	S wave velocity (km/s)	Vp / Vs ratio
0.00	1.60	0.90	1.78
0.35	2.10	1.20	1.75
0.80	2.60	1.50	1.73
1.40	3.48	2.60	1.84
2.40	5.20	2.90	1.79
4.00	5.70	3.30	1.73
6.00	6.00	3.50	1.71
13.00	6.20	3.42	1.81
19.00	6.80	3.90	1.74
29.50	8.00	4.60	1.74

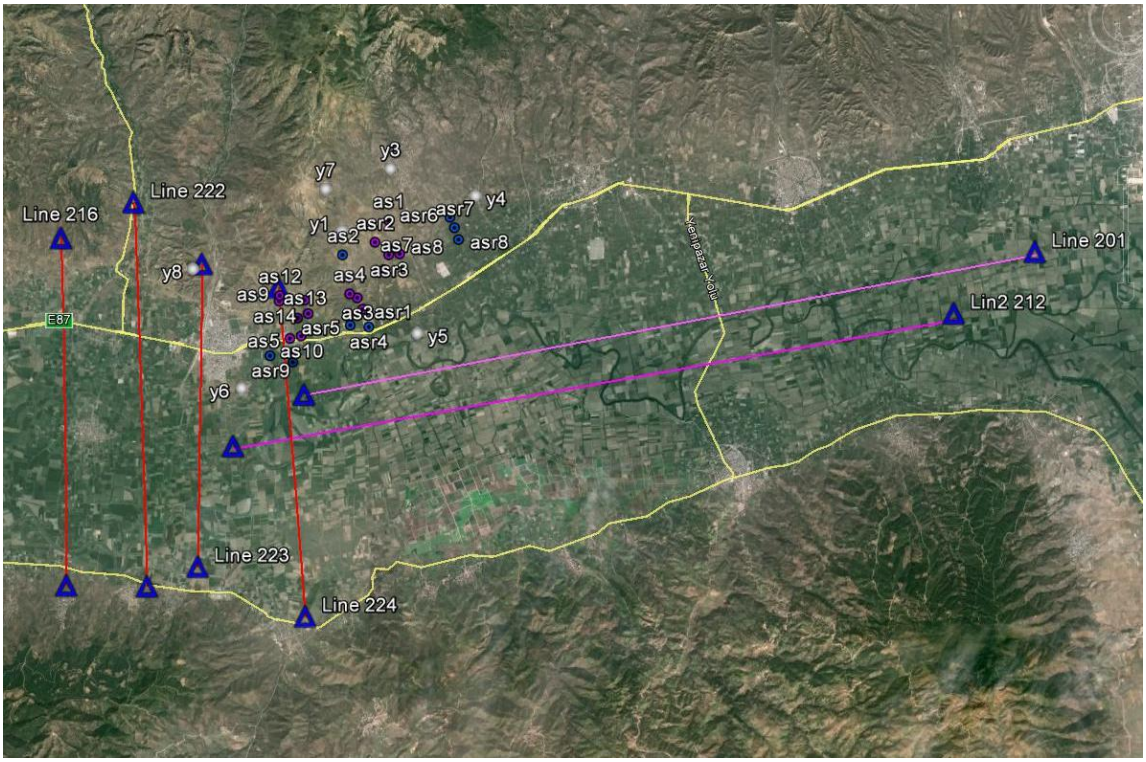

Figure 4.5. Location of the TPAO seismic reflection profiles, wells(purple circles) and seismic stations(white circles).

4.3.2. Phase Picking and Location of Earthquakes

Data at some stations were not clear enough to read P and S arrival times. Several samples from microeathquakes were selected and their Fourier Spectrum calculated to determine signal band range. From this analysis, a band of frequency was determined to filter the data. So, 2-10 Hz band pass filter was used to eliminate background noise. After finding microearthquakes, picking of the P and S arrival times were done using SEISAN. After picking arrival times microearthquakes were located with help of HYPO71 software using velocity model given in Section 4.3.1. Residuals of readings were checked, if they were greater than a predefined value (in this study, our value was 0.2s), the phase picking was repeated.

4.4. Correlation Analysis

In this study, the main goal was to find clusters by checking the microearthquake waveforms if they are coming from the same source or the same fault. First part of this study was mainly based on a program GISMO.

First of all, SAC data format were used for GISMO. As being said before, there are 9 broadband stations and the data quality strongly depended on their locations. Therefore, the data from the two best stations were used for the first step. One of these stations is AYD70 and the other one is AYD20. These two stations were chosen for their high quality data and also their high signal to noise ratio. There were over 977 microearthquakes recorded during three years, but for AYD70, there were 815 waveforms. For AYD20, there were 845 waveforms. The difference between the number of waveforms at two stations are due to data quality from the related station.

4.4.1. Making Clusters with GISMO

By looking at the output file from HYPO71 program, all the information about every station were determined. For these two stations, AYD70 and AYD20, all microearthquakes were found in their vertical component. After this, there are some steps to put the data into GISMO which are related to each other. They are :

1. All the waveforms were put into a directory.

2. Every waveform were checked in terms of their quality in SAC.

3.Their headers were checked so that they can be overwritten.

4. The header value LOVROK were set from false to true.

5. P wave arrivals were marked.

6. The waveforms were cut again before one second and after nine second from P wave arrival time.

7. Filename convention were set to microearthquakes occurance time. For example, if the waveform belongs to an earthquake which is occured in 4th of June, 2010 at 09.21.32

o'clock, then its name became 04062010092132.sac. This helps to find earthquakes easily after correlation results.

8. They were normalized by SAC to redoubled for ensuring the success of correlation.

9. With a small cshell program, all the data were loaded to GISMO toolbox.

After all these steps, the data are ready for correlation. There are some commands to make clusters from waveforms. For example it is up to user to determine the correlation coefficient. If it is chosen as 0.5, there will be clusters in which the waveforms similarity is equal to 0.5 or greater. In this study, the correlation coefficient was chosen as 0.9. The GISMO toolbox does not give every clusters at the first time. User has to eliminate waveforms before every run.

4.5. Location Accuracy of The Seismic Network

The accuracy of earthquake locations depends on the distribution of the stations, reading the phase arrival times accurately to each stations and how well the velocity structure represents the area. Today, the accurate timing in each stations can be ensured with GPS receivers, but we may not have a correct velocity structure. This requires a seismic refraction study or dense seismic seismic network. So, we can only improve the location by resonable distribution of the stations. This can be done by following,

1. An RMS value of noise in the frequency band of interest should be within an acceptable S/N level

2. Optimum distribution of the station locations depending on the activity in the area

3. Frequency response of the instruments should preferentially be same for all stations

4. P and S arrival times should be picked as accurate as possible.

5. P and S velocitiy model should be known with certain accuracy.

A software called LOK (Zivcic and Ravnik, 2002) was used to estimate epicenter and hypocenter location accuracy. The area is divided into squares in terms of longitude and latitude. A hypocenter error elipsoid is constructed for every grid point. The largest semi-axis of the error ellipse is named the hypocenter determination error, the largest of the projections of the ellipsoid semi-axis on the horizontal plane is named the epicenter determination error.

An area of 3.2 km x 6.5 km was modelled. The network consists of 9 stations and an earthquake of ML = 1.0 was assumed to occur at 3 km depth. The software can run for different hypocenter depths and magnitudes. Epicenter and hypocenter error calculations are shown in figures 1 and 2. Results are plotted using GMT software (Smith and Wessel, 2002). If the number of stations that recorded the event less than 4, output is a large number and this event discarded from the solution.

Errors in epicenters are within 0.8 km inside the network. It gets greater outside the network. This error can be reduced by using an accurate velocity model. Some improvement can be done first by obtainig a homogeneous 1-D velocity model by VELEST program. VELEST program also gives station corrections. By using new minimum 1-D velocity model and station corrections epicenters can be improved further. We see the similar results for the hypocenter locations. It is in the range of 0.6 - 1.0 km inside the network and gets larger outside the network. But error in hypocenter depths are smaller copared to the epicenter location errors inside and outside of the network. It starts getting larger jus after the network in the epicenter locations.

This test can be carried out for different hypocenter depths and magnitudes. We selected average hypocenter depth and magnitude in the calculations.

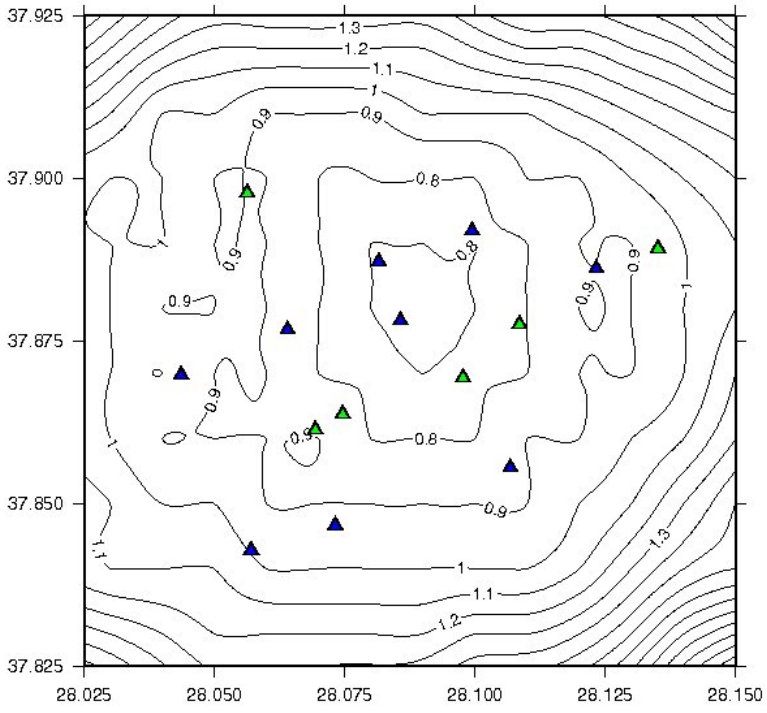

Figure 4.6. Error in epicenter location of the eathquakes in kms.

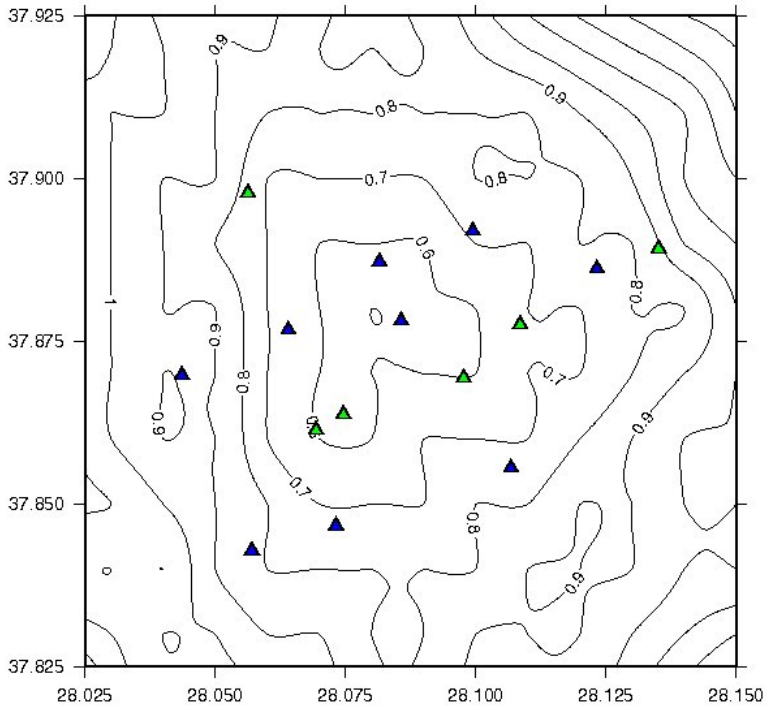

Figure 4.7. Location error of hypocenters in kms at the study area.

4.6. VELEST

VELEST (Kissling 1988; Kissling *et al*. 1994) computer program was used to obtain 1-D average velocity model for a region. Kissling *et al*. (1994) presented the method to calculate a 1-D model that may serve as reference model for 3-D seismic tomography and for routine earthquake location. Such 1-D velocity models with corresponding station corrections are the result of a simultaneous inversion which also gives the high quality hypocentral parameters.

Using an appropriate initial reference model, data are inverted to obtain station corrections and relocated hypocenter locations. After this procedure, we also obtain the minimum 1-D velocity model. Before running VELEST, geophysical studies in the region were examined to choose a priori initial velocity model. An initial model for VELEST runs was constructed from the model given in Section 4.3.1 (Table 4.2). Outputs of these runs were studied carefully in terms of average azimuthal gap values and changes compared with station delays and RMS residual errors to perceive a suitable velocity model for the study region. In conclusion, final velocity model for the target area were determined for the study area using earthquake data which was located with SEISAN.

In order to obtain the best velocity model, VELEST must be run more than one time. Best velocity model can be selected by looking at RMS residuals. If RMS residuals are under 0.1 and do not change after some iteration, which means the best velocity model is found. Also after every run, the program gives station correction for all stations.

At first 977 located events were used to obtain 1D velocity model. After first run, we have to select eartquakes which have best locations. It was done by using select routine in HYPO71 program. The only criteria for doing this is to pick the earthquakes which have azimuthal gap value under 180^0. Then 334 earthquakes were extracted for the analysis. These events are used for further VELEST runs. In every run, 9 iterations were enough to converge the solution. We have chosen the number of iteration where the RMS residual is the same in consecutive iterations. For this study, the best RMS residual was found as 0.0782. Also after every run, station corrections were changed. So, this value should be added to the Staion0 file for HYPO71 runs later.

Table 4.3. Final minimum 1D velocity model.

Velocity	**Depth**
1.742	-5.000
2.139	0.350
2.694	0.800
3.546	1.400
6.155	2.400
6.156	3.400
6.157	4.000
6.158	5.000
6.159	6.000
6.201	9.000
6.250	11.000
6.350	13.000
6.400	15.000
6.450	17.000
6.500	19.000
7.000	21.000
8.000	29.500

Table 4.4. Station corrections.

Station	Corrections
AYD10	-0,12
AYD20	-0,17
AYD30	-0,11
AYD40	-0,15
AYD41	0
AYD42	0
AYD50	-0,24
AYD51	0,18
AYD52	0
AYD60	-0,64
AYD61	0
AYD70	-0,16
AYD80	0
AYD90	0

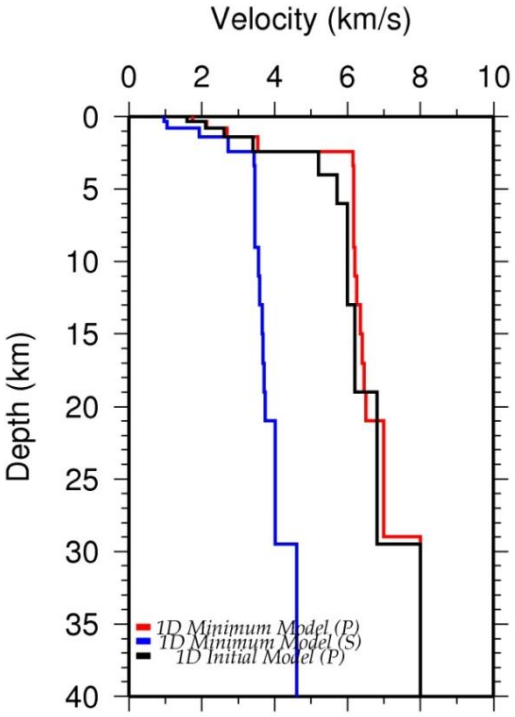

Figure 4.8. Initial and final 1D velocity model for the study area.

After all these process, microearthquakes can be ready to relocate. Results of relocation is given Chapter 5.

5. RESULTS

There were locatable 977 microearthquakes from June 2010 to April 2013 at the Salavatlı microseismic network. We selected 815 of them to find clusters in the study area. As it was given in chapter two, GISMO software was used for the cluster finding process. A correlation criteria was chosen to find similar earthquakes. For correlation criteria, correlation coefficient equals or greater than 0.9 was taken for the minimum similarity.

GISMO software uses waveforms for correlation rather than travel times. All waveforms have to be the same duration. Ten seconds duration data were used for GISMO run. It correlates waveforms by checking their waveforms. When all the waveforms were put in program, their raw form, similarity matrix, maximum correlation coefficient, lag matrix, realign traces, hierarchical cluster tree, event clusters, interferogram of clusters's waveform, main clusters's waveforms, cluster's data interval were given as the output of the program. Although we have 815 micro-earthquake waveforms, we have selected 334 best located events as given in previous chapter. The total number of similar waveforms are 86, which are related to 34 events. Maximum number of waveforms in these event groups are 7 and the minimum number is 2. The remaining waveforms (729) have their unique waveform and could not be possible to match any other waveforms with a given correlation coefficient (0.9). To get similar waveforms, program should be run over and over again. After each process, these waveforms were moved to another directory. This continued until the last waveform left in the process. Total number of event can be increased if we add more waveforms into the data set after getting new data from the field.

At the below, GISMO outputs could be seen when the correlation co-efficient was chosen as 0.8. This coefficient was chosen to demonstrate what if we chosed the correlation coefficient as 0.8.

Altough GISMO lists all the data with "wig" command, this could be useful when users have more than 50 waveforms. When it reaches the maximum, it shows only possible wavefoms and could not plot all of the waveforms because of its limitations. In raw data display, there are no filters, this part only contains untouched data. Figure 5.1 shows maximum number of raw waveforms which were put in GISMO for this study. The X axis of graphic shows relative times for waveforms and it is up to users to choose relative times. But relative times is related to trigger time. Without a trigger time, the correlation object has no

information about how the traces should be aligned. With clean data this may be remedied with the XCORR routine. If possible however, it is better to use one of the CORRELATION uses which include trigger times. In the absence of this information, trigger times are arbitrarily assigned to be one quarter of the time between the trace start and end times which are the relative times for this study. The reason why the left axis not readable is program gives it that way. It is not possible to put readable version of this table since there are more than 50 waveforms.

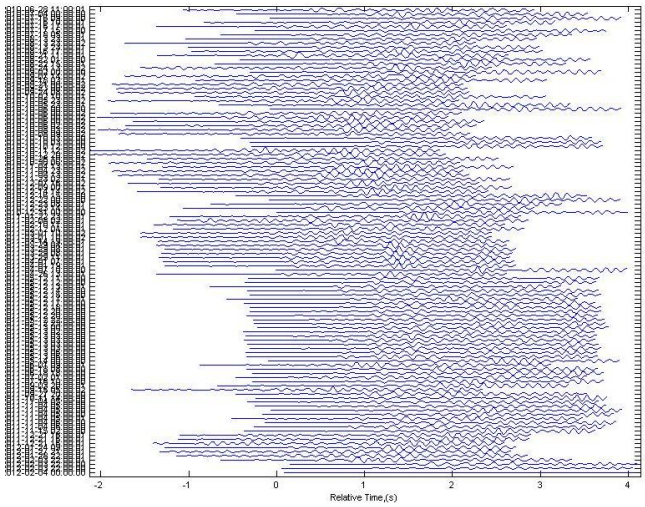

Figure 5.1. Raw form of maximum number of waveforms.

Figure 5.2 shows maximum correlation co-efficient for all waveforms for this study. Red dots show maximum similarity and dark blue color show no similarity between waveforms. Y axis of maximum correlation co-efficient graphic includes event date and X axis shows event number. With this information we could display similar micro-earthquakes.

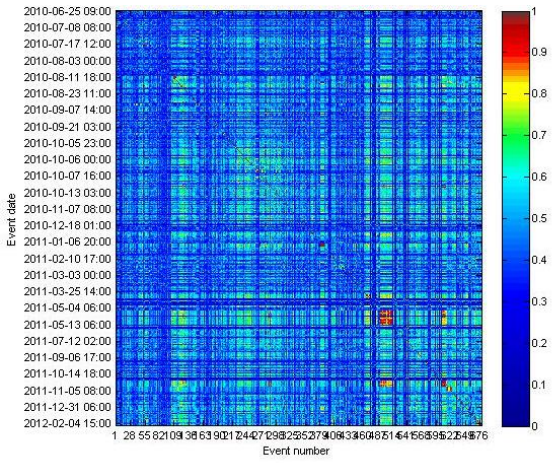

Figure 5.2. Maximum correlation coefficient.

Similar to maximum correalation co-efficient graphic, this graphic shows the matrix of lag times (in seconds) that yeild the maximum correlation between each pair of our traces. Same axis also valid for lag time for maximum correlations. Y axis shows event date and X axis shows event number. Figure 5.3 shows, lag times of the data for maximum correlations.

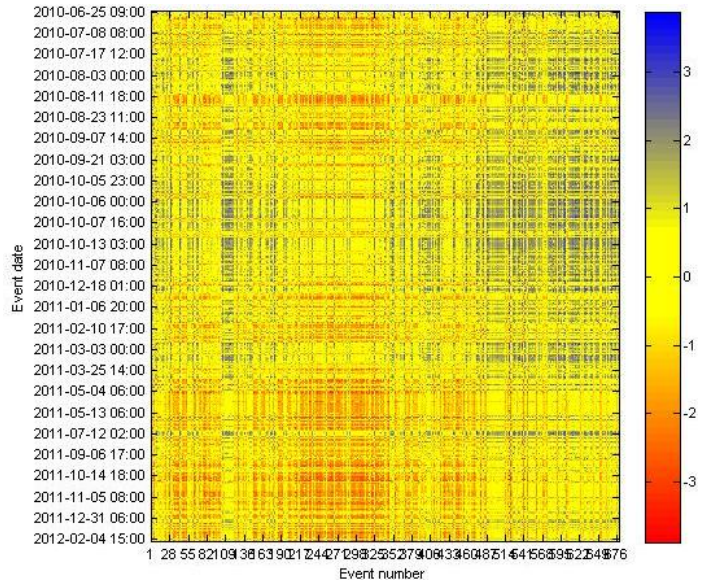

Figure 5.3. Lag time for maximum correlations.

When applying the time corrections in the lag matrix to the trigger times. This will result in highly correlated traces being well aligned. Figure 5.4 shows the realinged waveforms of exist in the waveform data set. As can be seen clearly, all waveforms were alinged by program and red-blue color shows similarity part of the waveforms. The list of waveforms were given by their dates at the Y axis of graphic and relative times were given at the X axis. It is up to users which part of the waveform taken as it was explained above.

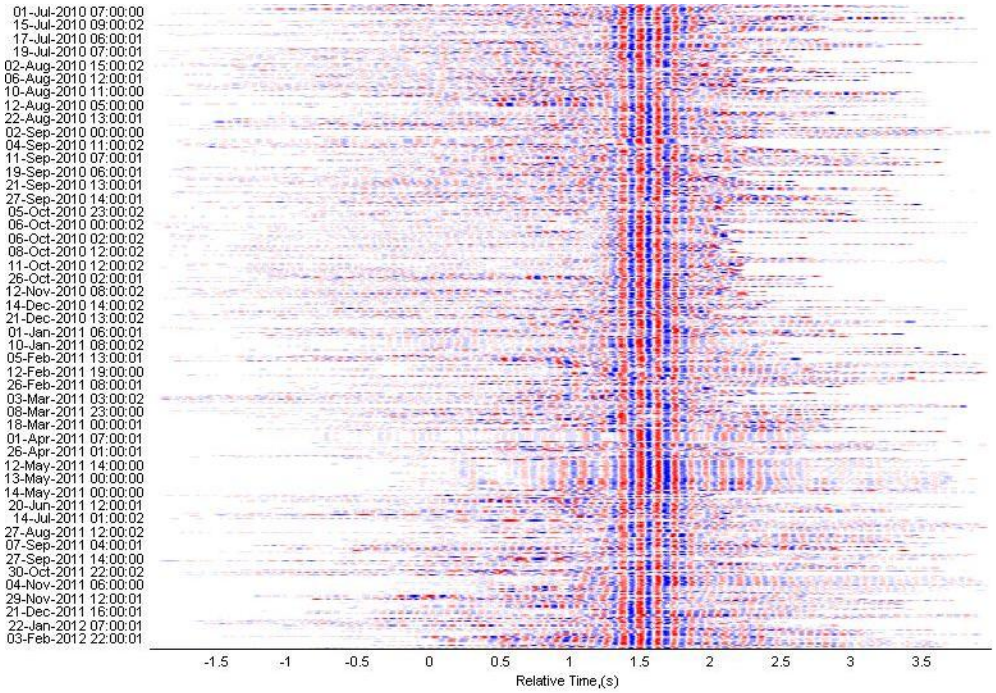

Figure 5.4. Relainged waveforms.

Figure 5.5 shows a hierarchical cluster tree relationship (denrogram) between all waveforms. It reorders traces such that they correspond with the ordering of traces on the cluster tree. Y axis of graphic shows event date and X axis of graphic shows inter cluster correlation co-efficient.

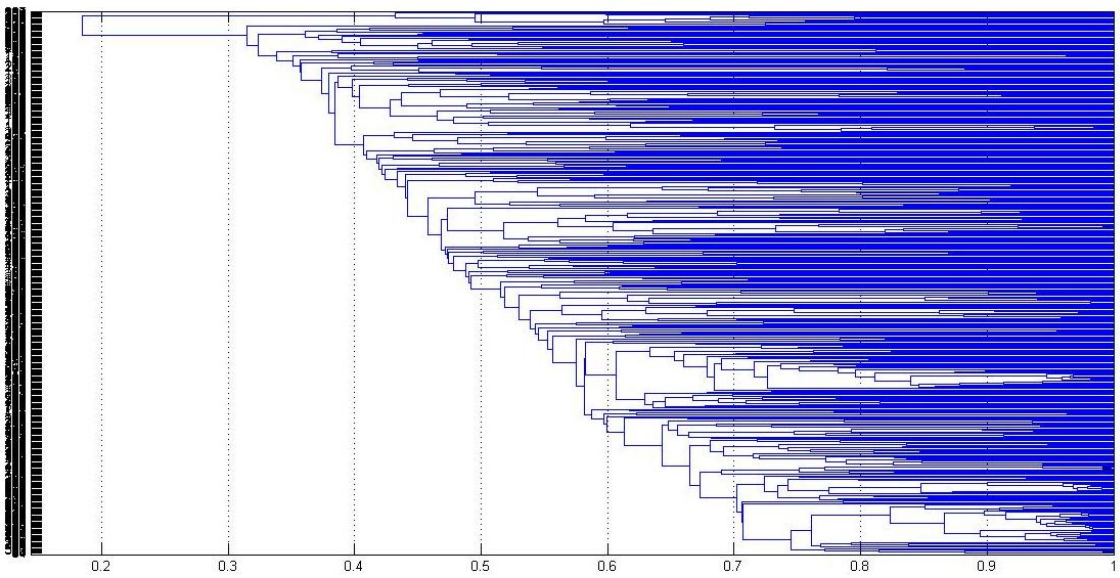

Figure 5.5. Hierarchical cluster tree.

Program trims the cluster tree relationship into discrete clusters of events. It subsets just the events of the largest cluster. Figure 5.6 shows the largest cluster's events which are the events of cluster 1. If users want to find the other clusters's events, they could change the

parameter of that command. By looking this graphic, similarity of the events's waveforms could be seen clearly. Y axis of graphics shows event dates and X axis shows relative times of waveforms.

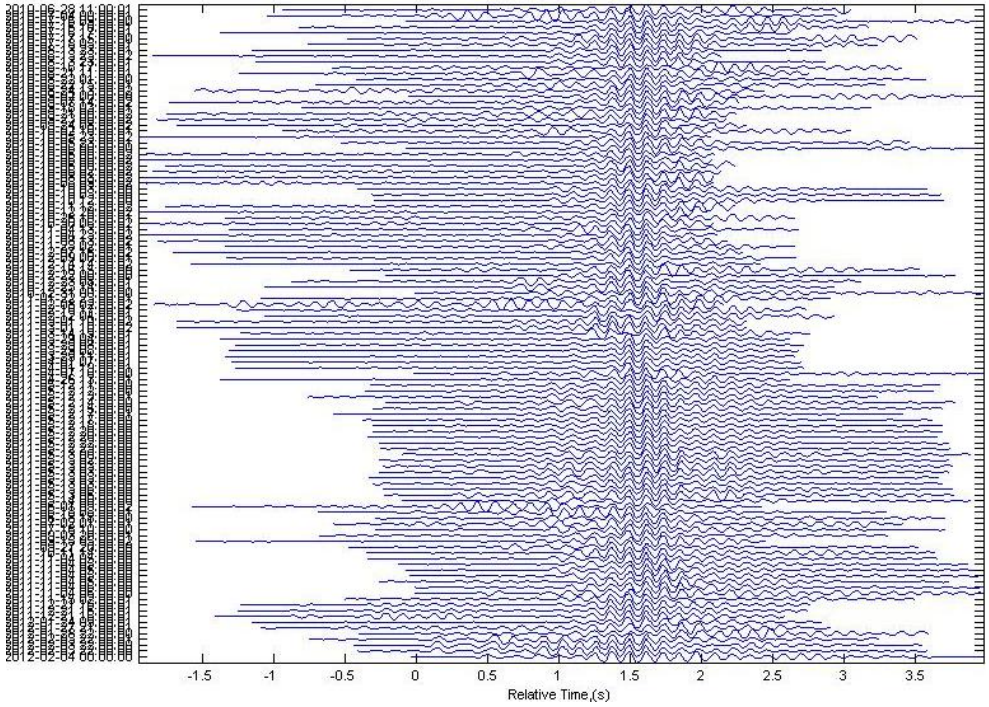

Figure 5.6. Events of largest cluster.

Then GISMO calculates the correlation and lag values on narrow time windows within each trace relative to a master event. By default, the final trace is used as the master event, which in this case is the trace stack. Both the maximum correlations and the lag times can be plotted behind a wiggle trace plot, or they can be exported as matrices which are called Interferogram. Figure 5.7 shows the interfefogram of the first run.

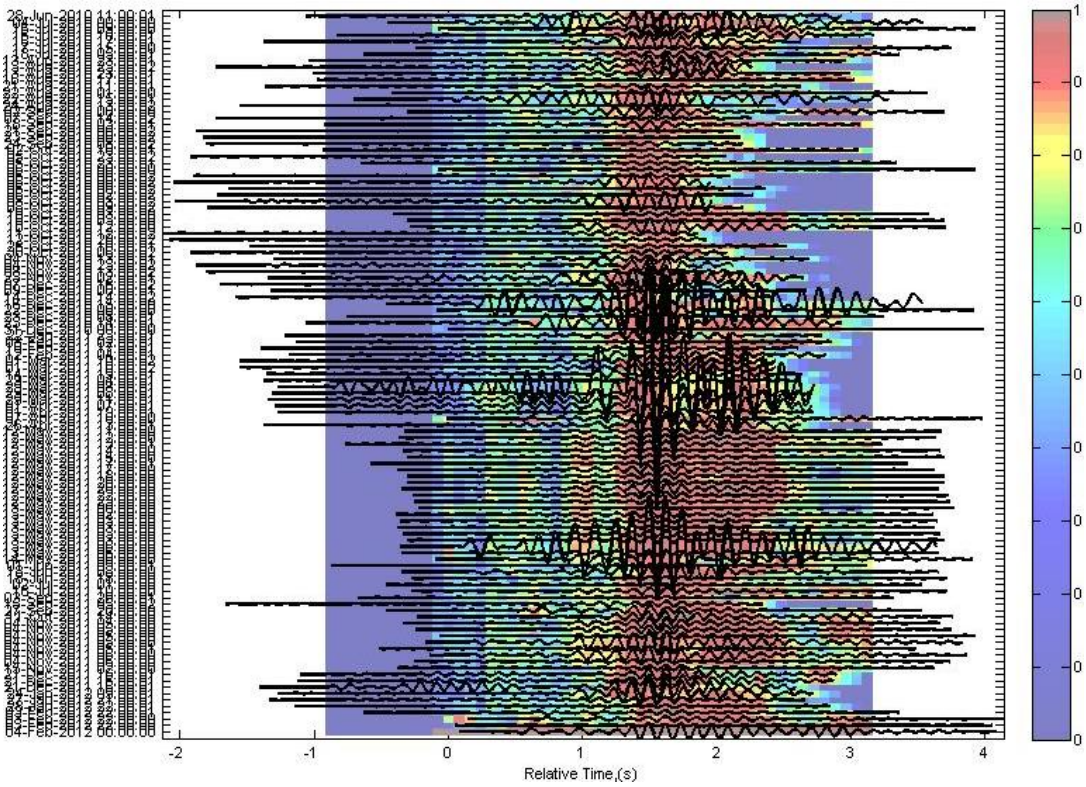

Figure 5.7. Interferogram of the first run.

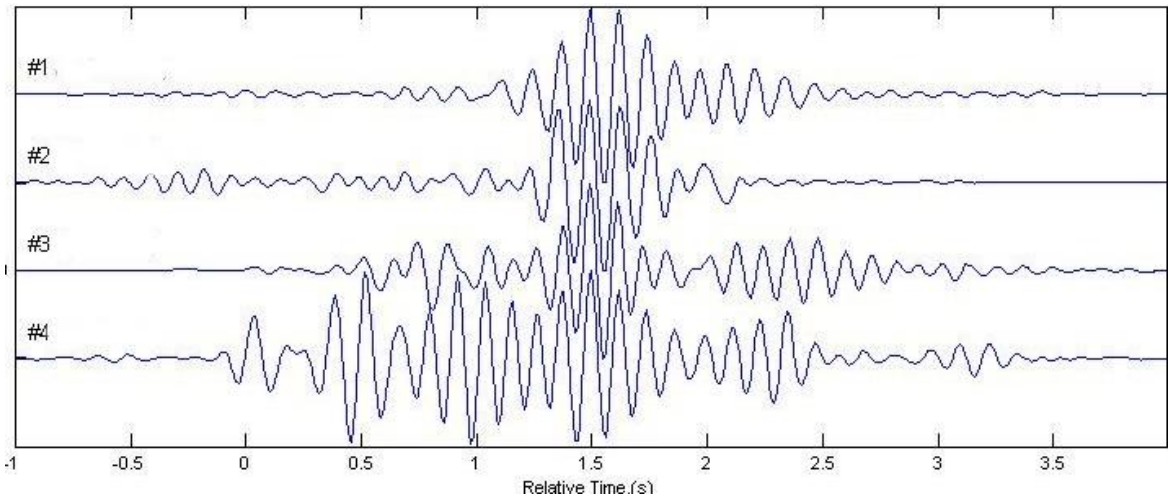

Figure 5.8. Shows master waveforms representing each cluster.

Since the correlation coefficient is 0.8, the program found 4 main waveforms which means 4 clusters. In Figure 5.9. data interval of clusters are shown. The Q values show the quarters of 2010, 2011 and 2012. For example, Q3-10 means the third quarter of 2010. Blue dots show waveforms of clusters. Some times blue dots are overlapping each other and because of this the number of waveforms which were represented by blue dots are less than real number of waveforms.

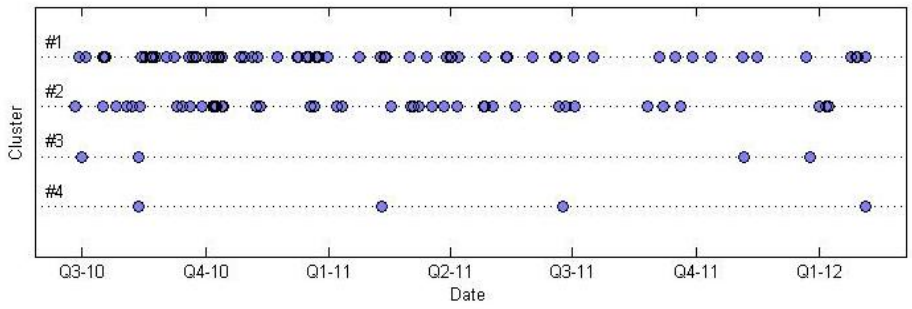

Figure 5.9. Date interval of the main clusters.

Our correlation coefficeint is 0.9. There are 34 event type and 86 waveforms for 0.9 correlation coefficient. The main reason why there is less cluster when we choose the correlation coefficient 0.8 is the clusters contains much more waveforms (about between 5-117) than the correlation coefficient is 0.9. Except from 86 waveforms, the other waveforms could not be classified because of the high rate of correlation coefficient . So some of these waveforms in SAC format were given at the end of the chapter. Since the maximum number of waveforms is 7, correlation matrices and waveforms were given for 4 events. Since the other event have very similar correlation matrices, only the waveforms of them will be given with their location in VELEST results.

As clearly seen in figures, waveforms are nearly identical. When we stack them, they look like as one waveform. The reason why the time axis starts from -2 is that program uses the trigger time of the first quater part of the waveforms (The waveforms have 10 seconds duration) .

5.1. Events of Similar Waveforms

5.1.1. Event Type 1

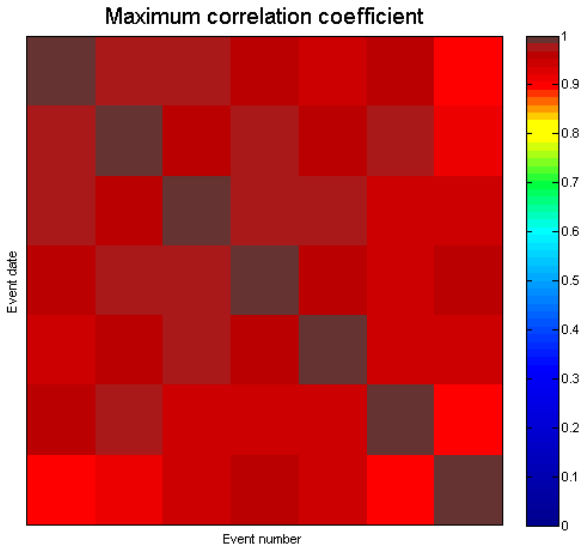

Figure 5.10 Correlation matrice for event 1.

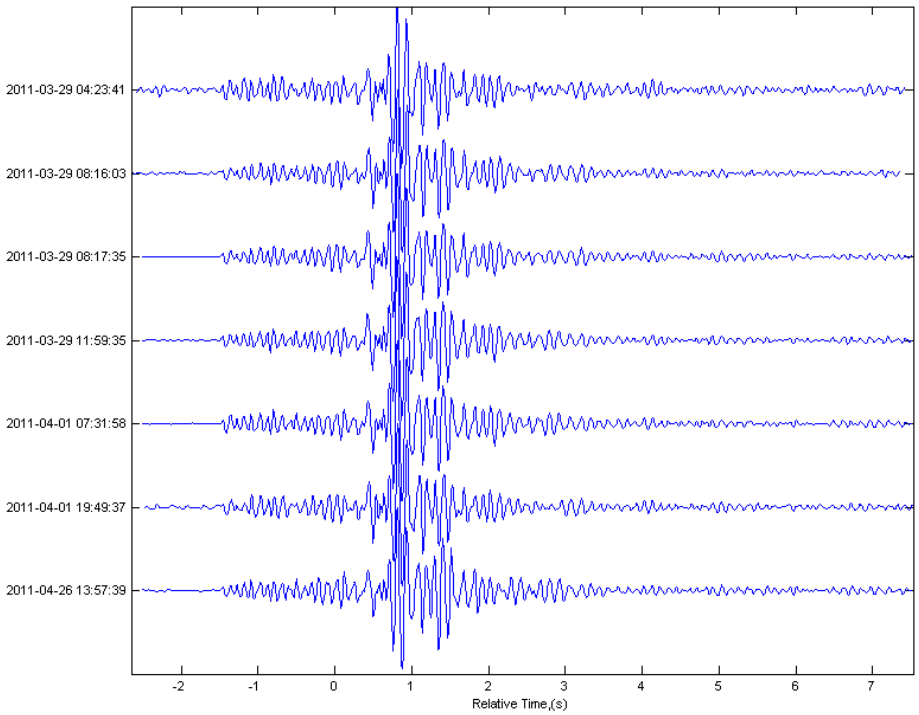

Figure 5.11. Waveforms of event 1.

Figure 5.11 shows the extracted waveforms for Event Type 1 with their dates along its vertical axis. The darker red squares along the diagonal of the plot shows the auto-correlation while the other red squares are cross correlation of the waveforms with one another. These

waveforms stack can be used as a reliable master event to look for its similar ones for the new data coming from the study area. It can also be used to get reliable phase picking for the events with low signal to noise ratios.

Similar explanations are valid for event type 2, 3, 4. From Figure 5.13 to 5.20 shows their correlation matrices and waveforms.

5.1.2. Event Type 2

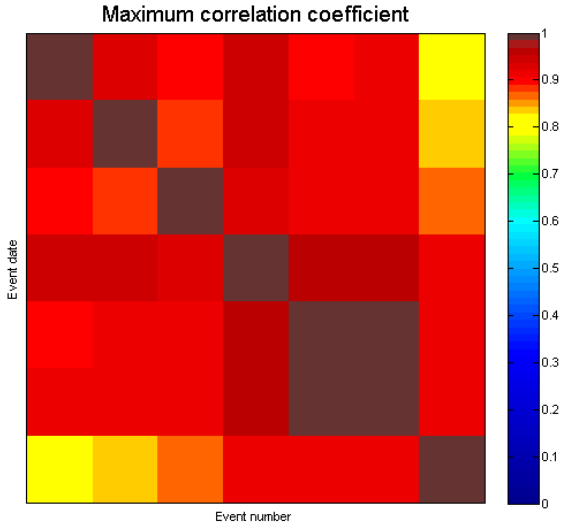

Figure 5.12. Correlation matrice of event 2.

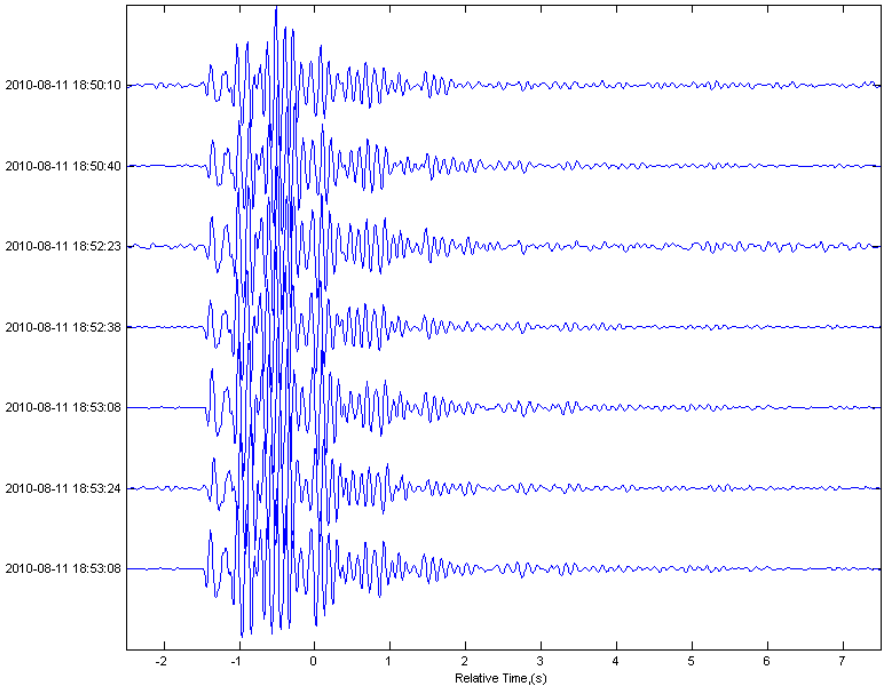

Figure 5.13. Waveforms of event 2.

5.1.3. Event Type 3

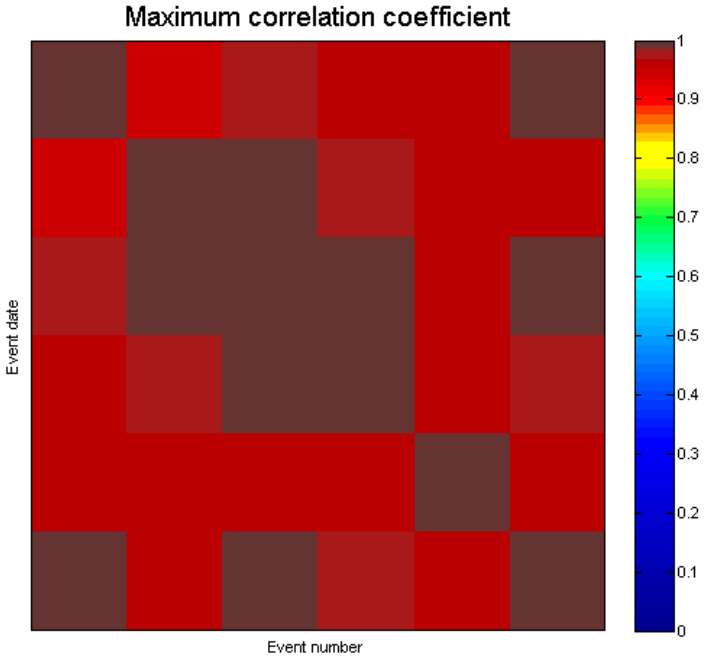

Figure 5.14. Correlation matrice of event 3.

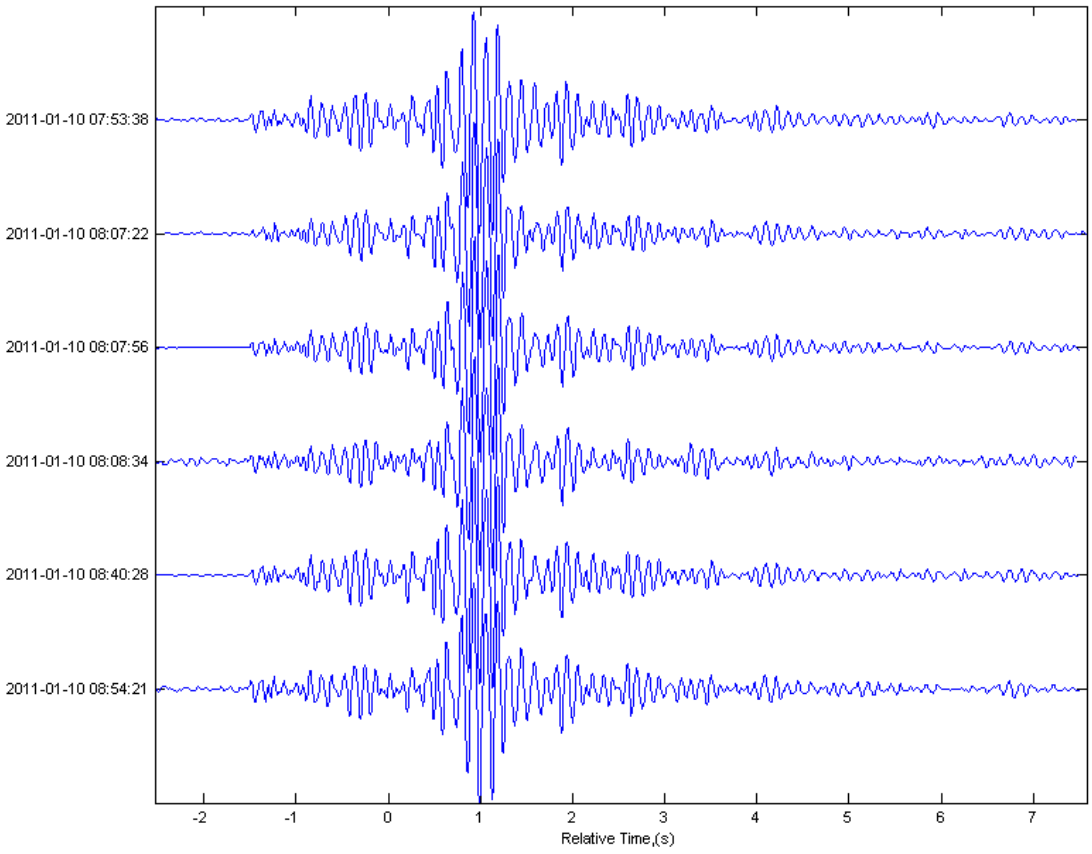

Figure 5.15. Waveforms of event 3.

5.1.4. Event Type 4

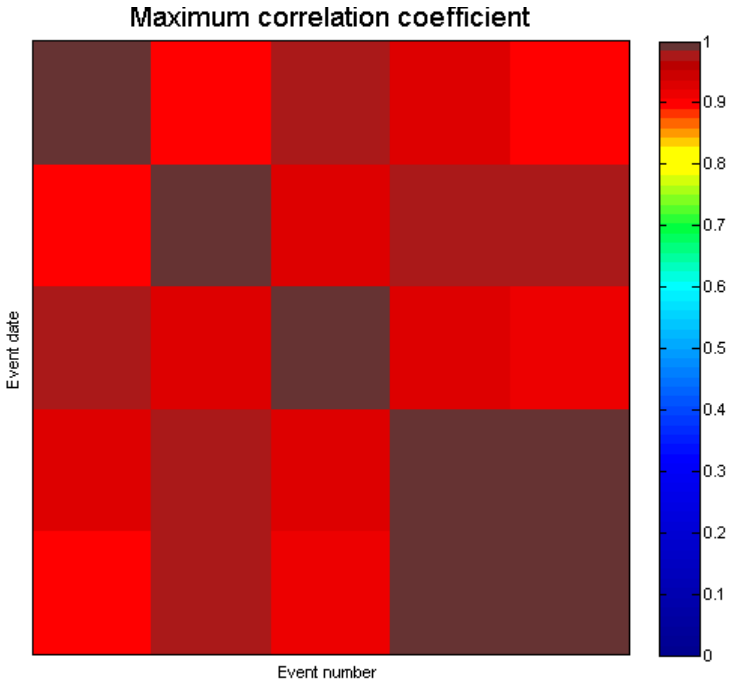

Figure 5.16. Correlation matrice of event 4.

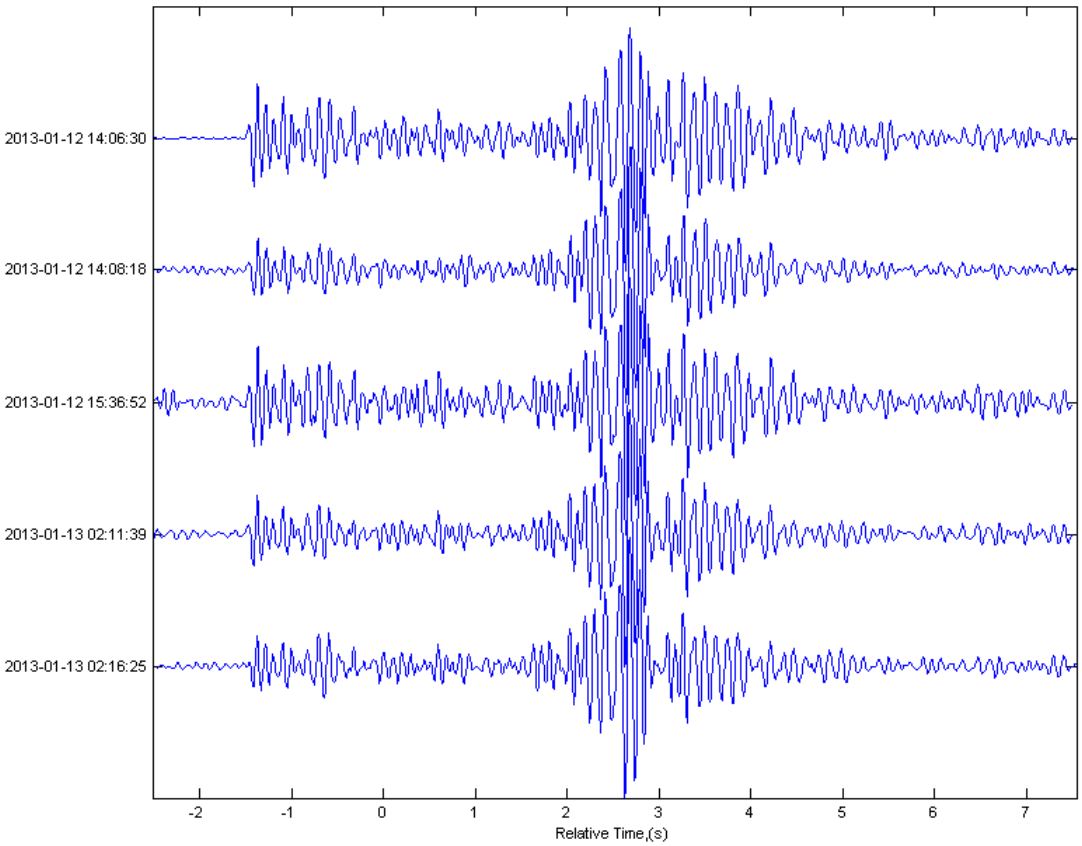

Figure 5.17. Waveforms of event 4.

5.2. Unclassified Micro-Earthquakes

With GISMO correlation toolbox, user could find best similarity with checking the waveforms. Apart from classified 34 events of waveforms, most of them could not be classified by the program. They have their unique forms. These waveforms could not be correlated. Some of the unclassified waveforms at the study area are shown at Figures 5.21 to 5.23.

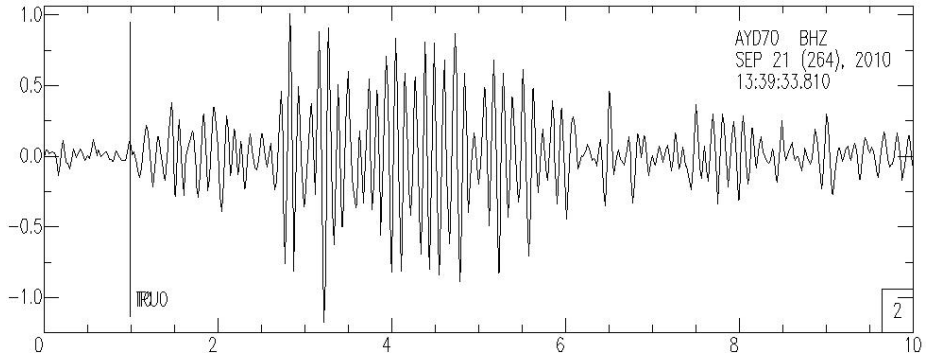

Figure 5.18. Unclassified waveform-1.

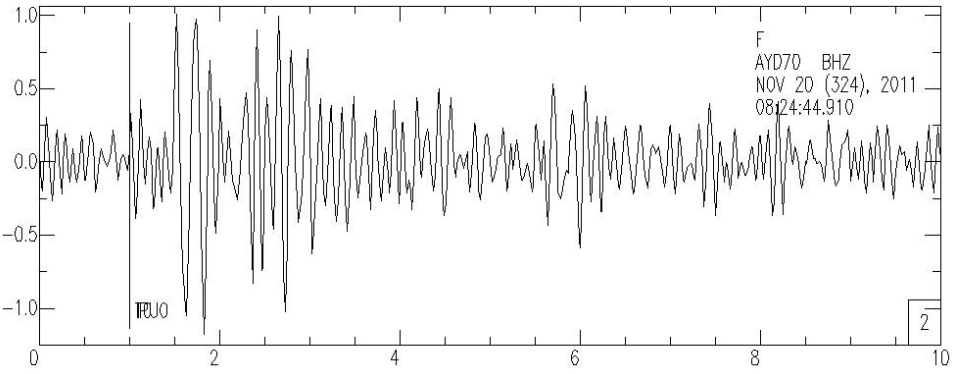

Figure 5.19. Unclassified waveform -2.

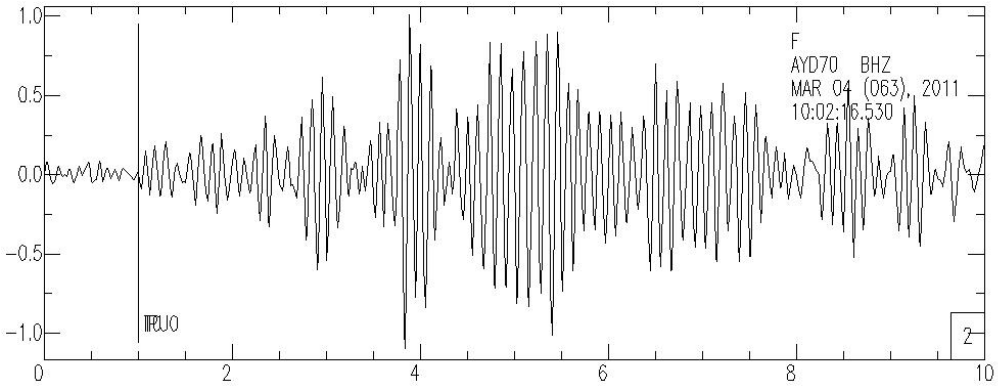

Figure 5.20. Unclassified waveform -3.

5.3. Location Improvement of Microearthquakes with VELEST

The initial model produced from existing well log, seismic reflection and other geophysical studies used locating the earthquakes. Later a minimum 1D velocity model and station corrections were obtained using VELEST software. All the earthquakes were relocated using VELEST results and new location maps were produced. At first, they look like scattered all over the study area. This can be due to two reasons. One of them is the velocity model and second one is unknown station residuals. After finding minimum 1D velocity model with VELEST and calculating station residuals, every event type had a concentration either around a circle or along a line. New locations of earthquakes are accumulated at certain areas. Figure 5.24 and Figure 5.25 shows location of all micro-earthquakes before and after the minimum 1D velocity model which was found by using VELEST.

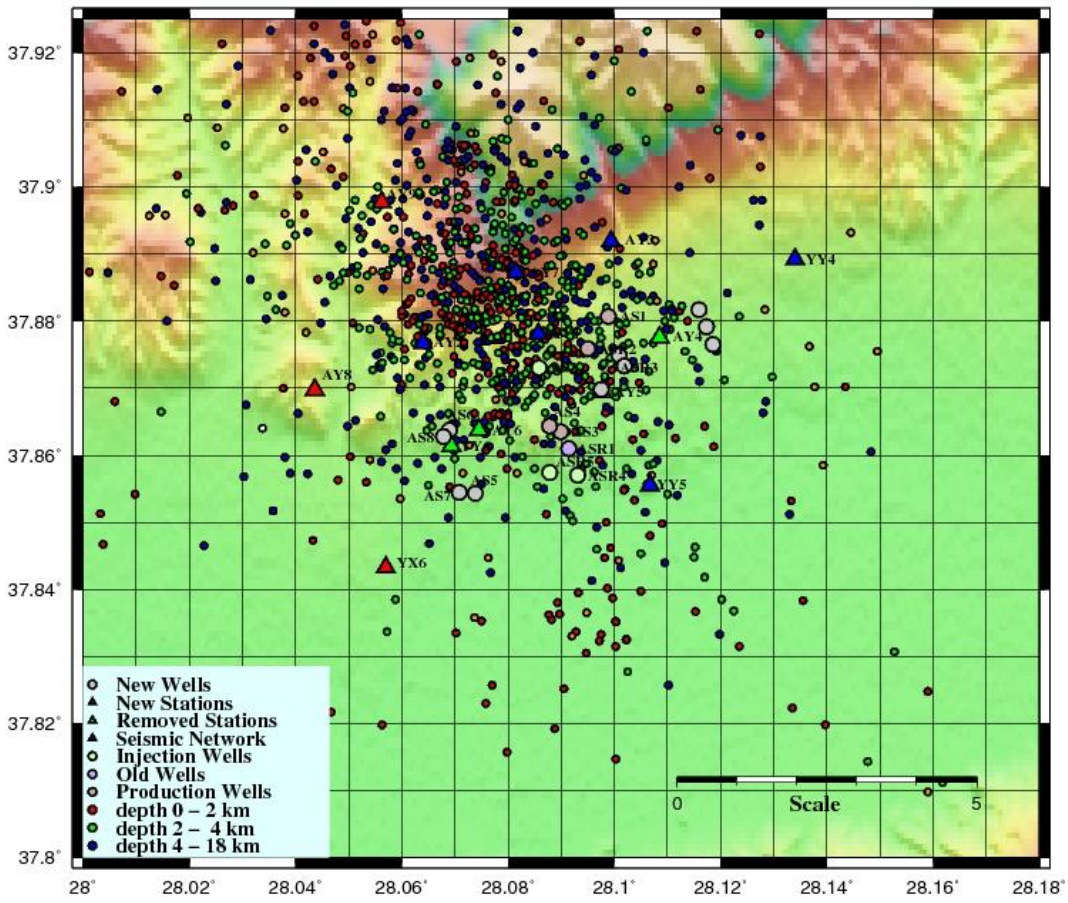

Figure 5.21. Microearthquake locations before VELEST run.

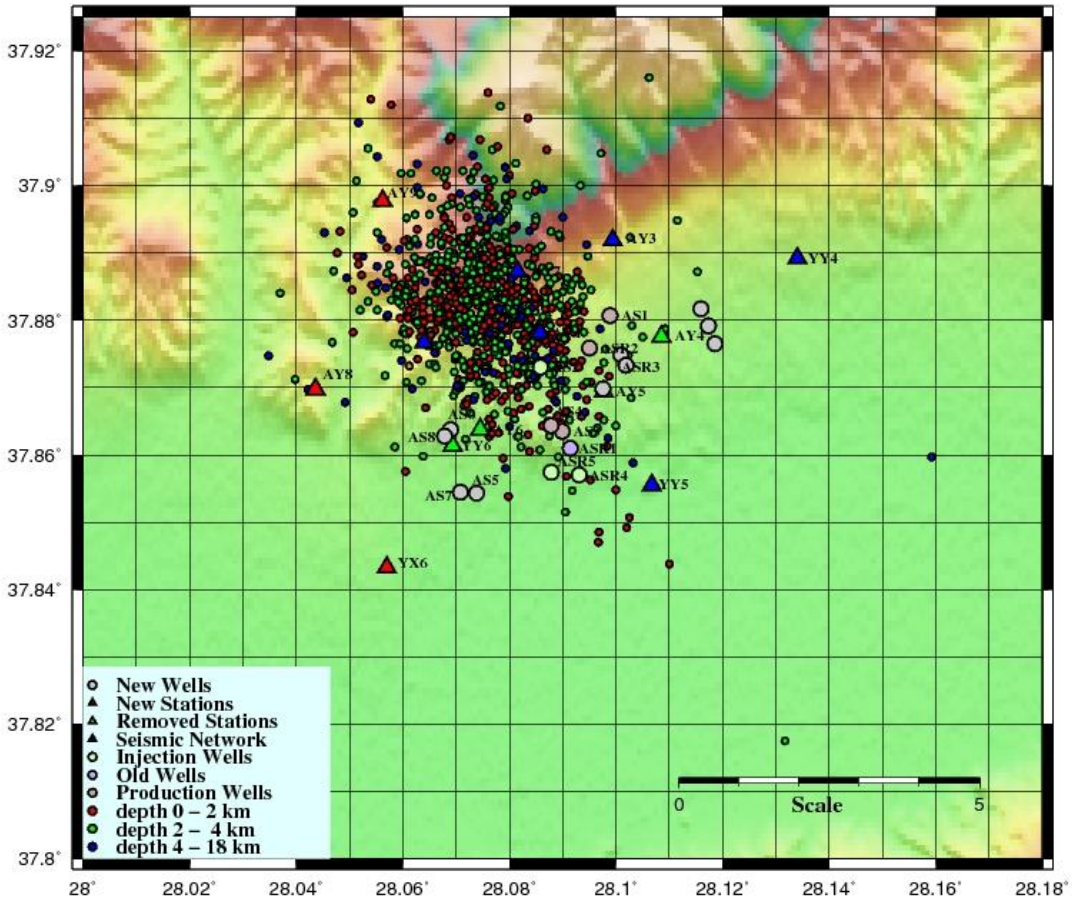

Figure 5.22. Microearthquake locations after VELEST run.

The difference between before and after VELEST run is very clearly seen on the maps. There are still some microearthquakes out of the study area.

Figure 5.23 to Figure 5.26 show the location of first 4 event types location after the VELEST. Their location will be given with their error ellipsoids. The reason why we used error ellipsoids is to show that how well we located the events. Within the error limits, they may be related to the same source. It is evidenced by the correlation method that their waveforms are very similar and they seems to be occuring at the same location. For example when we look at the Figure 5.23, the intersection of ellipsoids means there is a room that these earthquakes can be located to the same point.

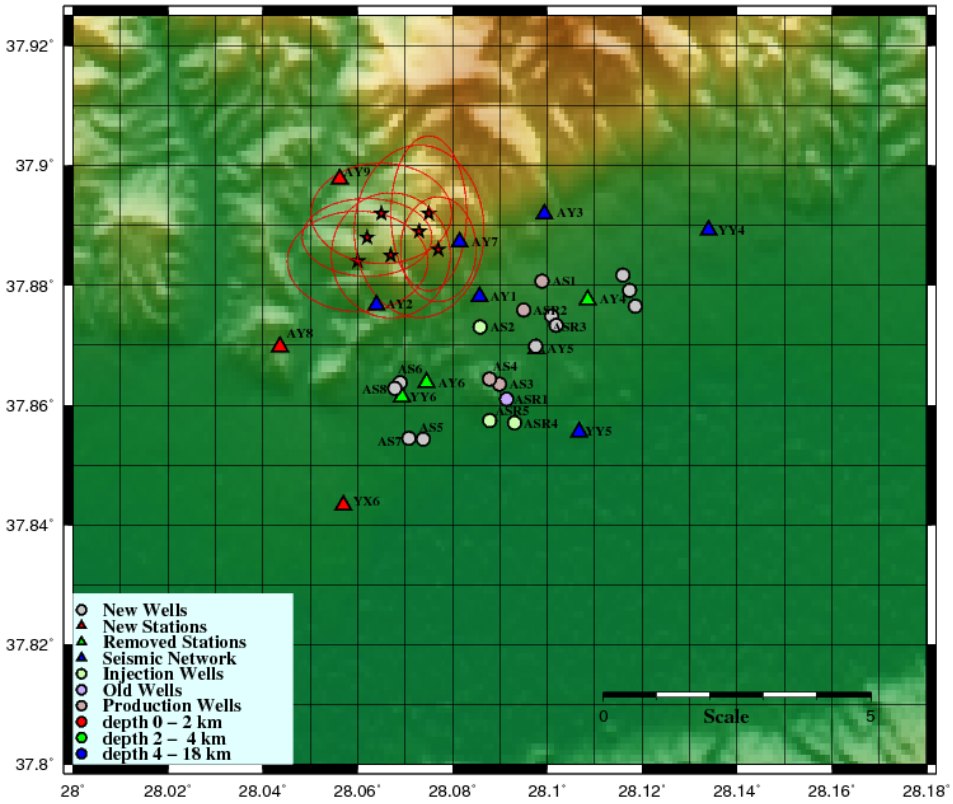

Figure 5.23. Locations of event type 1.

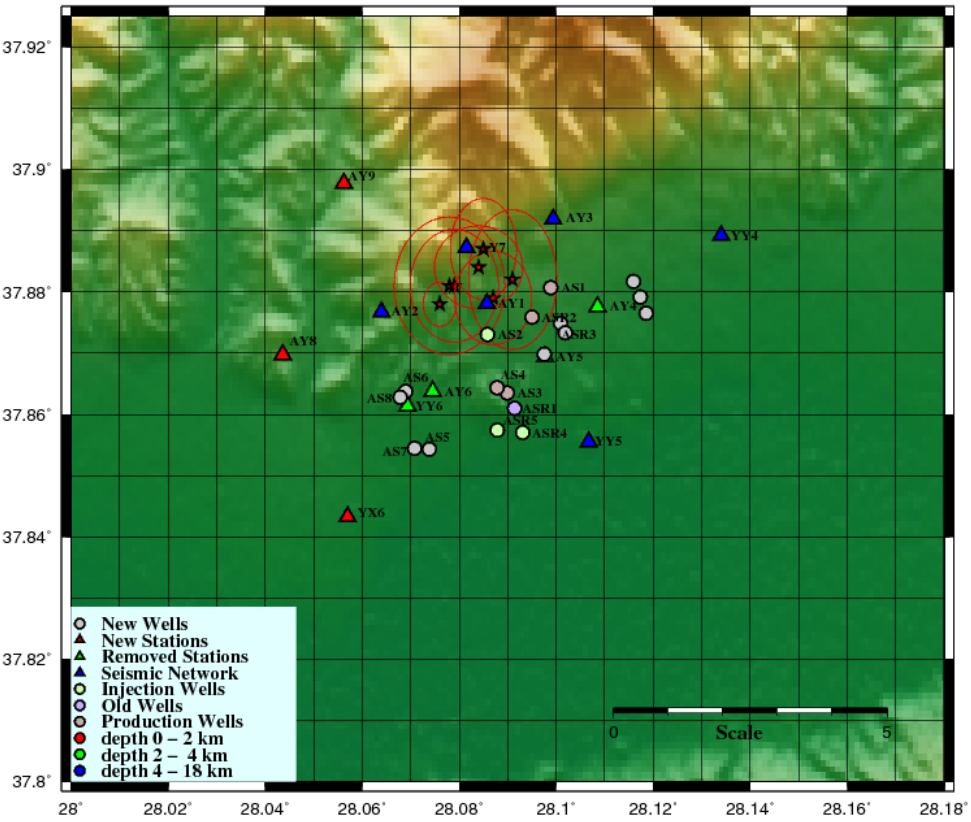

Figure 5.24. Locations of event type 2.

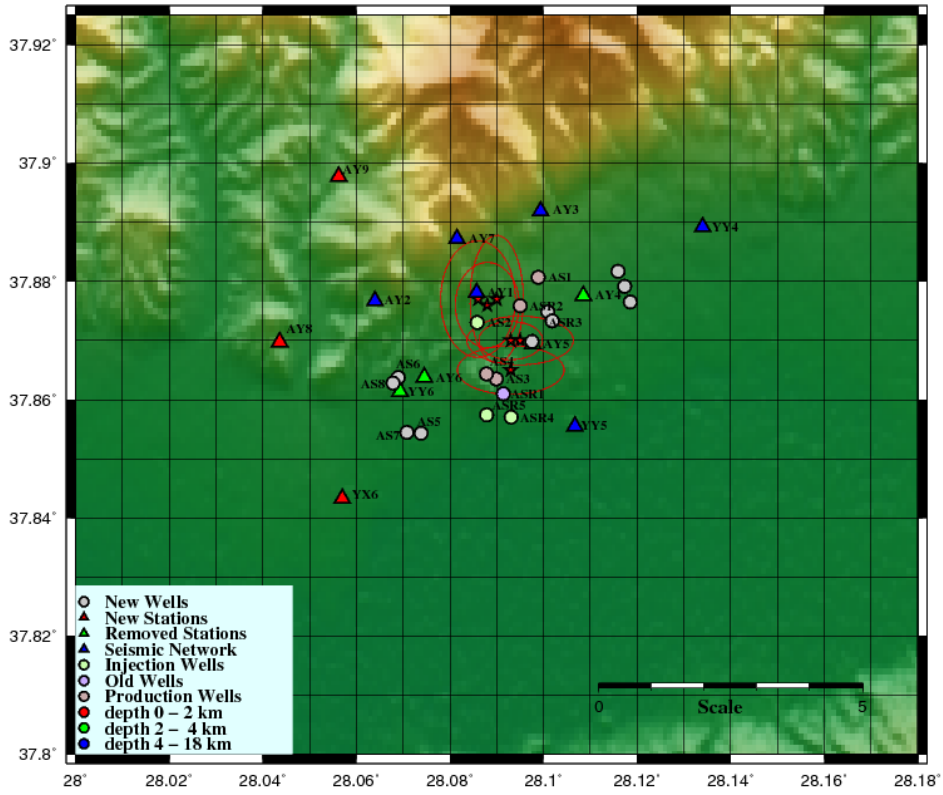

Figure 5.25. Locations of event type 3.

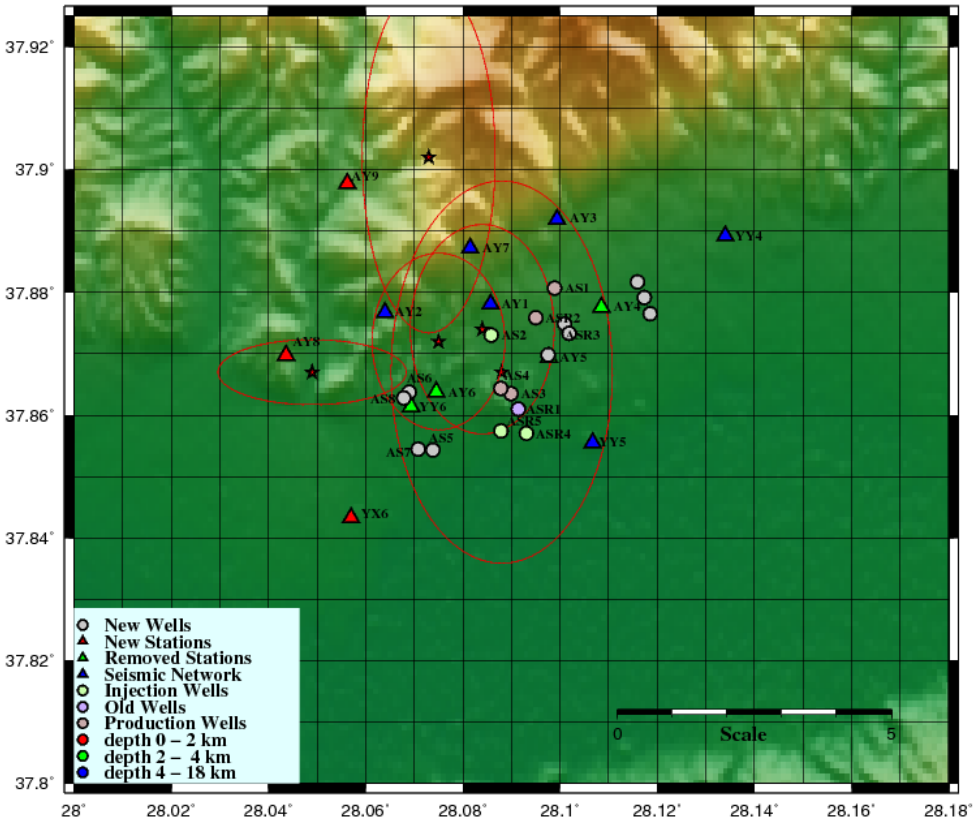

Figure 5.26. Locations of event type 4.

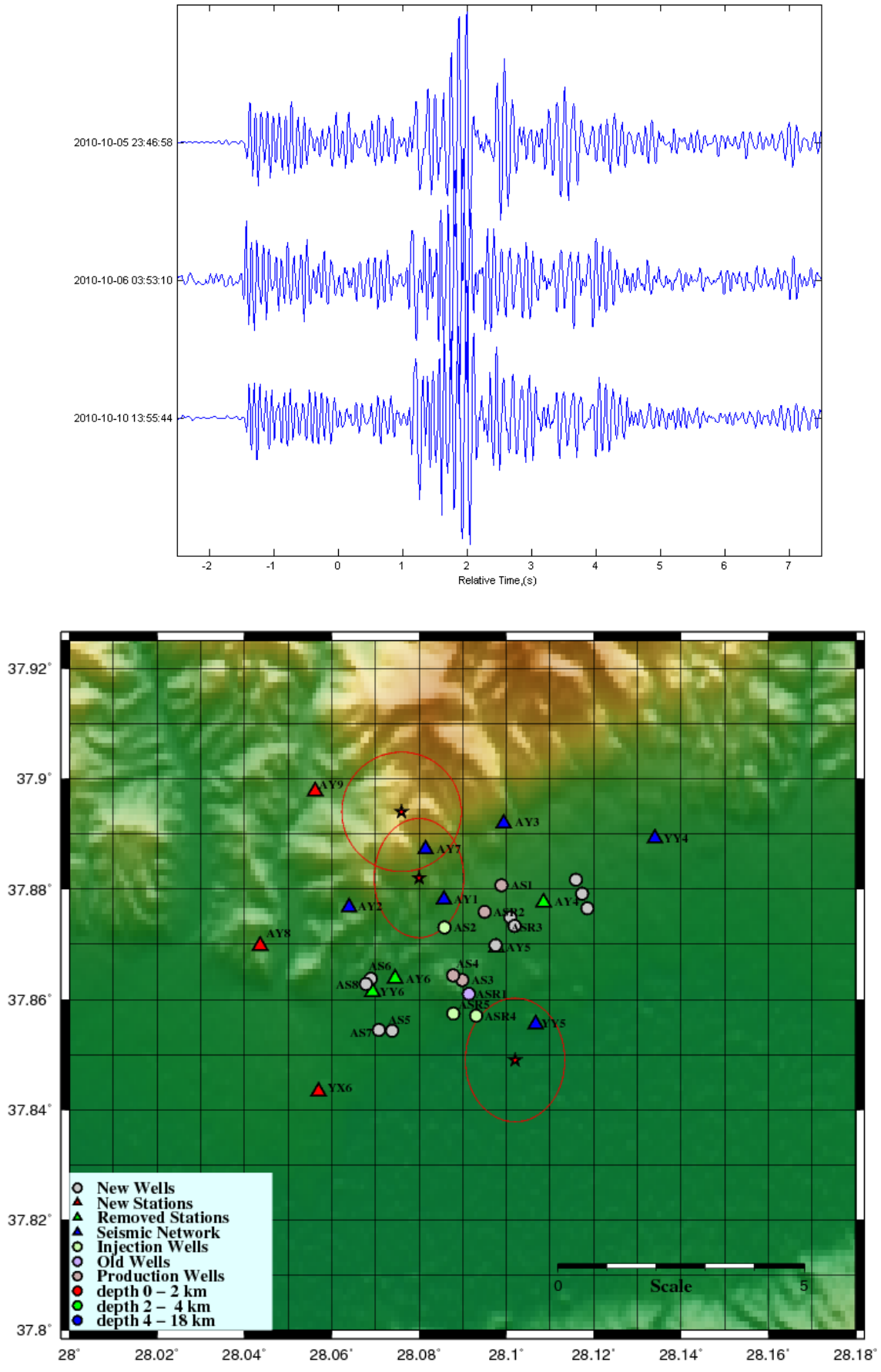

Figure 5.27. Waveforms and locations of event type 5.

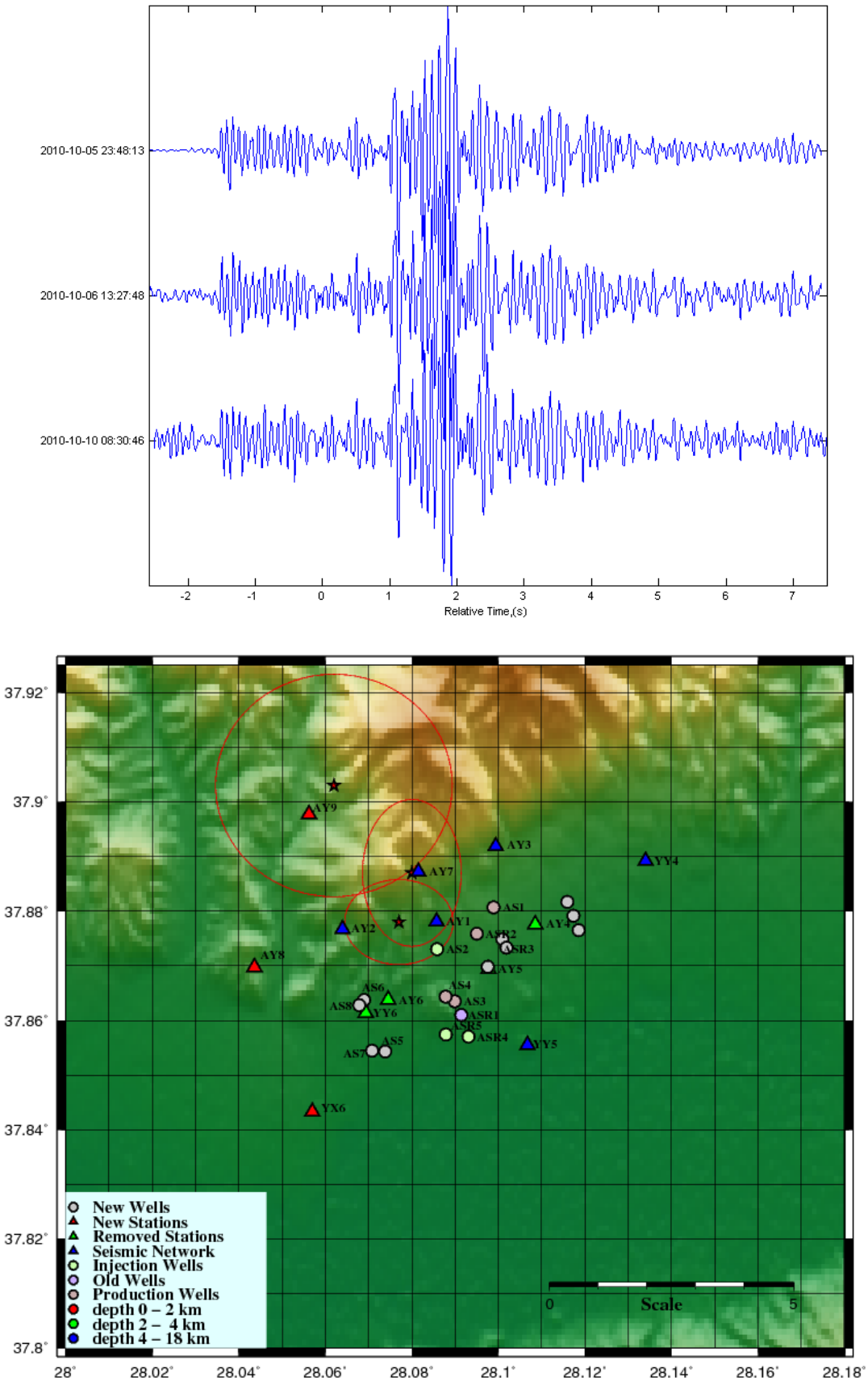

Figure 5.28. Waveforms and locations of event type 6.

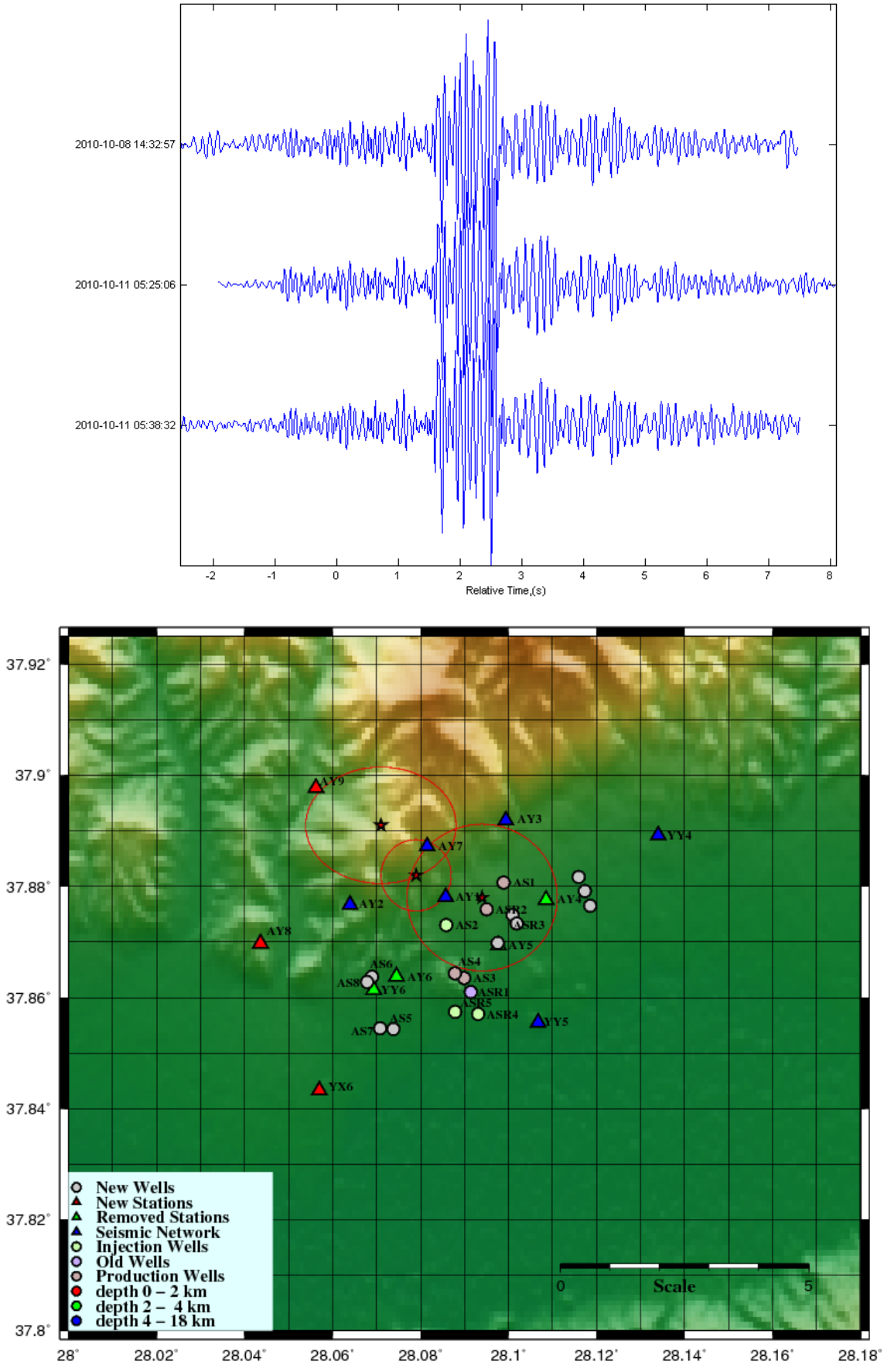

Figure 5.29. Waveforms and locations of event type 7.

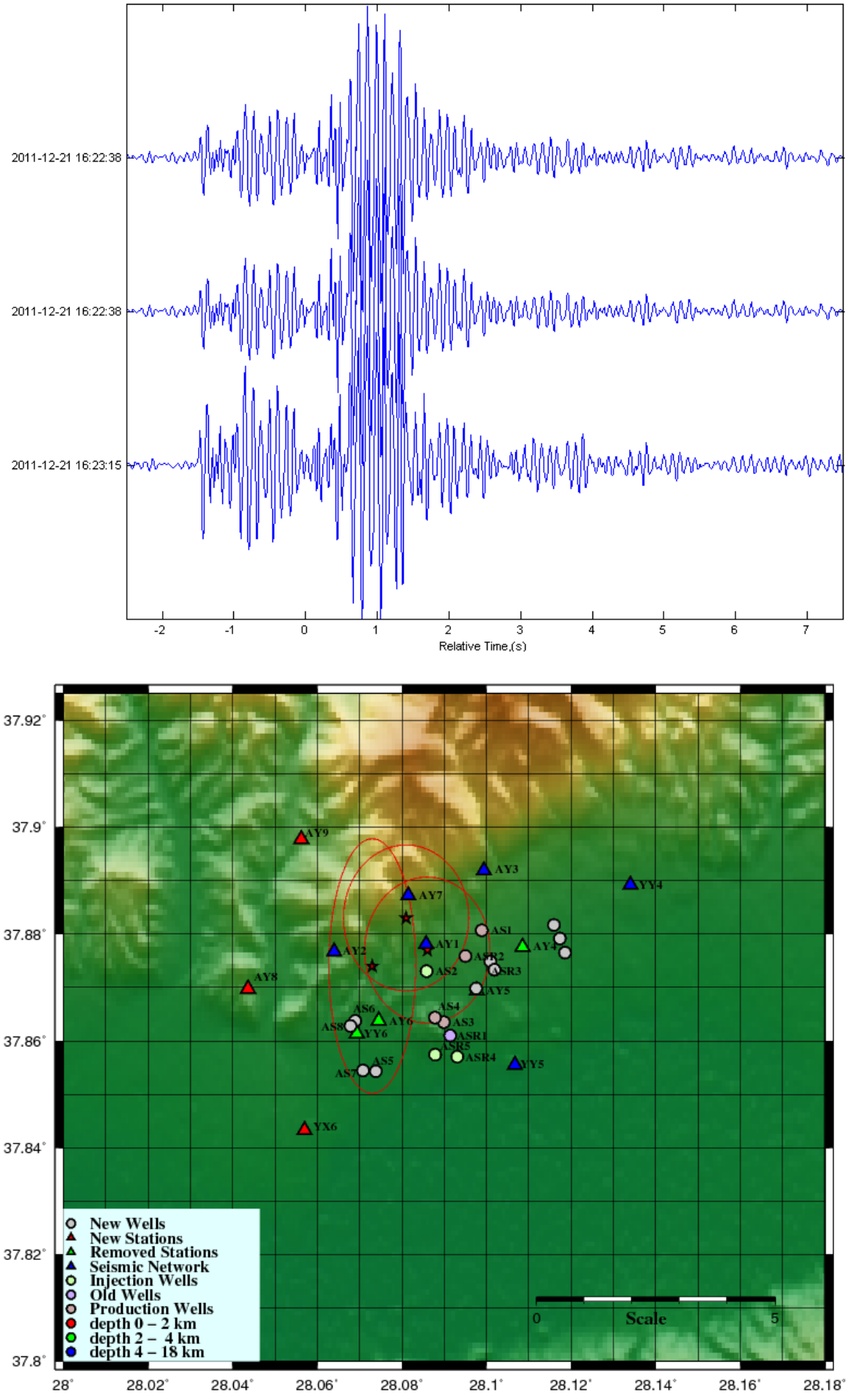

Figure 5.30. Waveforms and locations of event type 8.

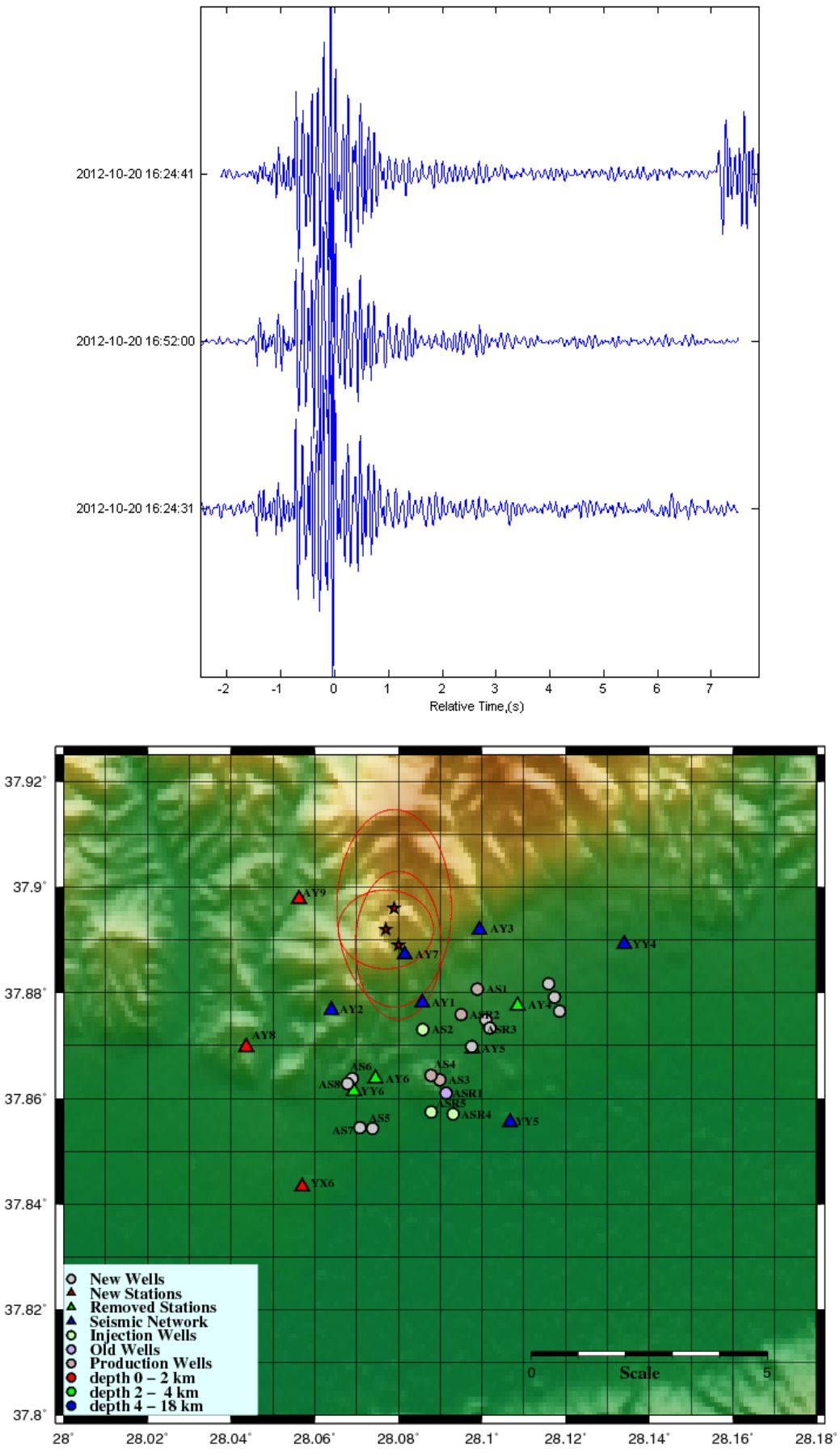

Figure 5.31. Waveforms and locations of event type 9.

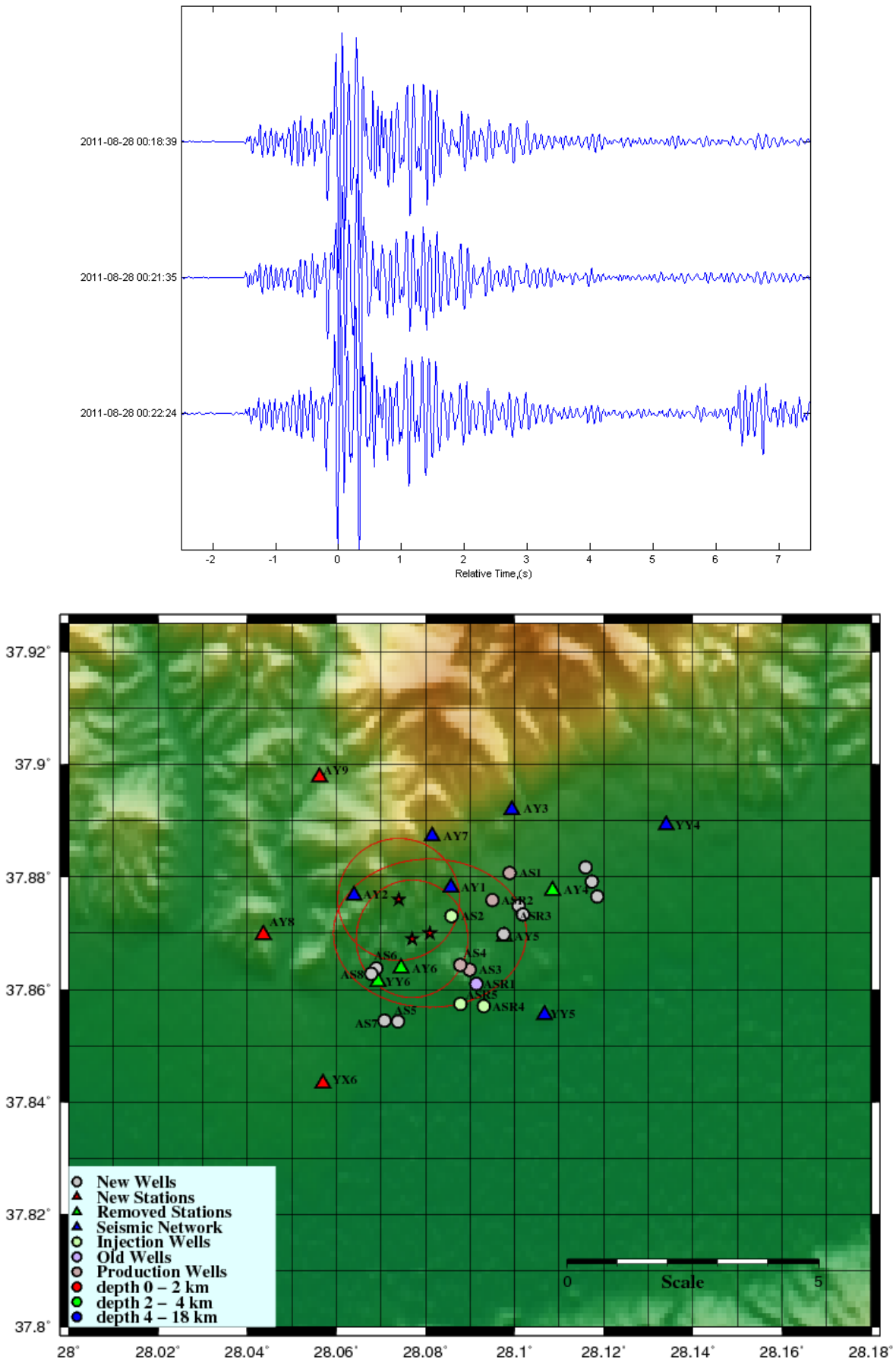

Figure 5.32. Waveforms and locations of event type 10.

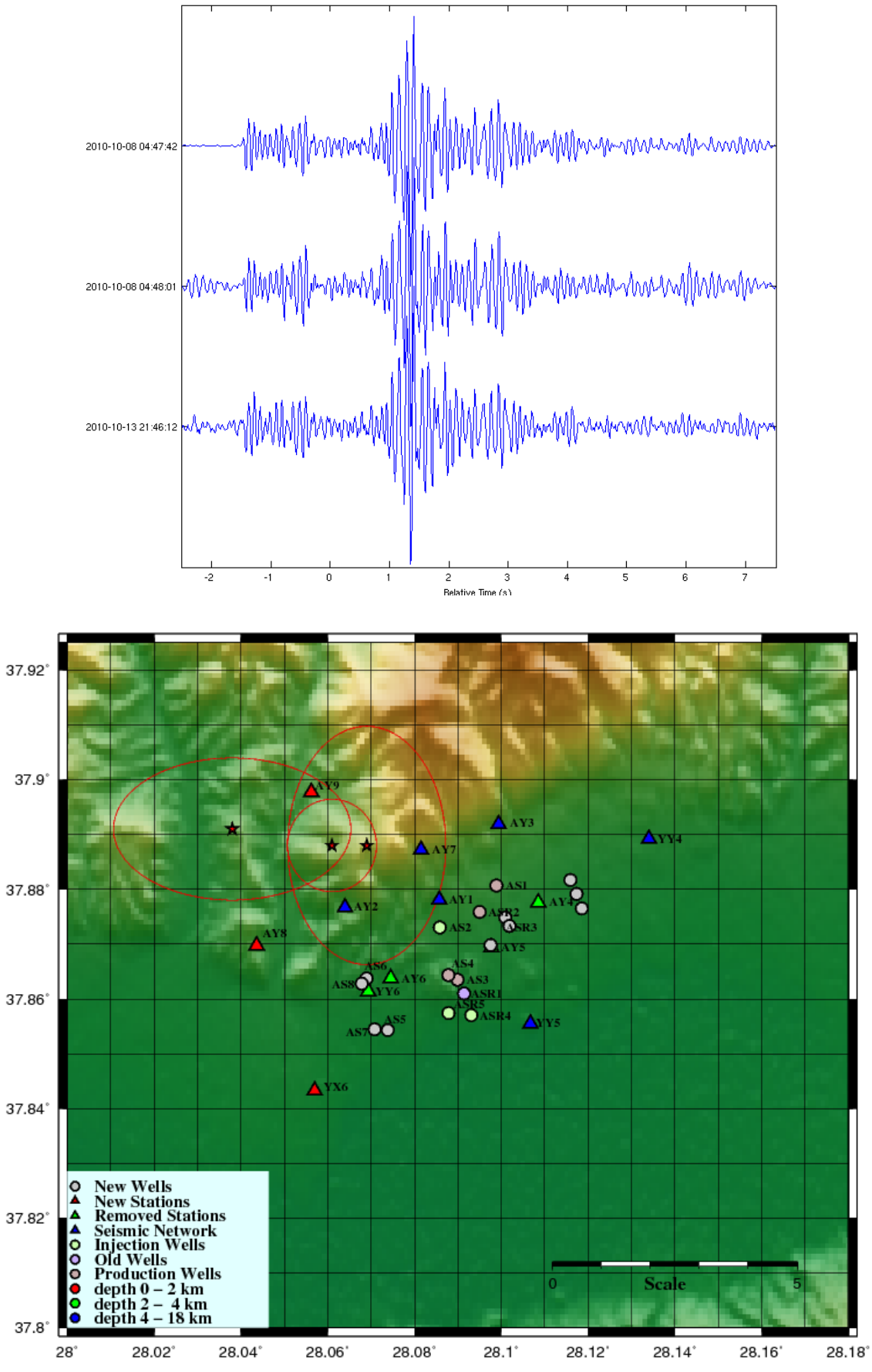

Figure 5.33. Waveforms and locations of event type 11.

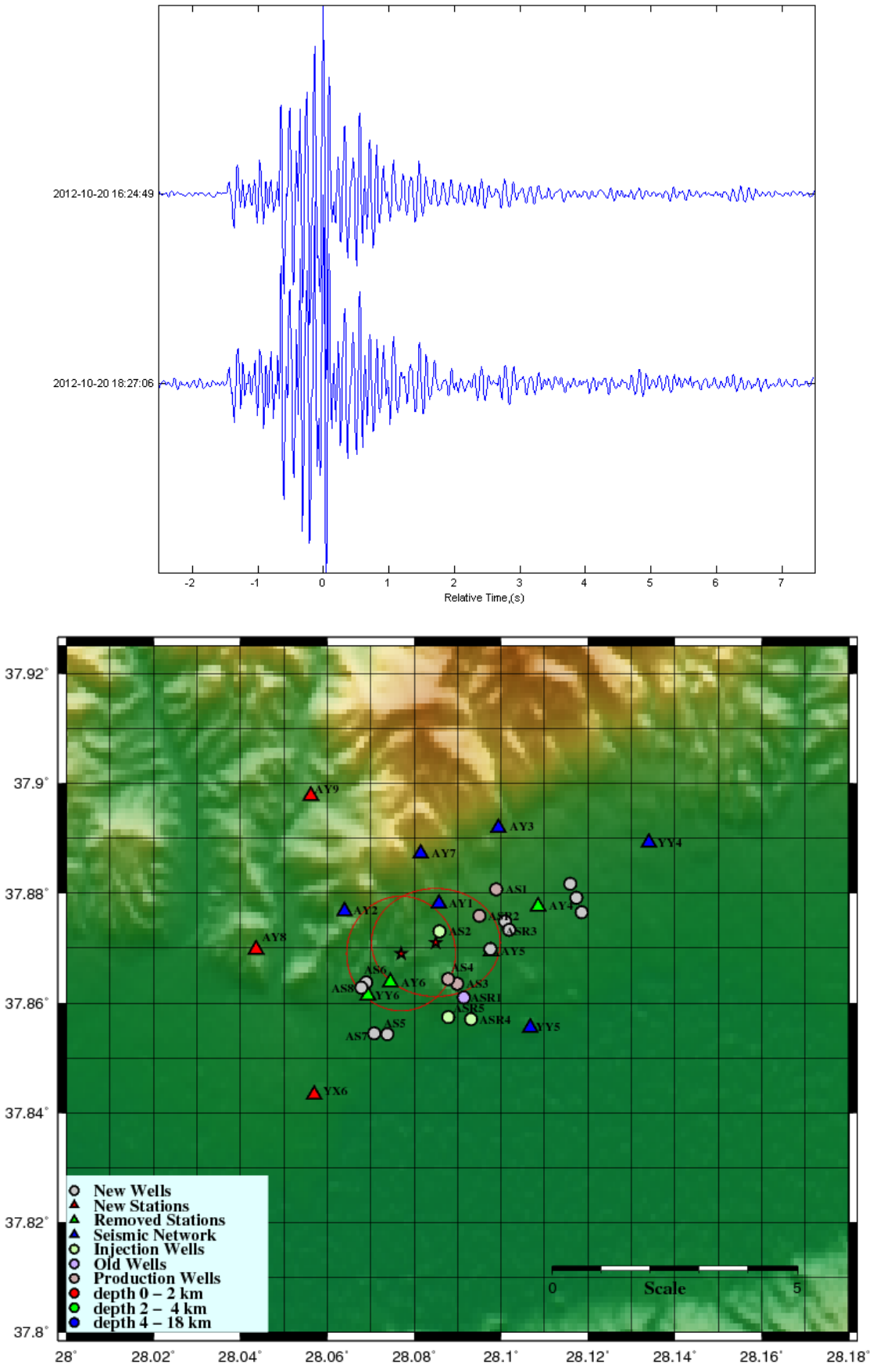

Figure 5.34. Waveforms and locations of event type 12.

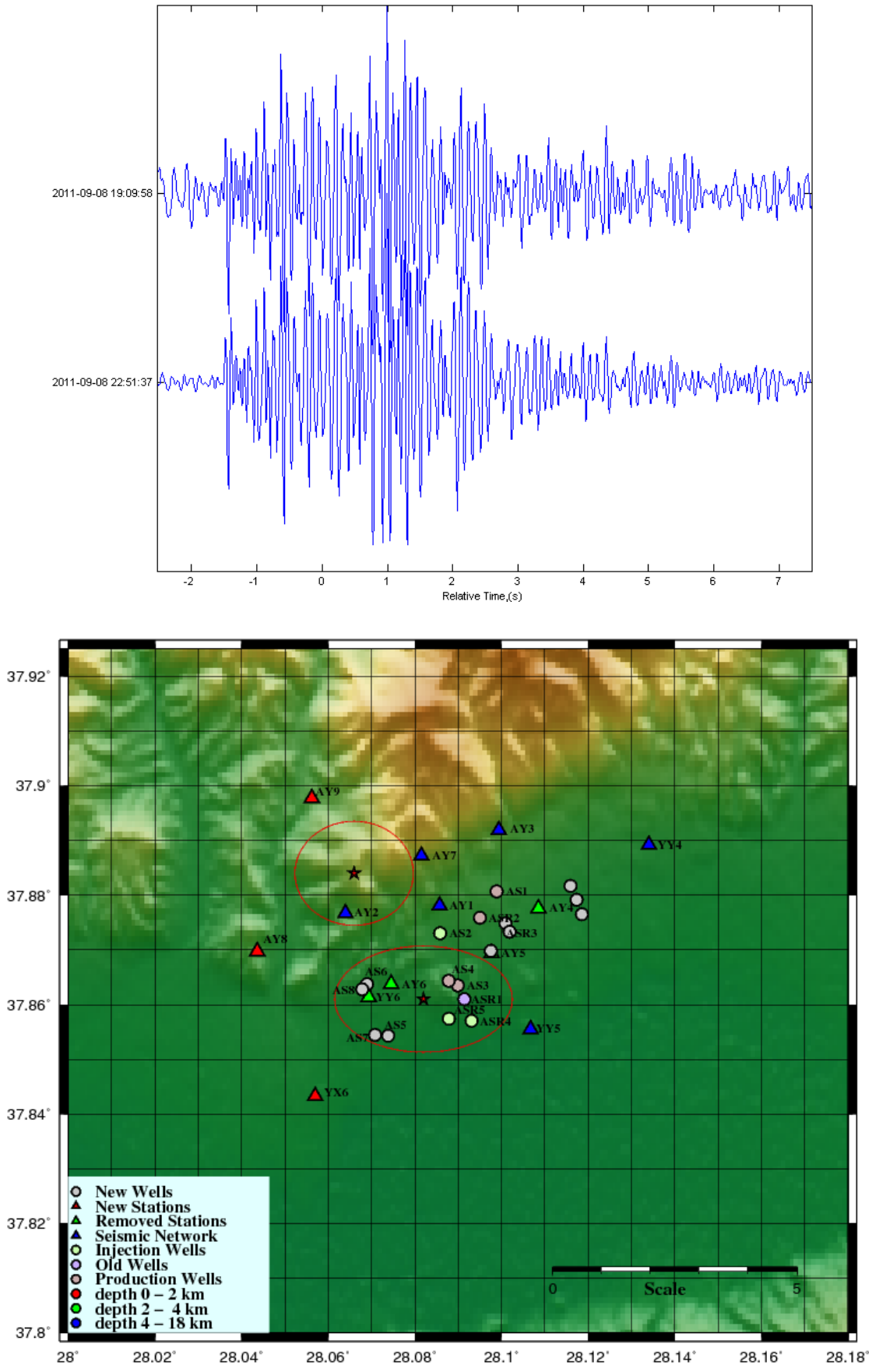

Figure 5.35. Waveforms and locations of event type 13.

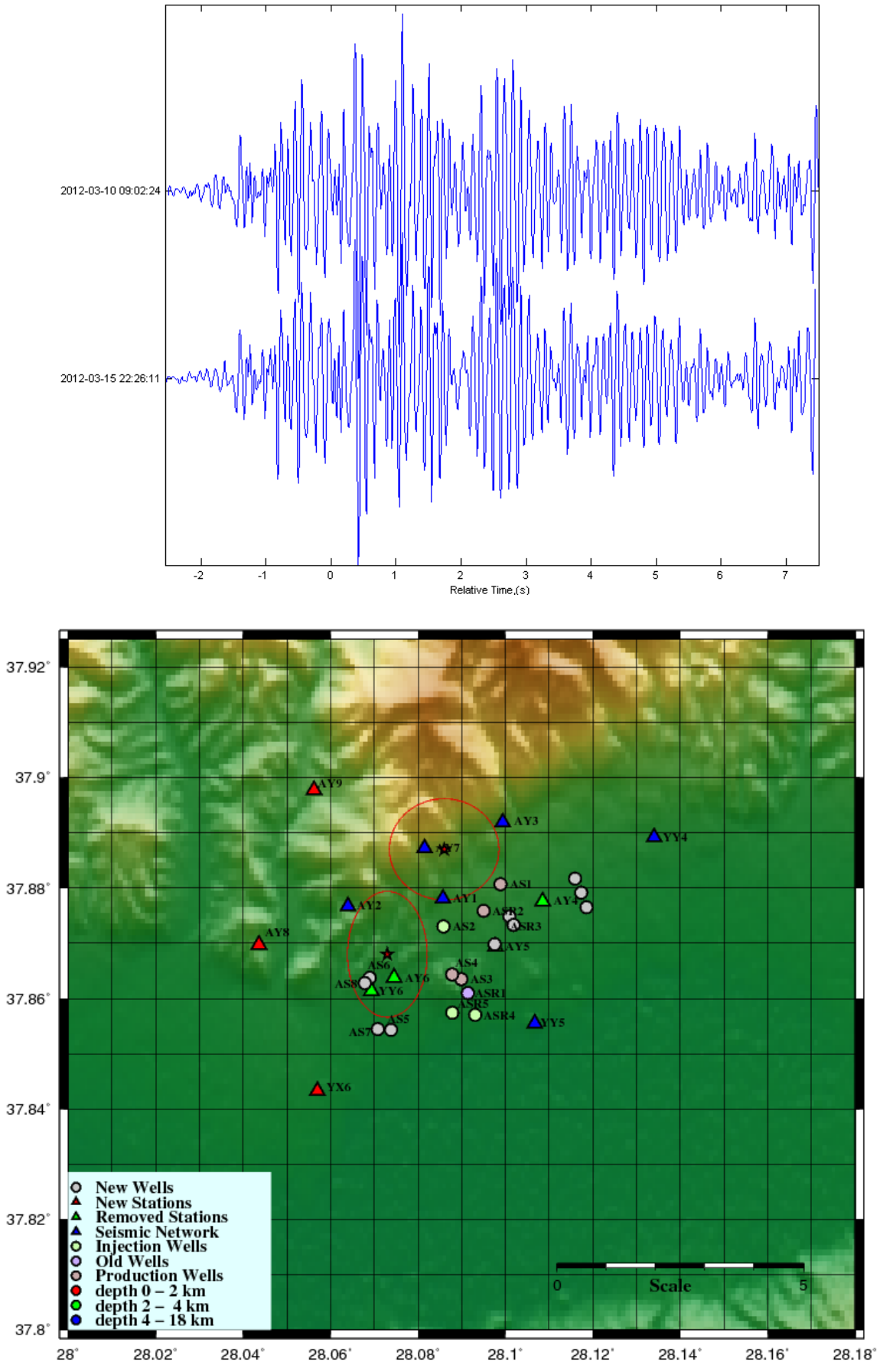

Figure 5.36. Waveforms and locations of event type 14.

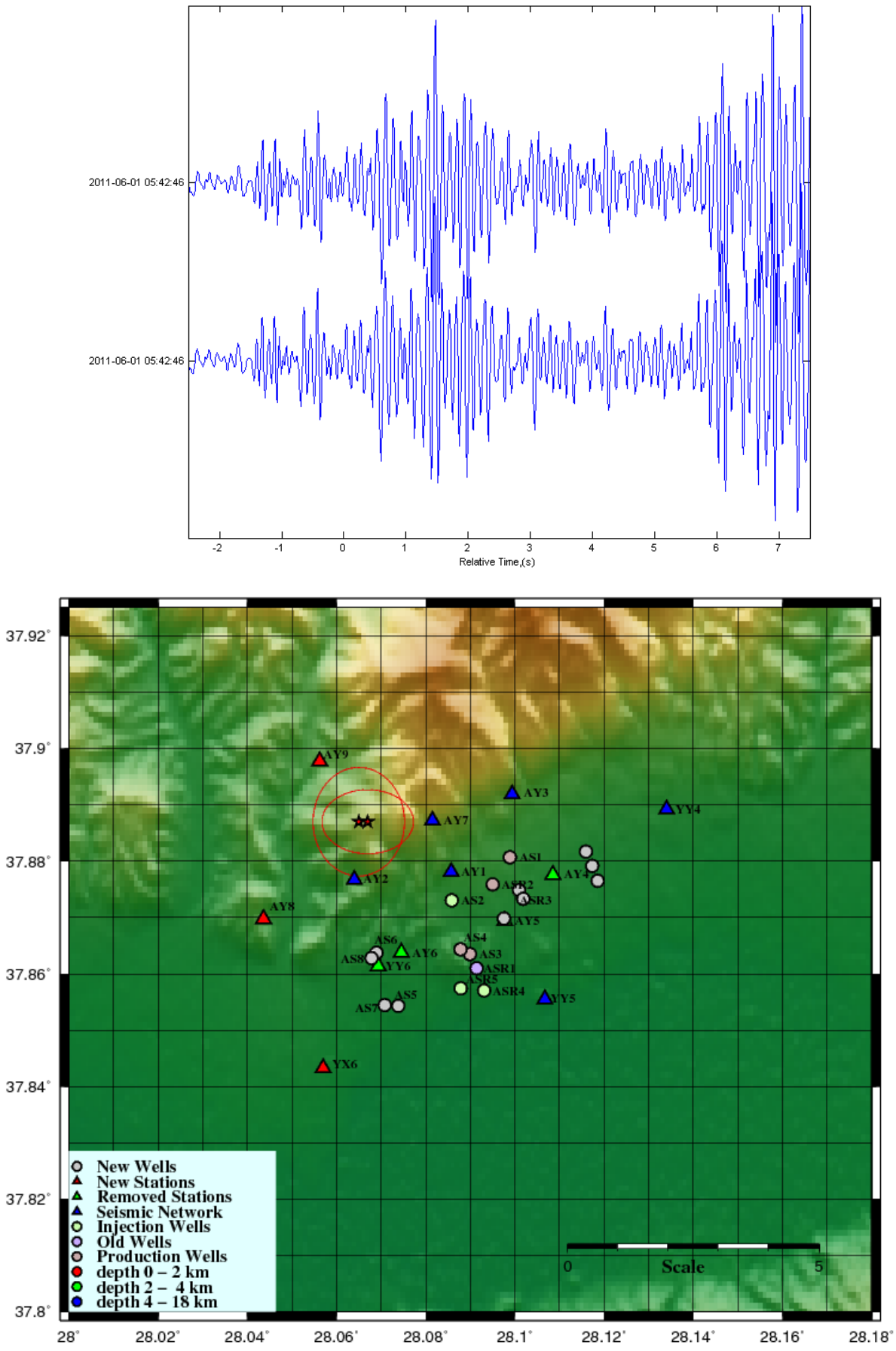

Figure 5.37. Waveforms and locations of event type 15.

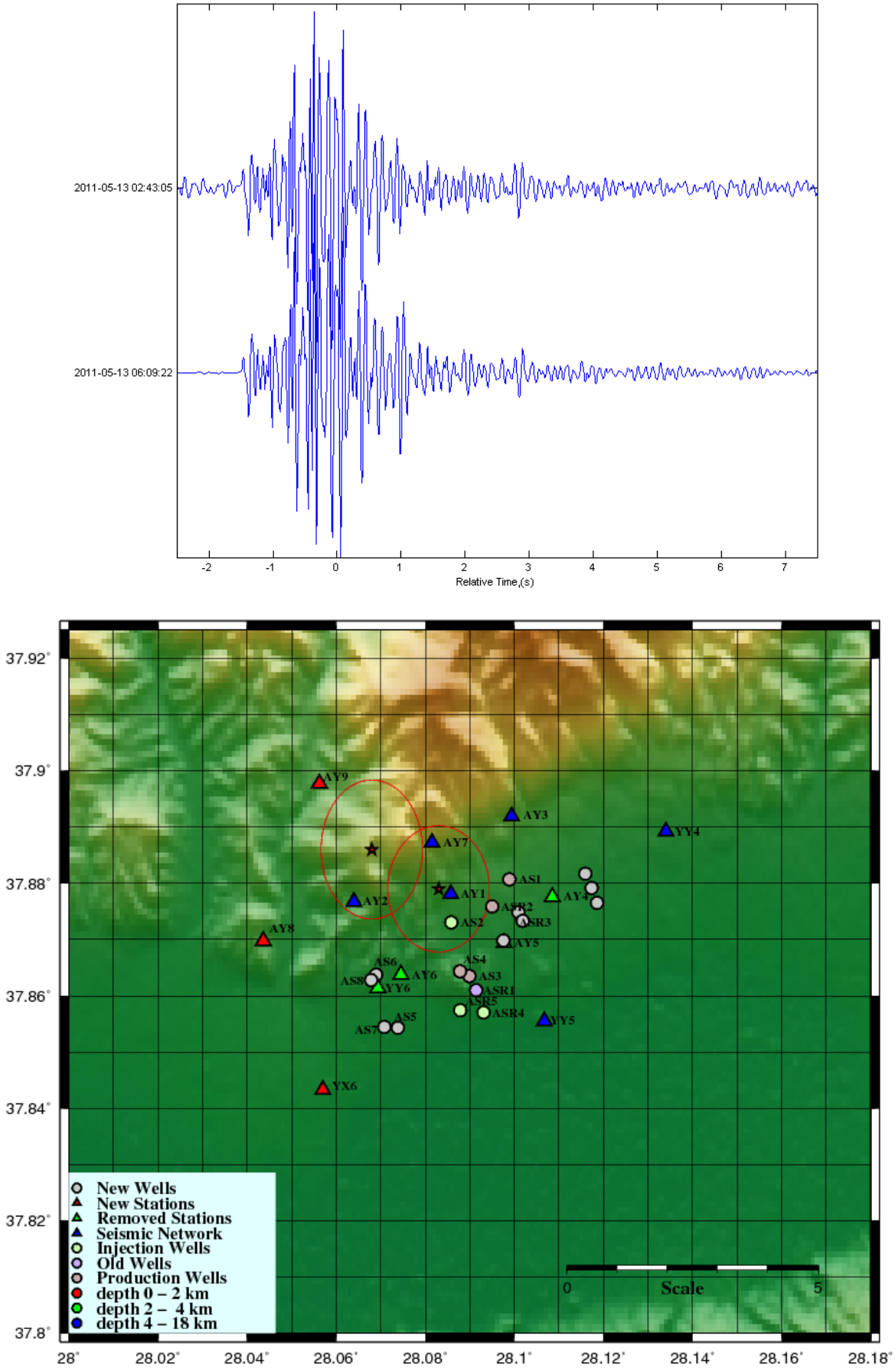

Figure 5.38. Waveforms and locations of event type 16.

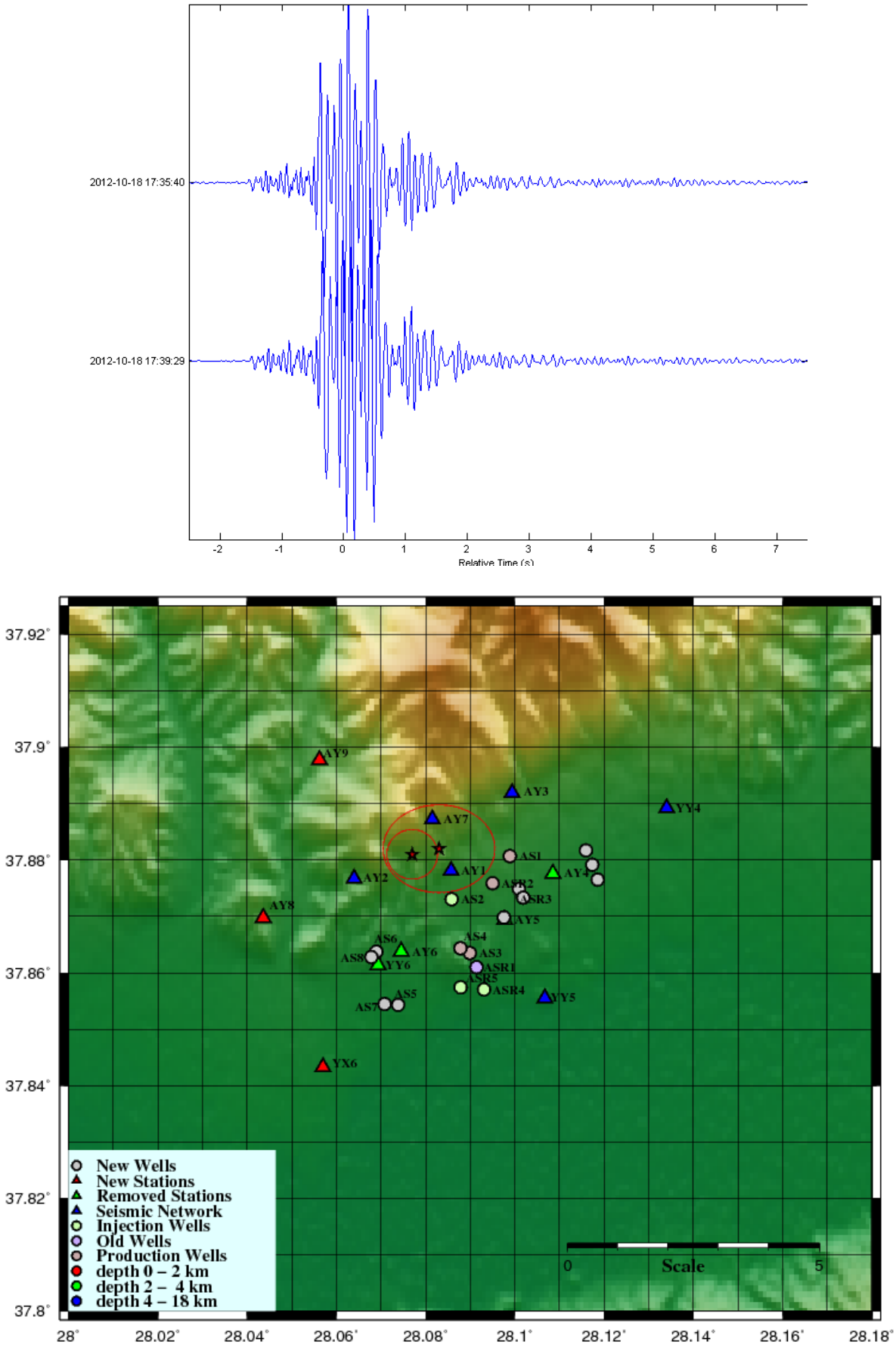

Figure 5.39. Waveforms and locations of event type 17.

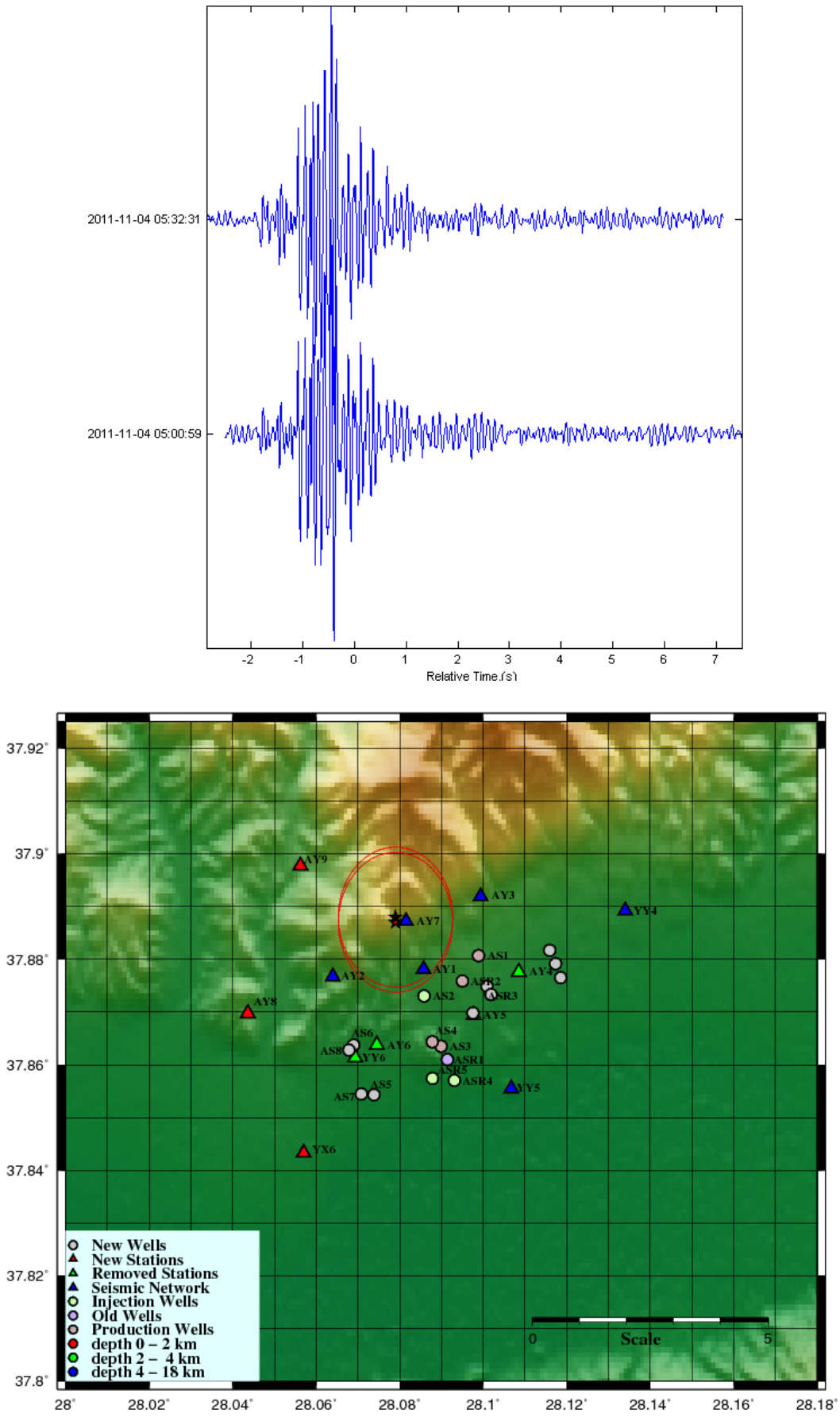

Figure 5.40. Waveforms and locations of event type 18.

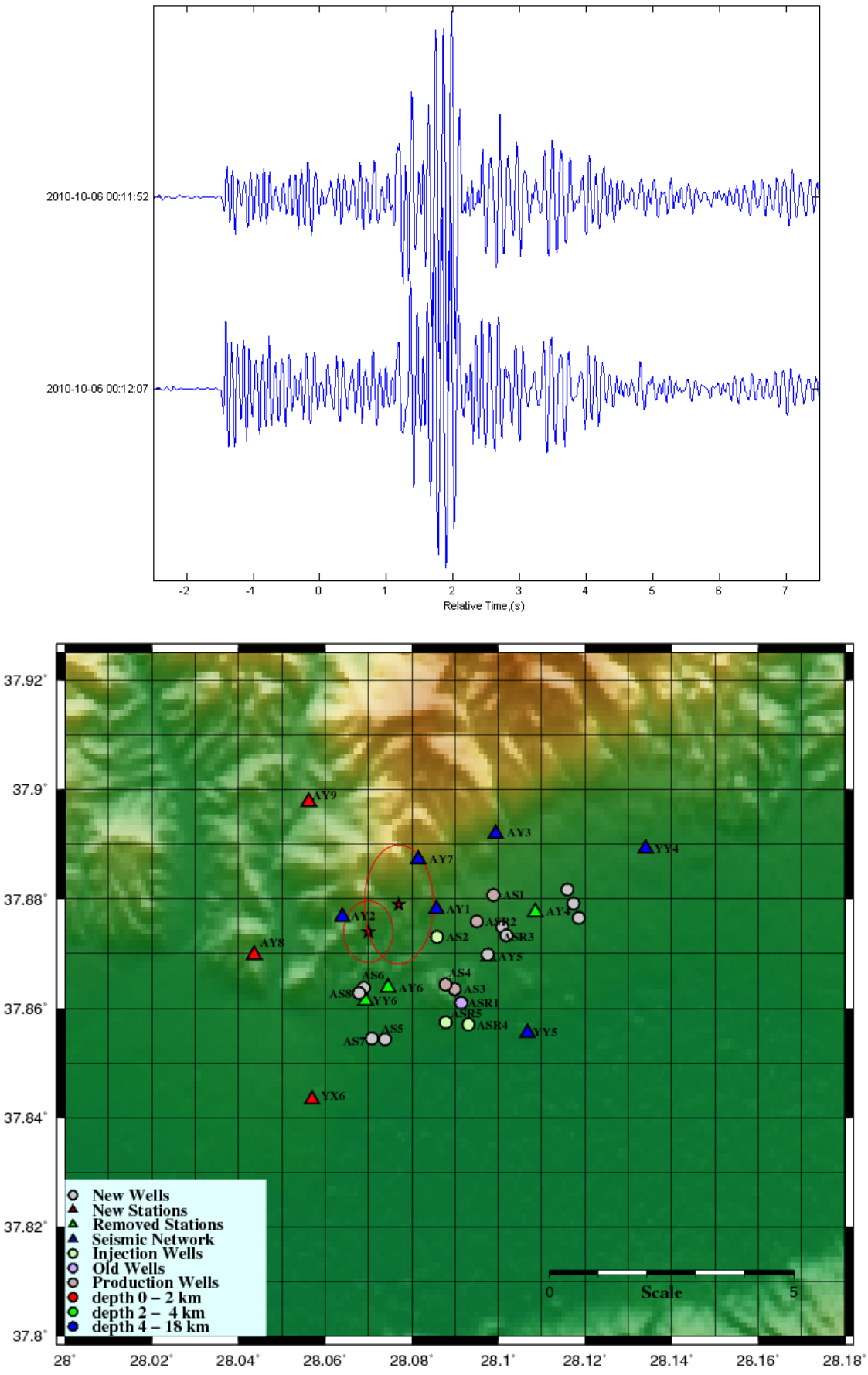

Figure 5.41. Waveforms and locations of event type 19.

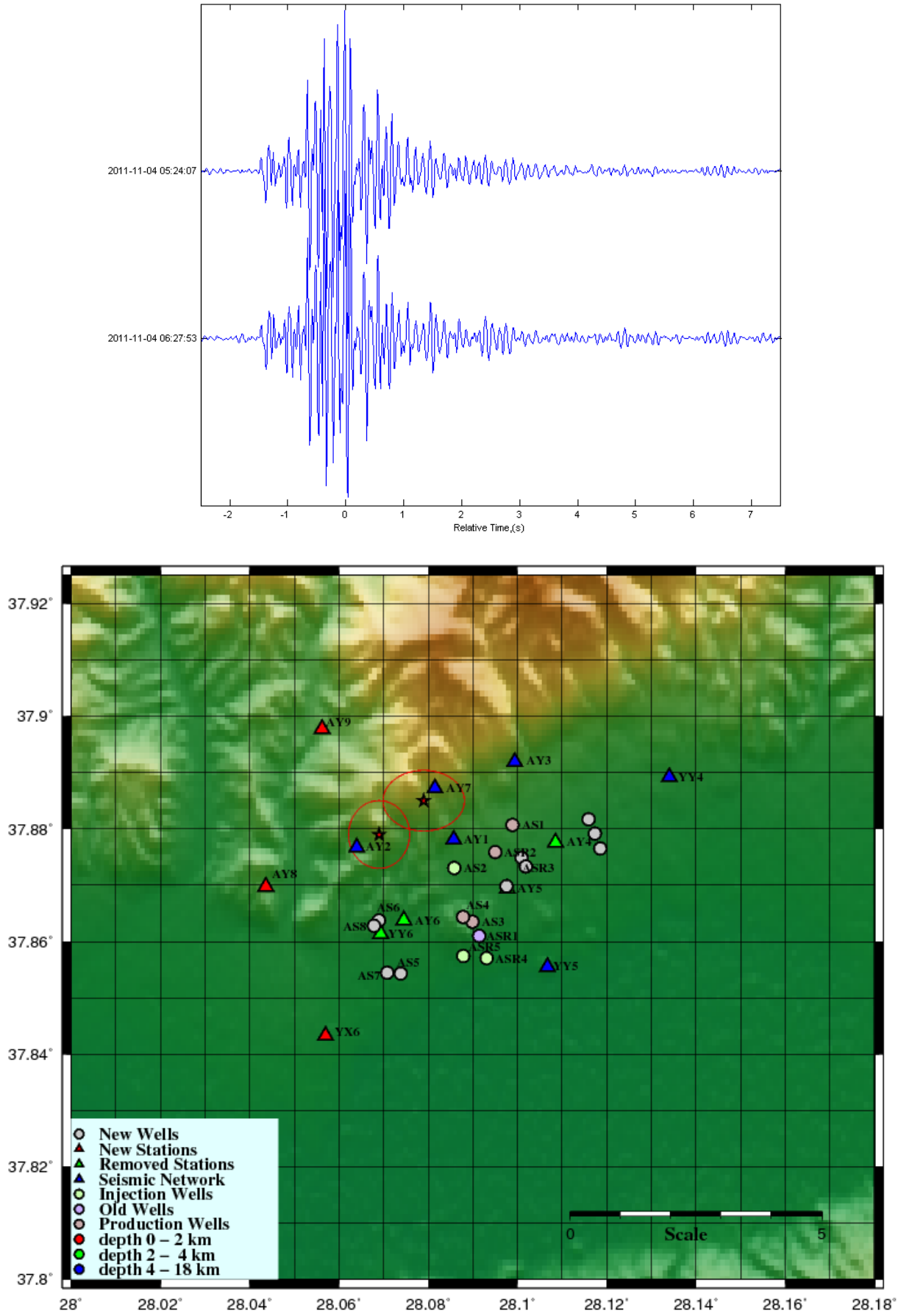

Figure 5.42. Waveforms and locations of event type 20.

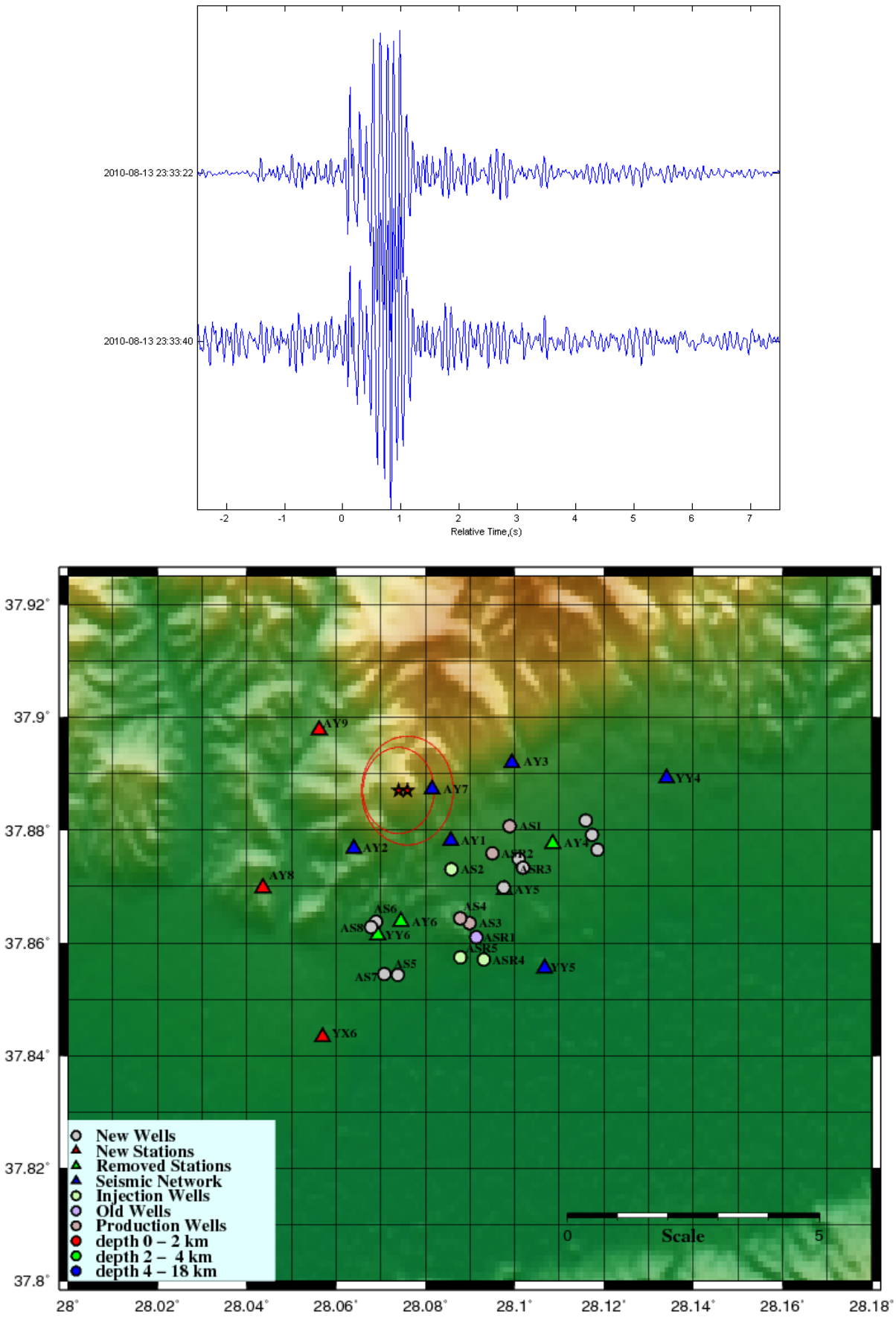

Figure 5.43. Waveforms and locations of event type 21.

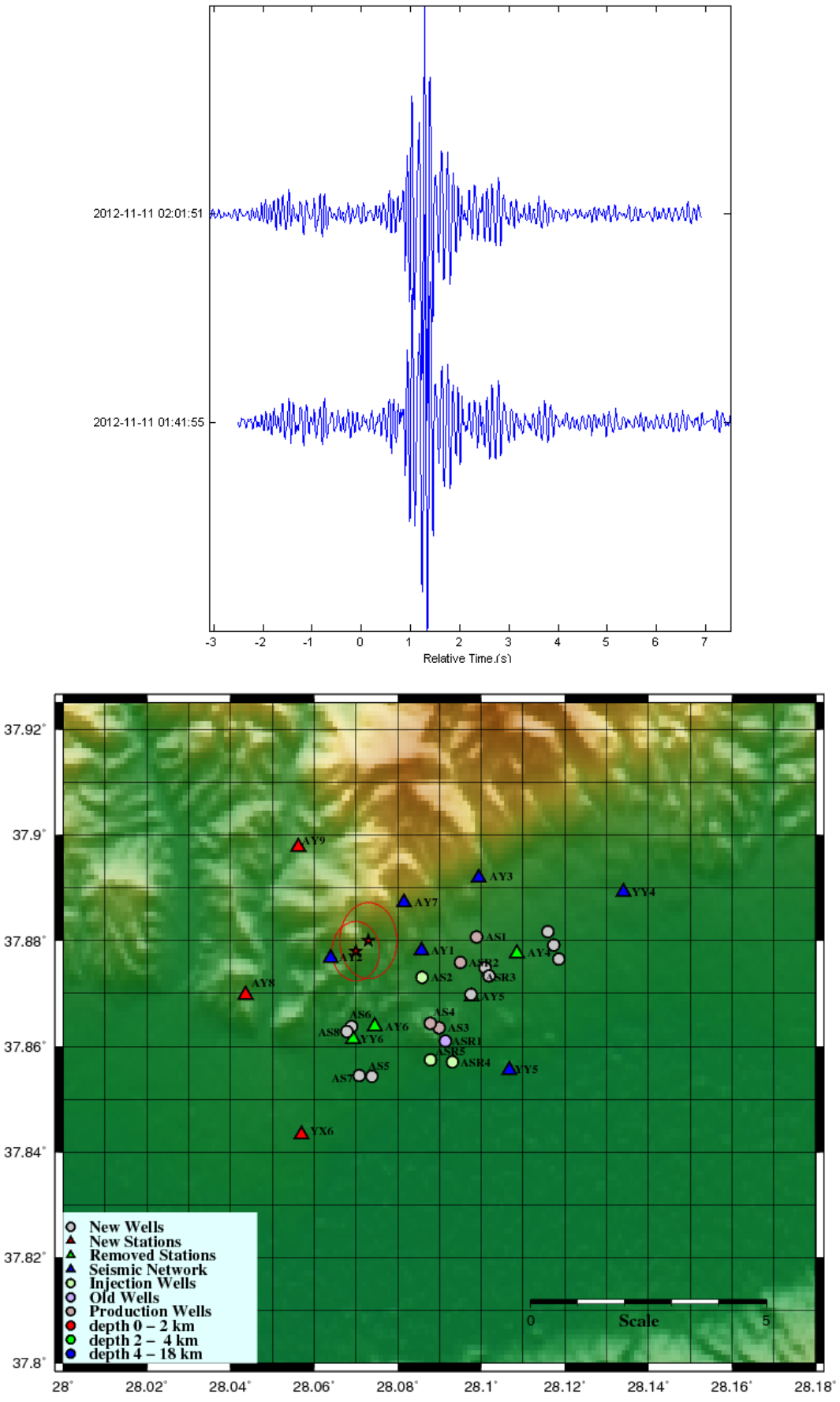

Figure 5.44. Waveforms and locations of event type 22.

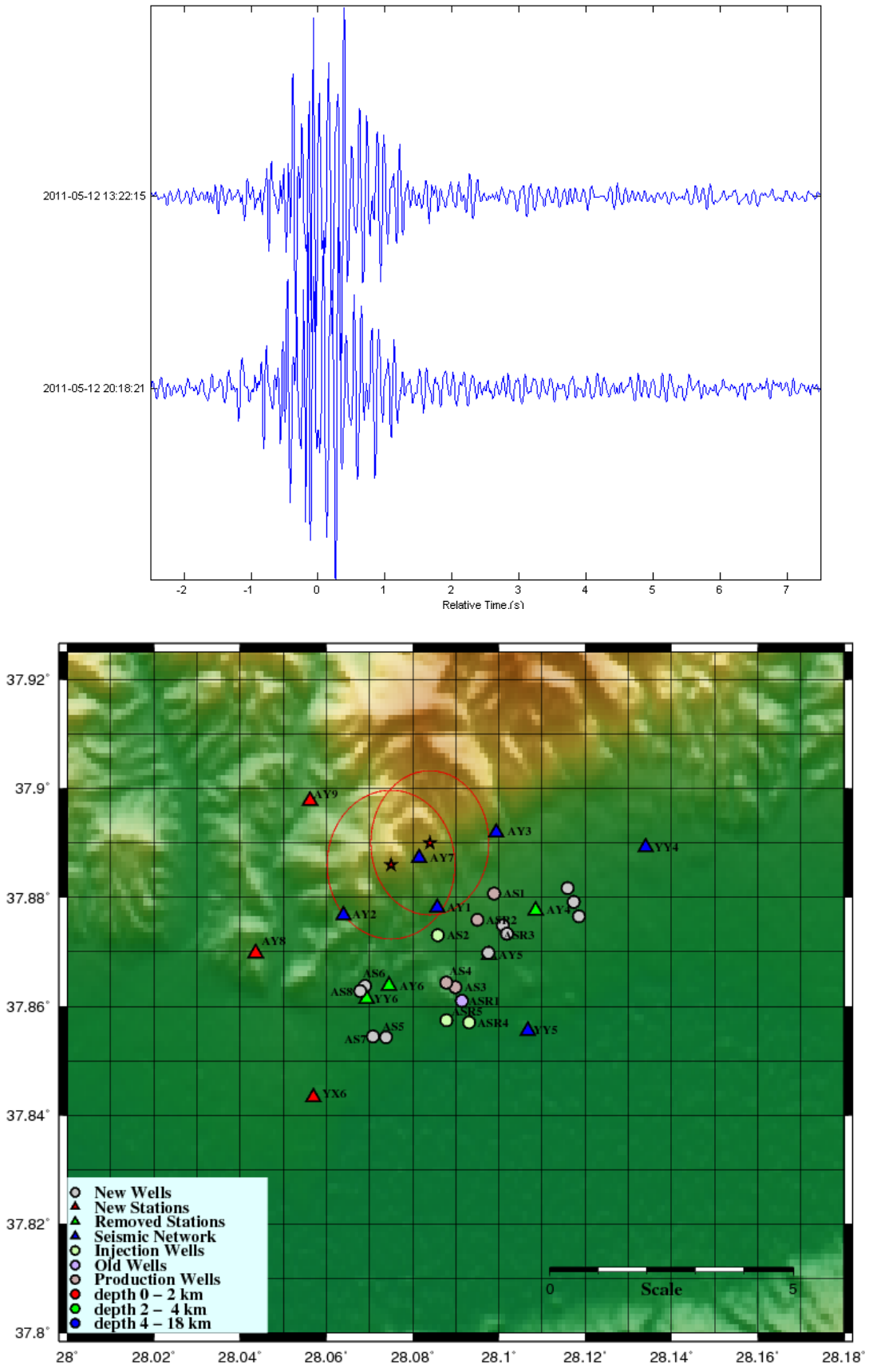

Figure 5.45. Waveforms and locations of event type 23.

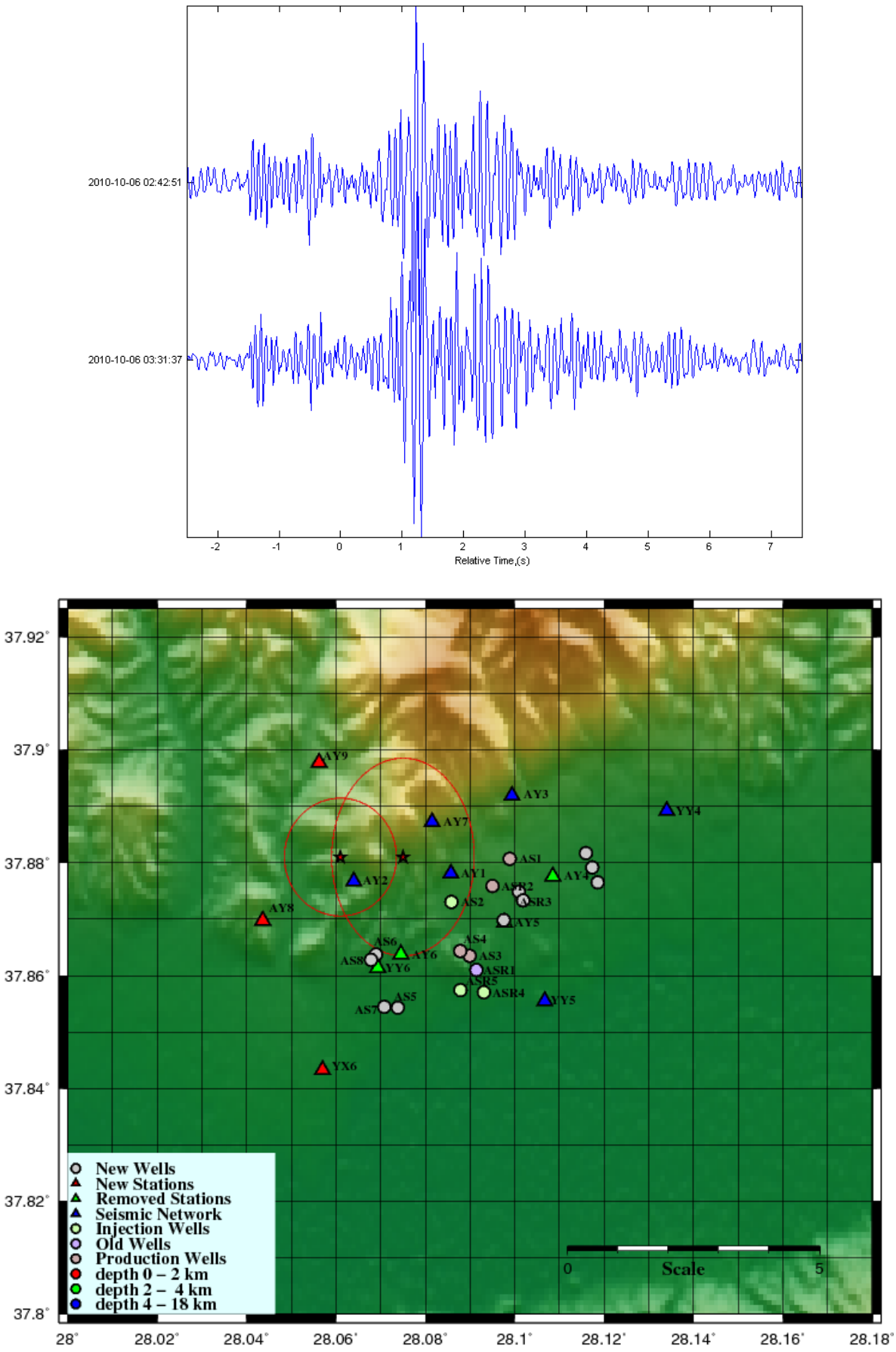

Figure 5.46. Waveforms and locations of event type 24.

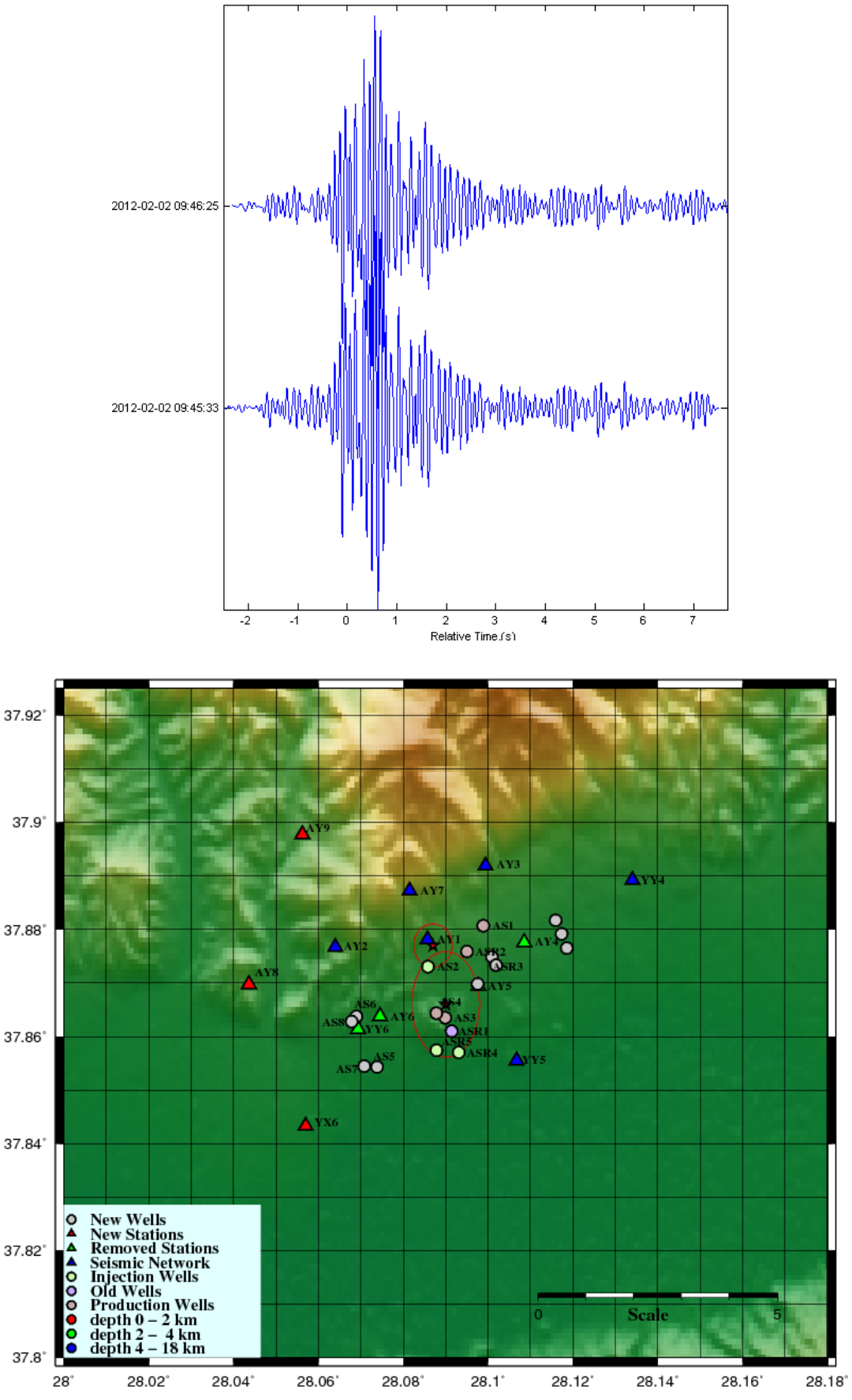

Figure 5.47. Waveforms and locations of event type 25.

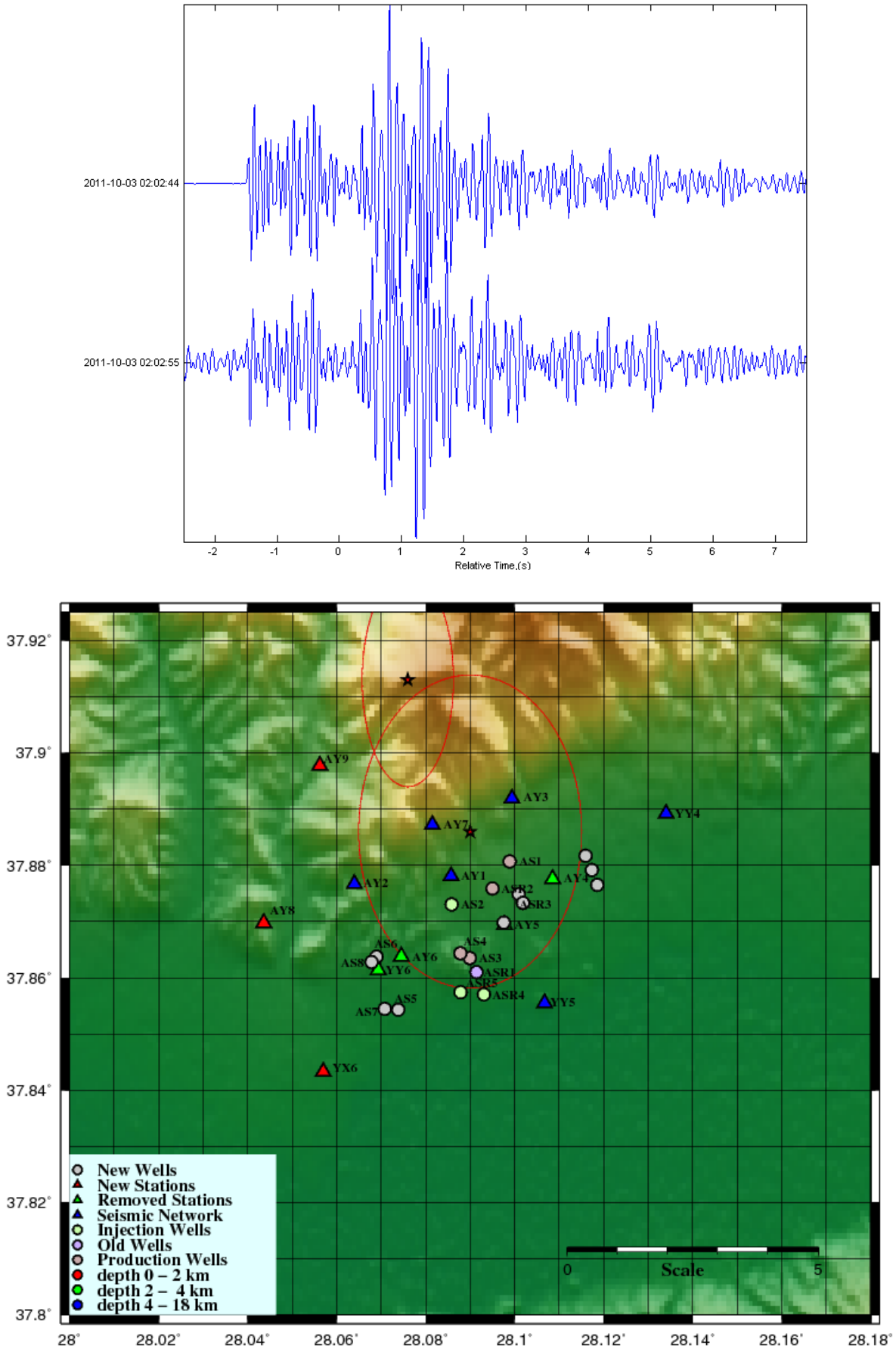

Figure 5.48. Waveforms and locations of event type 26.

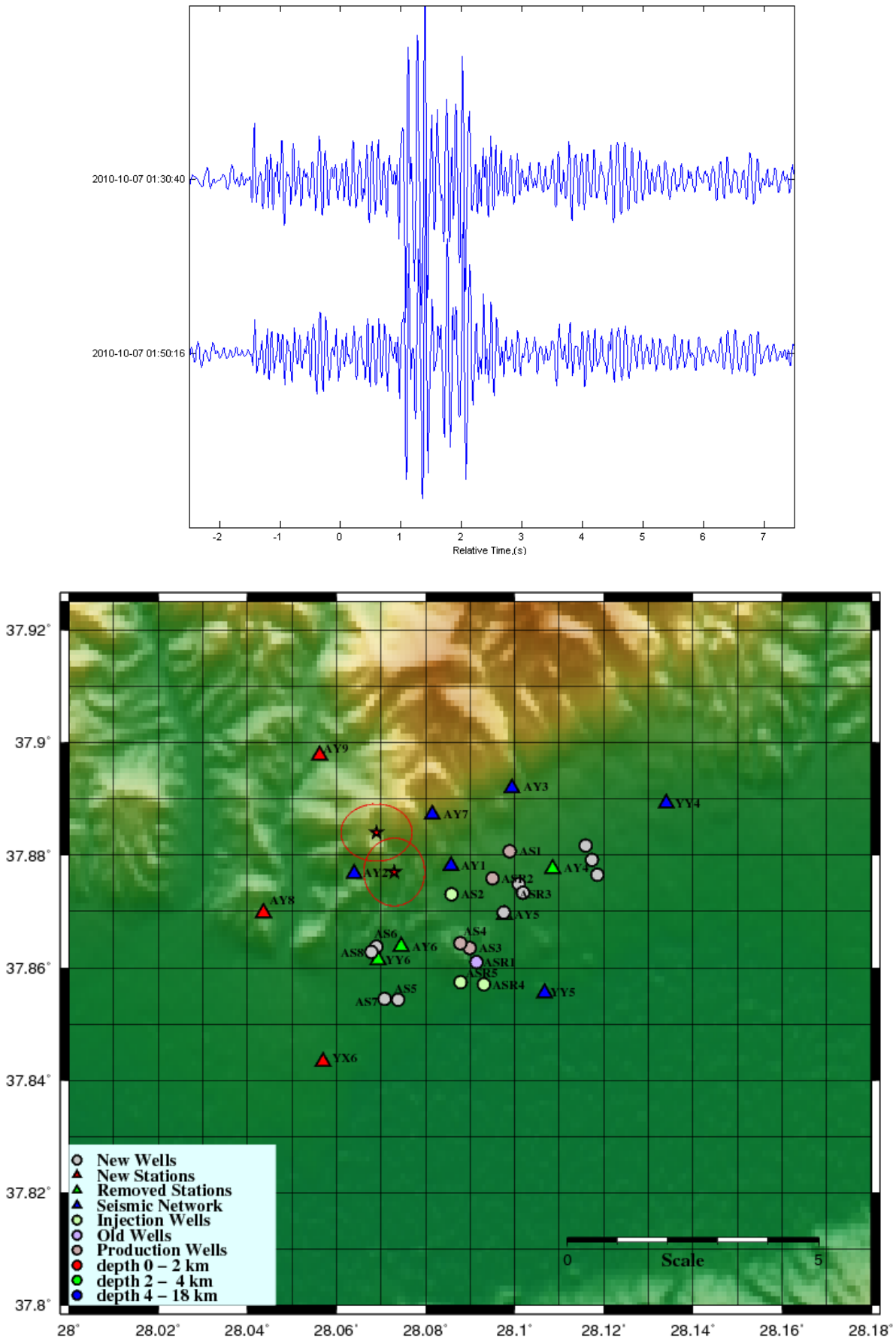

Figure 5.49. Waveforms and locations of event type 27.

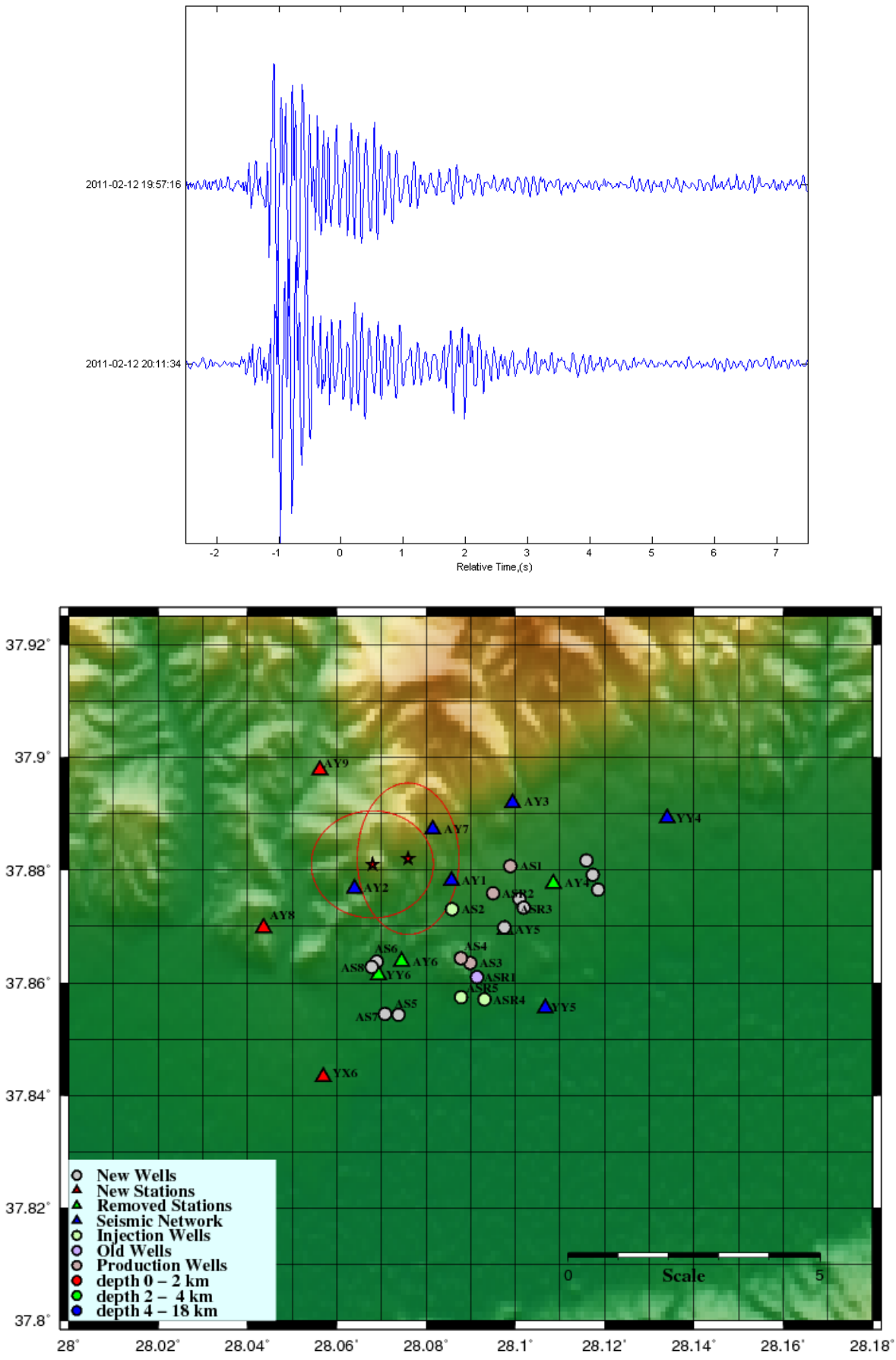

Figure 5.50. Waveforms and locations of event type 28.

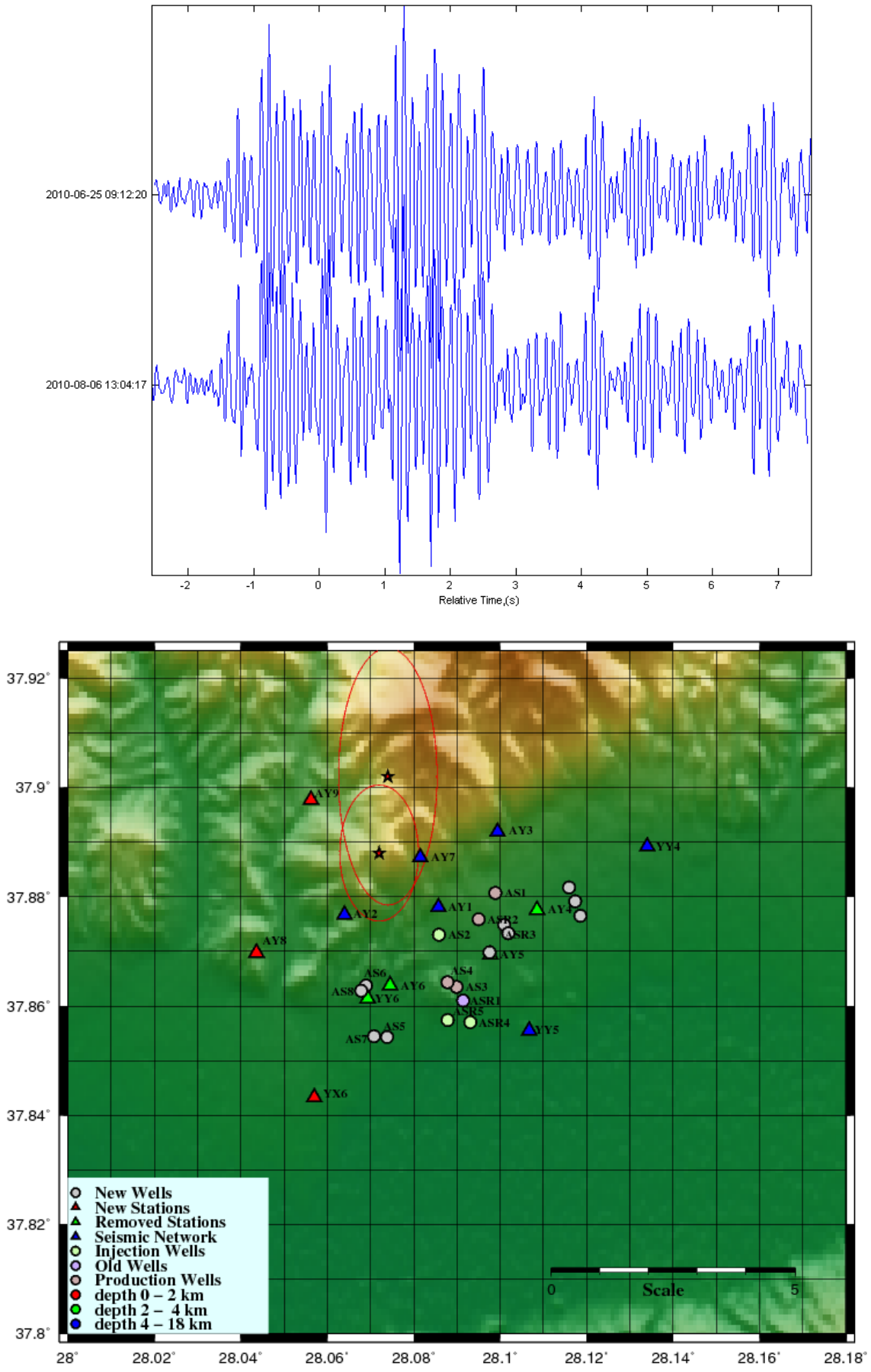

Figure 5.51. Waveforms and locations of event type 29.

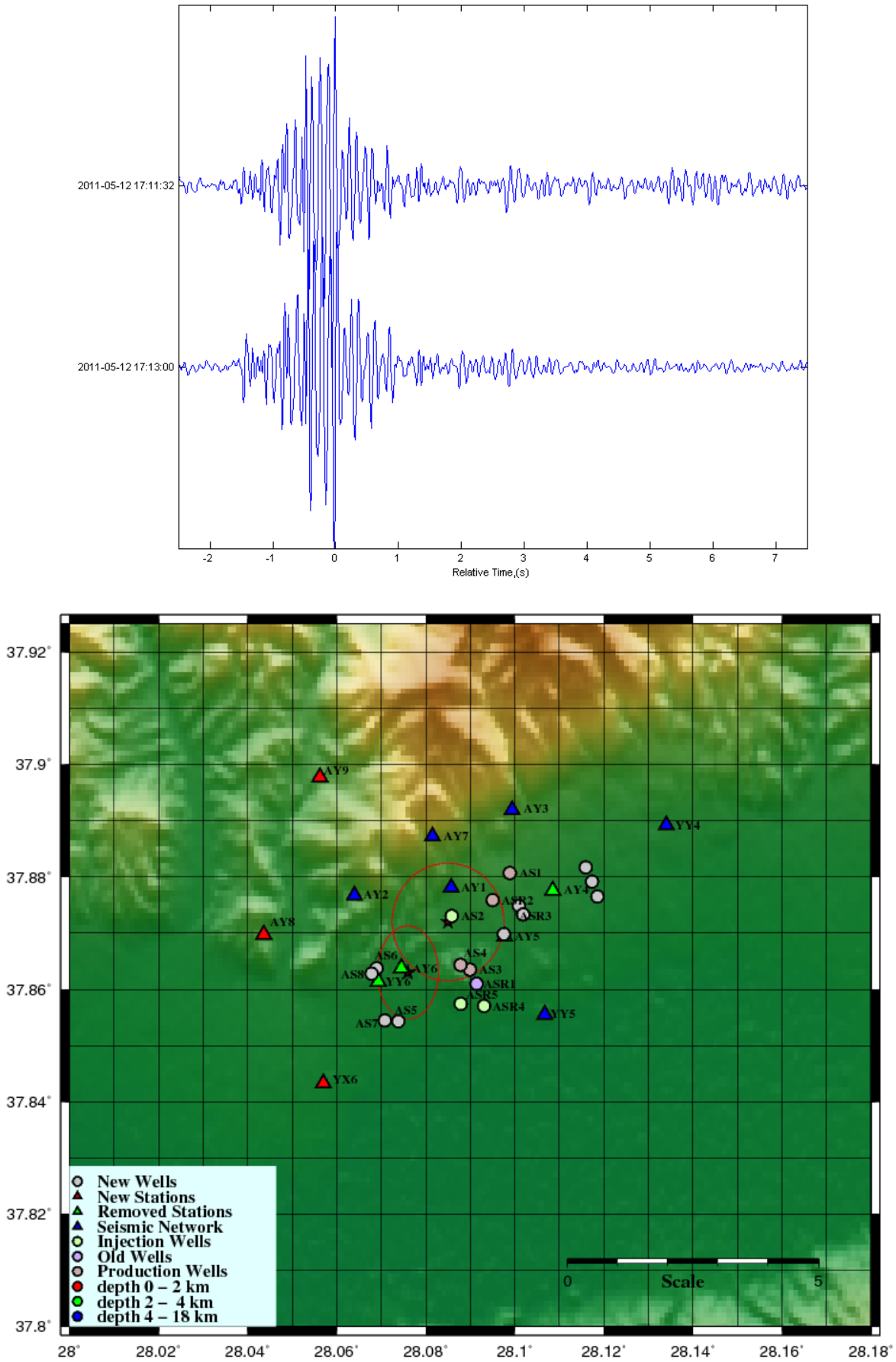

Figure 5.52. Waveforms and locations of event type 30.

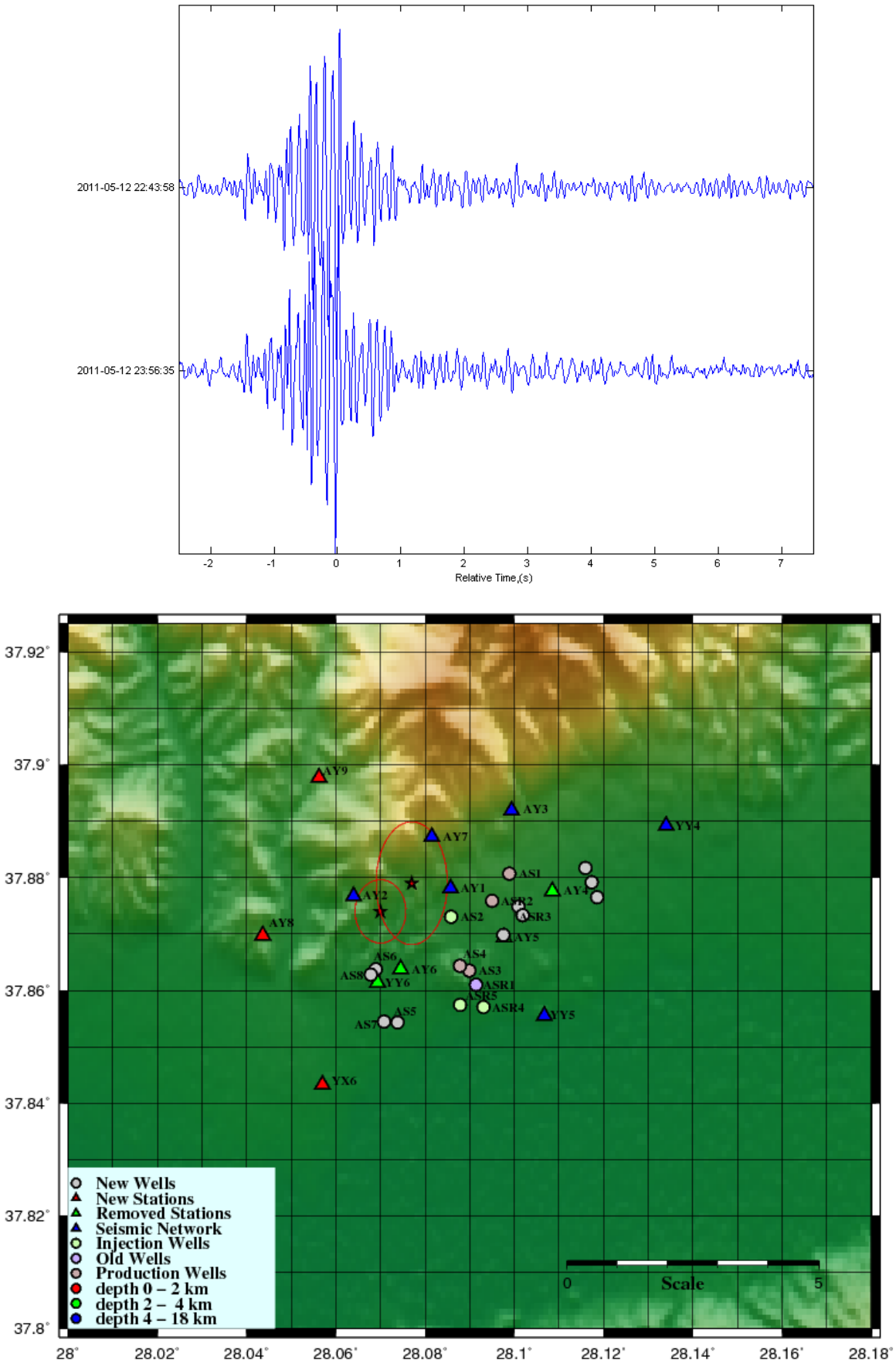

Figure 5.53. Waveforms and locations of event type 31.

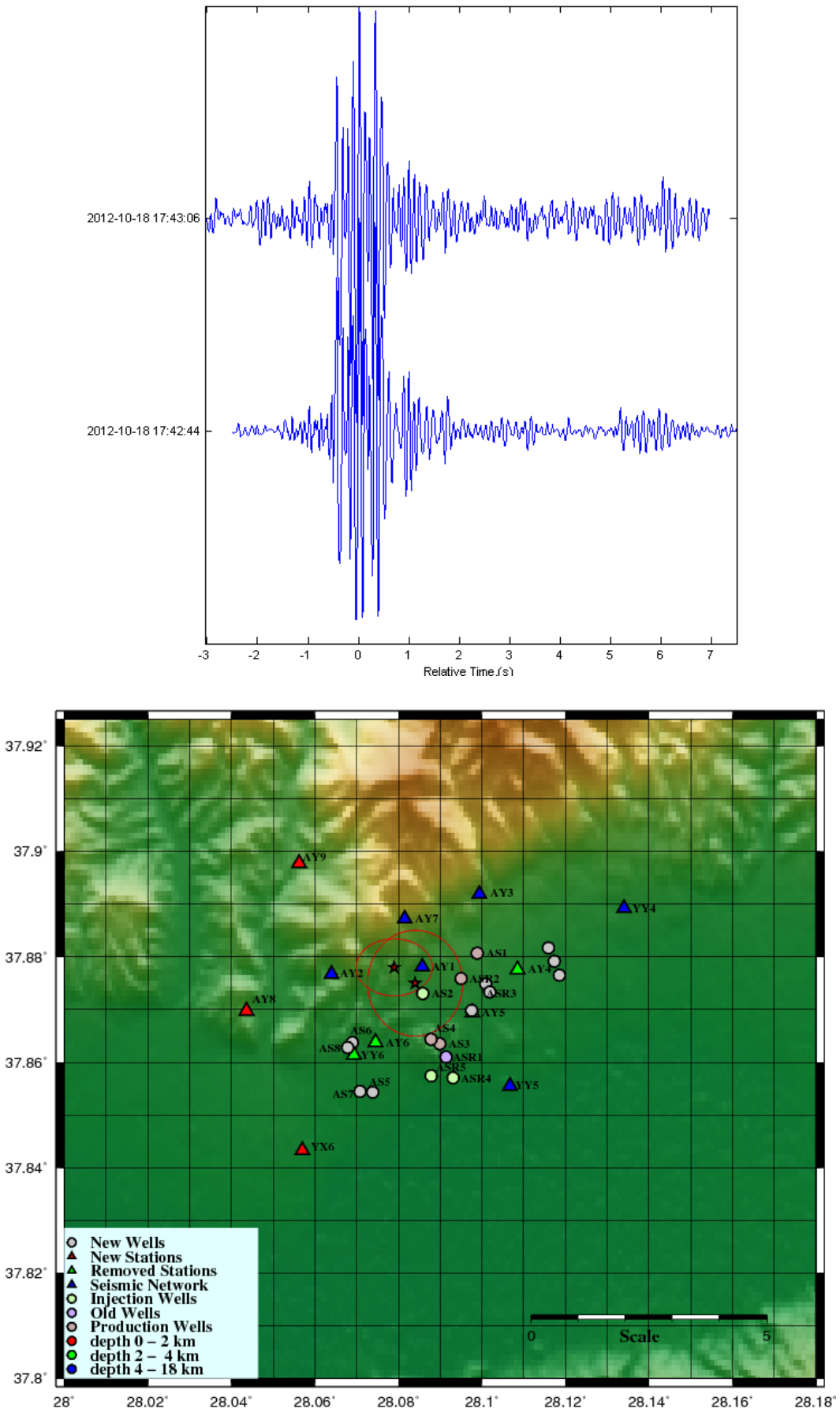

Figure 5.54. Waveforms and locations of event type 32.

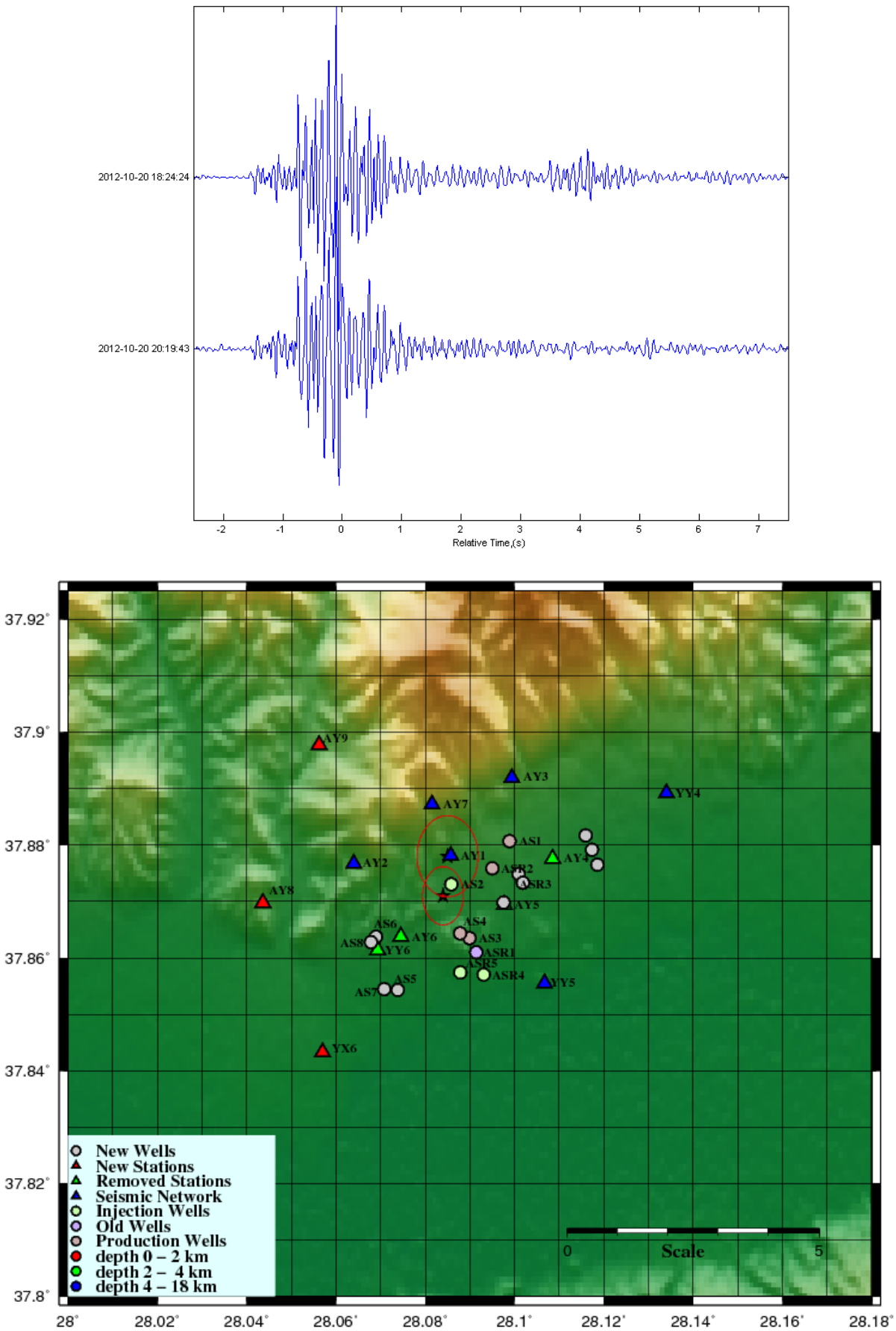

Figure 5.55. Waveforms and locations of event type 33.

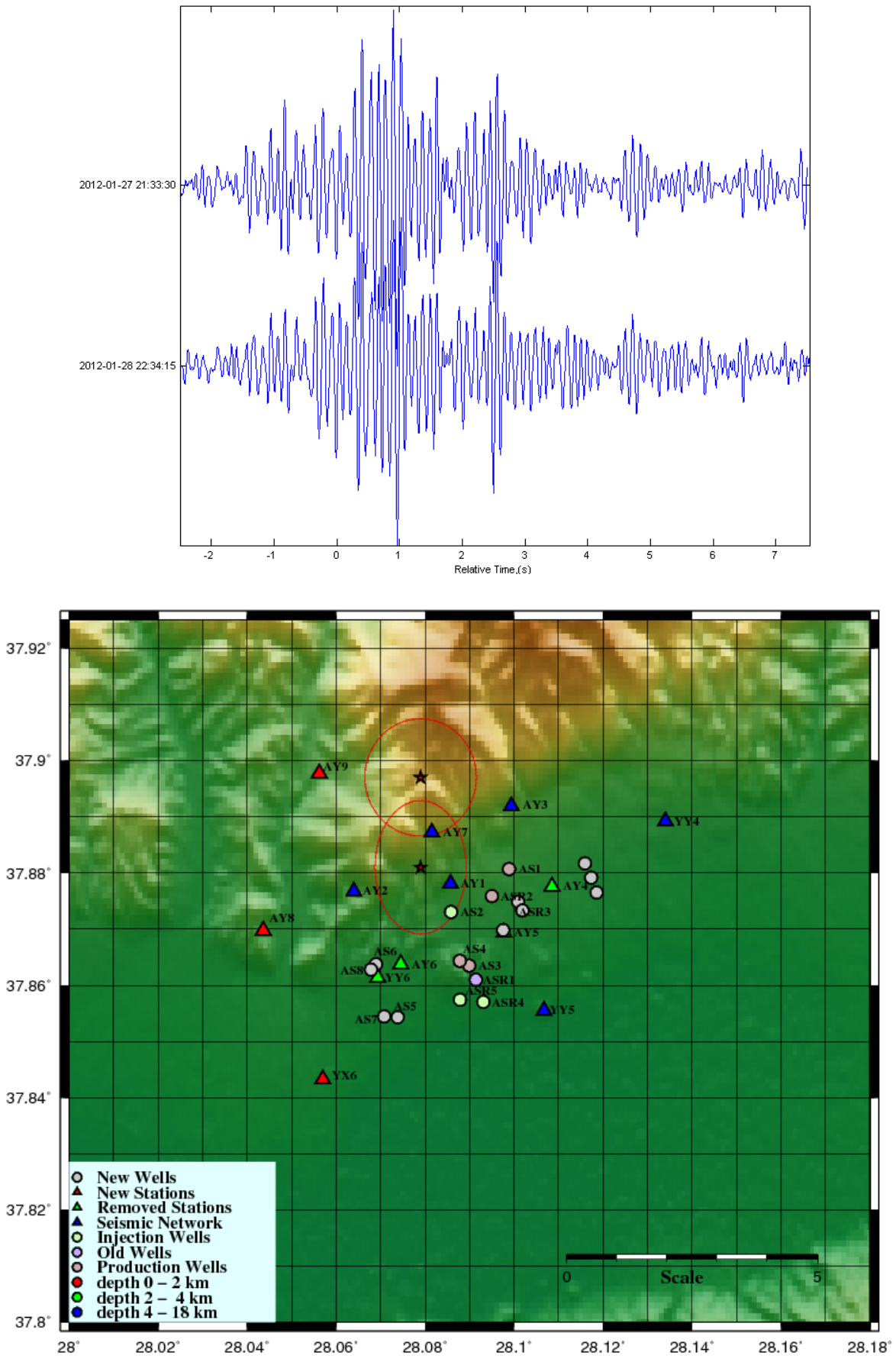

Figure 5.56. Waveforms and locations of event type 34.

6. CONCLUSION

Geothermal areas are very active areas to observe and micro-earthquakes. For this reason,the Salavatlı Geothermal Area, Aydın was chosen as a recording site of micro-earthquakes. At this area, hot water production and re-injection of cold water processes are still in operation. Through these processes many micro-earthquakes are occurring at every geothermal site.

The main purpose of this study is to find similar micro-earthquakes which were occurred at the study area, with a correlation method. The waveform of micro-earthquakes were used for the correlation analysis. The data were collected from June, 2010 to April 2013 from 9 broadband stations. These stations were deployed to the study area surrounding the geothermal wells. About 977 micro-earthquakes were located during this study. 815 of them were used for the correlation analysis.

For the correlation analysis, GISMO correlation toolbox was used. The data was put into GISMO and clusters were found by checking their waveforms. The Threshold for the minimum correlation co-efficient was chosen as 0.9. 34 groups of similar micro-earthquakes found and every group has its unique waveform and they are nearly identical to each other.

VELEST software was used to get a minimum 1Dvelocity model that can represent average velocity structure for the study area and the stations corrections for P and S waves due to different elevation and site geology of the seismological stations,. We have used 380 best located micro-earthquakes for VELEST run. Later, all the events were relocated with the best 1D velocity model by using HYPO71 program. The new location of the micro-earthquakes wereless scattered than before and the distribution of the epicenters became more focused as one big cluster. It is impossible to separate any group of events in relation to any special activity like fluid injection on a mapvieew of the all events by looking at only the epicenter distribution. In this thesis, an attempt has been made to find similar waveforms coming from similar sites.

We have found 34 event groups. Their waveforms are nearly identical, but their locations are little apart from each other. By looking at their waveforms similarity, they should be in the same place. A Further attempt can be made to correct phase arrival picking using correlation lag times, this will likely to map them closer.

When we look at the location of event type 1,2,3 or 4 we can say that they are coming from the same source. Also the other types of the events by looking their error ellipsoids, it is highly possible to say they also come from the same source or fault. When we look closer event type 2 location and time, they occurred at the same day in 10 minutes, the events in this event type 2 might be related to the re-injection process from the wells AS1 and AS2 but we do not have the information about these processes. This will be the focus for a future work.

REFERENCES

Çiftçi, G., O Pamukçu. , C. Çoruh, S. Copur., H. Sözbilir, 2010, "Shallow and Deep Structure of a Supradetachment Basin Based on Geological, Conventional Deep Seismic Reflection Sections and Gravity Data in the Büyük Menderes Graben, Western Anatolia" *Survey Geophysic*, DOI 10.1007/s10712-010-9109-8.

Colberg, P. and Höfling, F. 2011, "Highly Accelerated Simulations of glassy Dynamics Using GPUs: Caveats on Limited Floating-Point Precision". *Comp. Phys. Comm.* 182 (5): 1120–1129. doi:10.1016/j.cpc.2011.01.009.

Dunn, P. F. 2005, *Measurement and Data Analysis for Engineering and Science* New York: McGraw–Hill. ISBN 0-07-282538-3.

Erişen, B., Akkuş, I., Uygur, N. and Koçak, A., 1996, Geothermal Inventory of Turkey MTA, Ankara.

Frenkel, D. and Smit, B. 2002, "Chap. 4.4.2". *Understanding Molecular Simulation (2nd ed.)* London: Academic Press. ISBN 0122673514.

Kissling, E., and J. C. Lahr, 1991. "Tomographic Image of the Pacific Slab Under Southern Alaska" *Eclogae Geol. Helv*., 84/2, 297-315.

Kissling, E. 1988, Geotomography with Local Earthquake Data, *Rev. Geophys*., 26, 659-698.

National Research Council, 2012. *Induced Seismicity Potential in Energy Technologies,* The National Academic Press. ISBN 0-309-0XXXX-X

Ozalaybey, S. ,2010, Personal Communication.

Percival, Donald B. Andrew T. Walden 1993, *Spectral Analysis for Physical Applications: Multitaper and Conventional Univariate Techniques* Cambridge University Press. pp. 190–195. ISBN 0-521-43541-2.

Priestley, M. B. 1982. *"Spectral Analysis and Time Series"* London, New York: Academic Press. ISBN 0125649010.

Reyes, Celso G. and West, Michael E. 2011, "The Waveform Suite: A Robust Platform for Manipulating Waveforms in MATLAB" *Ssa*.

Sözbilir, H., 2001, "Extensional Tectonics and The Geometry of Related Macroscopic Structures: Field Evidence from The gediz Detachment, Western Turkey" *Turkish Journal of Earth Sciences* 10, 51–67.

Sözbilir, H., Emre, T., 1990. "Neogene Stratigraphy and Structure of The Northern Rim of The Büyük Menderes Graben" *Proceedings of International Earth Science Colloquium on the Aegean Region*, 2, pp. 314–322.

Serpen U. and Aksoy N., (2005), "Reinjection Problems in Overpressured Reservoirs. Proceedings" *Thirtieth Workshop on Geothermal Reservoir Engineering Stanford University*, Stanford, California, January 31-February 2.

Serpen, U., and Aksoy, N., (2010), Reassessment of Reinjection in Salavatlı-Sultanhisar Field, Turkey. Proceedings World Geothermal Congress 2010 Bali, Indonesia, 25-29 April 2010.

Serpen, U. and Tüfekçioğlu, H., 2003, Developments in Salavatli Geothermal Field of Turkey. Transactions of GRC 2003 Annual Meeting. Oct. 12-15, Morelia, Michoacan, Mexico.

SUMET, 2010, "Resistivity Surveying in Salavatlı Geothermal Field" Report to Menderes Geothermal, İzmir.

Şahin, H., 1985, Resistivity Surveying in Salavatlı-Sultanhisar Area, MTA Report, Ankara.

Tezel, T., Shibutanip, T., Kaypak, B., (2010), Crustal Structure Variation in Western Turkey Inferred from The Receiver Function Analysis, Tectonophysics, doi: 10.1016/j.tecto.2010. 06.006.

Tezel, T., Erduran, M., Alptekin, O., (2007), "Crustal Shear Wave Velocity Structure of Turkey by Surface Wave Dispersion Analysis", *Annals of Geopgysics*, 50, No 2, 177-190.